# Oriented 3D Printing

# Oriented 3D Printing

by

Simon Boliver El Sahi

A thesis submitted to the
School of Computational Engineering and Science
in conformity with the requirements for the degree of
Master of Applied Science


Hamilton, Ontario, Canada
2008

MASTER OF APPLIED SCIENCES (2008) MCMASTER UNIVERSITY

(Computational Engineering and Sciences) Hamilton, Ontario

TITLE: Oriented 3D Printing

AUTHOR: Simon Boliver El Sahi, B.S. Engineering

SUPERVISOR: Dr. Allan Spence

NUMBER OF PAGES: xii, 113

*To my best friend and shelter*

*Amber*

# Abstract

Ink-jet printing onto flat paper is a widely established process. In this thesis, we make extensions to printing on target surfaces such as metals and glass, using a 5-axis orientable head. Original artwork is created using CAD, and is sampled to create the ink jet point cloud. The target surface location is registered using a standard Coordinate Measuring Machine (CMM) 5-axis touch trigger probe. The probe is then replaced with the ink jet head and the printing process is carried out. Demonstration of the system is illustrated using flat metal and glass samples, as well as rapid prototyped 3-D plastic shapes.

# Acknowledgments

I would like to express my deepest gratitude to my supervisor, Dr. Allan Spence. His encouragement, guidance, and support have been outstanding. The experience that I was privileged to live throughout the past two years was gratifying and rewarding, its lessons helped me develop both academically and most importantly as an individual. For this, I can't stress enough the multitude of my respect and admiration to Dr. Spence as an educator and a human being.

Special thanks to Dr. Spence's research group for their valuable advice, support and friendship. In particular, I would like to thank Dave Chang and Mike Kinsner for their help in setting up the hardware environment.

I would also like to express my gratitude to Mark McKenzie and Ron Lodewyks for their valuable advice and assistance in the machine shop.

To my wife, Amber, the encouragement, motivation, inspiration, and support you've provided me have been invaluable. Words fail me to express my gratitude and love to you. Thank you so much for your presence in my life.

# Nomenclature

| | |
|---|---|
| $e$ | Width of the Half Cylinder Extrusion |
| $\beta$ | Plane Angle of Inclination |
| $M_P$ | PCS to MCS Transformation Matrix |
| A | Probe Angle A rotation around an axis in the xy plane |
| ABS | Acrylonitrile butadiene styrene |
| B | Probe Angle B rotation around z-axis |
| CCS | Calibration Coordinate System |
| CMM | Coordinate Measuring Machine |
| DOF | Degrees of Freedom |
| DPI | Dots per Inch |
| EEPROM | Electrically Erasable Programmable Read-Only Memory |
| FDM | Fused Deposition Modeling |
| MCS | Machine Coordinate System |
| PCS | Part Coordinate Cystem |

RGB Red Green Blue

RP Rapid Prototyping

SLA Stereolithography Apparatus

TTL Transistor Transistor Logic

# Contents

# List of Figures

# Chapter 1

# Introduction

Rapid prototyping and manufacturing continues to be a useful addition to the design cycle. Designers are able to produce a prototype that conveys their vision about scale, shape, and functionality in less time and at a lower cost. According to Ming et al [1] adding color to a design would significantly increase the range of potential applications and the information presented with a colored model. Colored rapid prototyping has been available in the market through ZCorp, however their coloring approach is irreversible because it takes place during the building process, and their rapid prototyped parts are too brittle for functionality.

In this thesis three objectives are addressed: 1) exploring the possibility of taking an already built RP model and applying a color on it accurately to resemble the original CAD model. 2) converting decal images to point clouds that can be viewed independently with or without the model and be accepted by the printer head apparatus used for this thesis. 3) experimenting with coating materials to extend the outreach of the printing apparatus where finer than the available market resolution grids can be printed on the edges or faces of metal sheets to check the effects of manufacturing processes such as: stamping and bending, or printing on glass where

these grids can be picked up by laser scanners or computer vision to research the deformation of glass. The remainder of the thesis is organized as follows. Chapter 2 gives a brief introduction about Rapid Prototyping, decoration technologies, and CAD systems. Chapter 3 talks about the image processing approach, and the conversion of a 2D image into a 3D point cloud. Chapter 4 describes the 3D ink-jet printing hardware, its calibration, and coating materials. Chapter 5 describes the path generation for the CMM, and the progression of the calibration and printing methods from 2D to 3D, about image angular sectioning. Chapter 6 shows the results achieved in printing on planes, inclined planes, half cylinders, elliptical extrusions, spline extrusions, planar coated glass sheets, edges and faces of aluminum sheets. The final chapter states a conclusion about this work and recommends follow up avenues for future work.

# Chapter 2

# Literature Survey

Product design is becoming a more challenging field with an increasingly selective clientele. Focusing on the functionality and utility of products, while ignoring their attractiveness, has been the norm in the designing process. Such was the case with Sinclair C5 electric car [2] where the customers were not allowed to see how it would look until its extremely disappointing release, causing the production of a functional and easily usable product to come to an end. On the other side the iPod mp3 players proved to be a huge success mainly due to their aesthetic design and appeal. The notion of analyzing customer needs and wishes and appealing to their emotional needs, be it positive or negative, can identify the design aspects (Reactive, Behavioral, and Reflective) [3, 4] that can satisfy the consumer. To capture the mood of consumers it is critical be able to provide them with a feedback mechanism that can accurately gauge what they like about a design and what they don't. This iterative approach has been realized better with Rapid Prototyping (RP).

## 2.1 Rapid Prototyping

All manufacturing processes fall under three categories: additive, subtractive, or formative, and the production of a certain part can involve one or more processes [2]. Rapid Prototyping is the use of a CAD-based automated additive manufacturing process to construct parts that are used directly as finished products or components with little or no human intervention once the process has begun [5]. This technology has offered unlimited possibilities for designers, medical specialists [6, 7], sculpturers and artists [8, 9] who were constrained by Design For Manufacturing guidelines. With this technology, products can be built as long as they can be drawn in the CAD system, while providing designers an insight about the form, scale, fit, functionality, and reliability of their design[10]. There is no need to think about draft angles, part complexity, sharp corners, and the constraints of the molding or tool making processes. This freedom in geometry comes at a cost of the surface roughness, accuracy, and repeatability. The relative ease of use and rapidity of the RP machines provides designers with the luxury of visualization, verification, iteration, and fabrication. "A Prototype is worth a thousand pictures" [5], thus the ability to visualize and get a sense of scale, and check for hidden features that can puzzle the best blue print and CAD file readers. Due to the rapidity and low cost of the Rapid Prototyping product iteration or design debugging [11] can be achieved through multiple cycles. This approach would have been avoided in the past due the time and cost of producing one single prototype. While iteration could be a good road map for product quality, optimizing the iterated part would be an extra step that designers could afford to have with RP, because it would help research the product sensitivity to distinct factors. Most useful is RP's ability to produce a functional test model (FTM), where the functionality of the part can be surveyed before committing any time or money to

produce the final tooling. The flowchart shown in figure 2.2 illustrates how using RP could save time and money, and how it would enable the designer to communicate their ideas about products at a every stage of the design.

### 2.1.1 File Format

STL file format is the language of interchange between the CAD system and the RP machines. This format was first introduced by 3D Systems and is widely used for rapid prototyping and manufacturing. STL is a facet representation that approximates surface geometry only, while disregarding entities like points, lines, and curves and attributes like color, texture [12].

An STL file contains a variable density triangulation facet data as shown in Fig. 2.1. Each facet is determined by a normal and by three vertices, where each facet should share two vertices with the one adjacent to it. A sample syntax generated by Autodesk Inventor is listed below, where one can infer that there can exist more than one solid in a file, more than one loop in a facet, and more than three vertices in a loop; however, the example syntax uses only simple triangles.

Using this file format has several advantages such as: easy conversion to a simple file format, wide range of 3D geometry input, simple slicing algorithm, and the ability to split these files to accommodate the RP building size. The disadvantages are: floating point approximation, and deficiency of important information about the model features [13].

```
solid ascii
  facet normal -3.612417e-001 9.324722e-001 0.000000e+000
    outer loop
      vertex   -1.661774e+001 4.715772e+001 0.000000e+000
      vertex   -1.948929e+001 4.604528e+001 1.000000e+002
      vertex   -1.661774e+001 4.715772e+001 1.000000e+002
    endloop
  endfacet
```

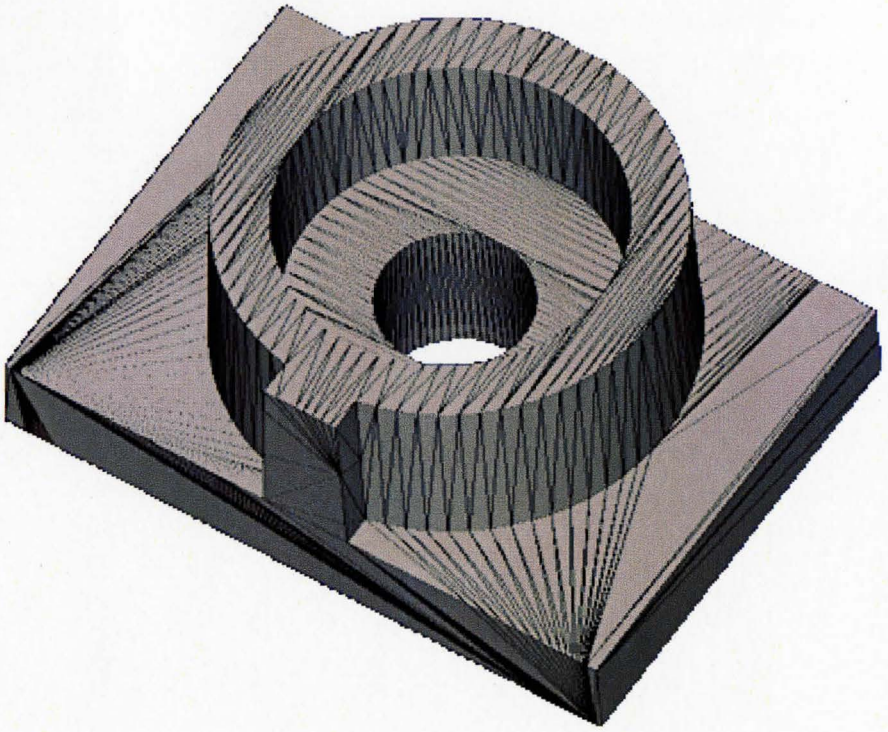

Figure 2.1: Visualization of Triangulation in STL Files [12]

### 2.1.2 RP Technologies

RP is defined as "the use of CAD-based automated additive manufacturing process" to build finished parts or components with no human interference once the process starts [2]. When the produced parts are functional and intended for end use,

the process is called Rapid Manufacturing and is used for specialist, low-volume and customized products. Currently there are several competing RP technologies in the market, some of these technologies are shown in Table 2.1

| Technology Base | Sample Technologies |
|---|---|
| Solid-Based Systems | • Fused Deposition Modeling[14]<br>• Laminated Object Manufacturing [15] |
| Liquid-Based Systems | • Stereolithography [16]<br>• Jetting Systems [17]<br>• Direct Light Processing [18] |
| Powder-Based Systems | • Selective Laser Sintering [19]<br>• Three Dimensional Printing [20] |

Table 2.1: Major Rapid Prototyping Technologies[2, 21]

**Stereolithography**

Stereolithography is the oldest and most preeminent RP process, and considered as the founding process in the RP industry [2, 22, 23]. The process works by focusing a concentrated beam of ultraviolet (UV) laser onto the surface of a liquid photo-curable vat, which solidifies whenever the beam hits its surface. Using a CAD software that slices the part model into a large number cross-sections layers that can be as thin as $50\mu m$, the (UV) laser traces the cross-section triggering the curing the photo-polymer. By tracing cross-sections, the beam finishes the part by building it layer by layer starting with the bottom layer, on an stepper motor platform that descends into the vat after the solidification of each layer. When the build is complete, the platform raises above the vat, draining the excess resin away from the part as shown in Fig. 2.3.

Due to their high accuracy and large size Stereolithography Apparatus (SLA) ma-

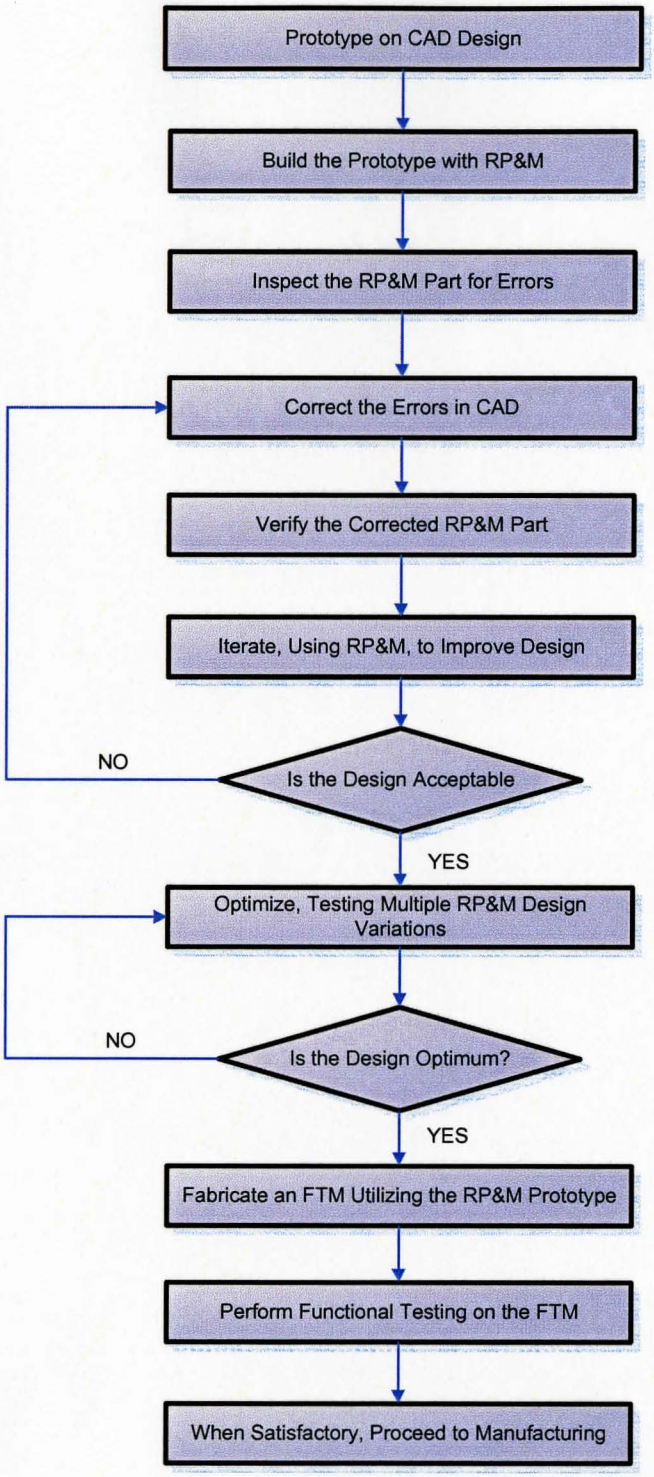


Figure 2.2: Application of RP&M Flow Chart [5]

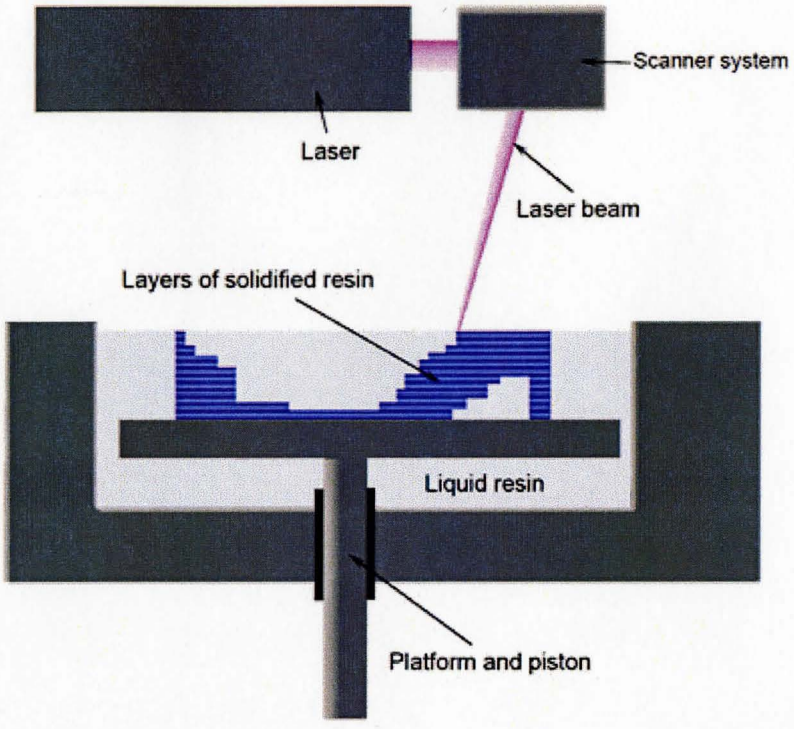


Figure 2.3: Stereolithography System Schematic Drawing [23]

chines and their ability to build complex geometries and intricate details[16], Stereolithography is becoming a dependable tool for rapid manufacturing. On the other side, SLA are the most expensive RP machines with a price tag that ranges from $100,000 to $400,000, and photo-curable resin that costs $75 - $200 a litre [21, 23].

### Fused Deposition Modeling (FDM)

FDM is a solid-based RP process that was first commercialized by Stratasys in 1991 [14, 2]. It builds models by extruding materials through a head that travels in the $xy$ plane, thus creating 2D layers [2, 6, 24], where a plastic filament is unwound from a coil and then supplied to a heated extrusion head that controls the flow of the semi-liquid state plastic.

When the head travels in the plane of deposition according to the slice geometry, it squirts a thin bead of extruded material to form each layer which solidifies instantly and bonds to the layers below due the chamber air flow [21]. After building each layer the table drops in the $z$ direction by the resolution of the system which can be as low as $127\mu m$ [2]. The process is repeated until the model is completely built. The apparatus shown in Fig. 2.4 is contained within a chamber where the temperature is just below the solidification point of the plastic [21].

Materials such as Acrylonitrile Butadiene Styrene (ABS) and other thermoplastic polymers or eutectic metals are used in FDM, due to the simplicity of the process and the properties of the polymers. Support structures for overhanging geometries are built using a different coil, and are later removed by breaking them away from the model or simply by washing them off if the support material is water-soluble [21].

FDM machines are popular due to their relative low cost and clean non-toxic operation that make them office friendly. On the other hand their building process is slow and their limitations can be reached easily due to their relative low resolution. The closest competitor to the FDM process in terms of cost and popularity is three dimensional printing, where FDM has the advantage in the variety and strength of its building material [21].

### 3D Printing

3D printing is an ink-jet based process that builds the model's slice geometry on layers of powder (plaster, corn starch, or resins). As shown in Fig. 2.5 the ink-jet head sprays a liquid adhesive compound onto the top layer of a bed of powder object material in the shape of the cross-section geometry, which binds the powder particles where the adhesive is deposited. The powder bed is lowered by the resolution of the machine, while the powder supply is raised by the same amount enabling powder

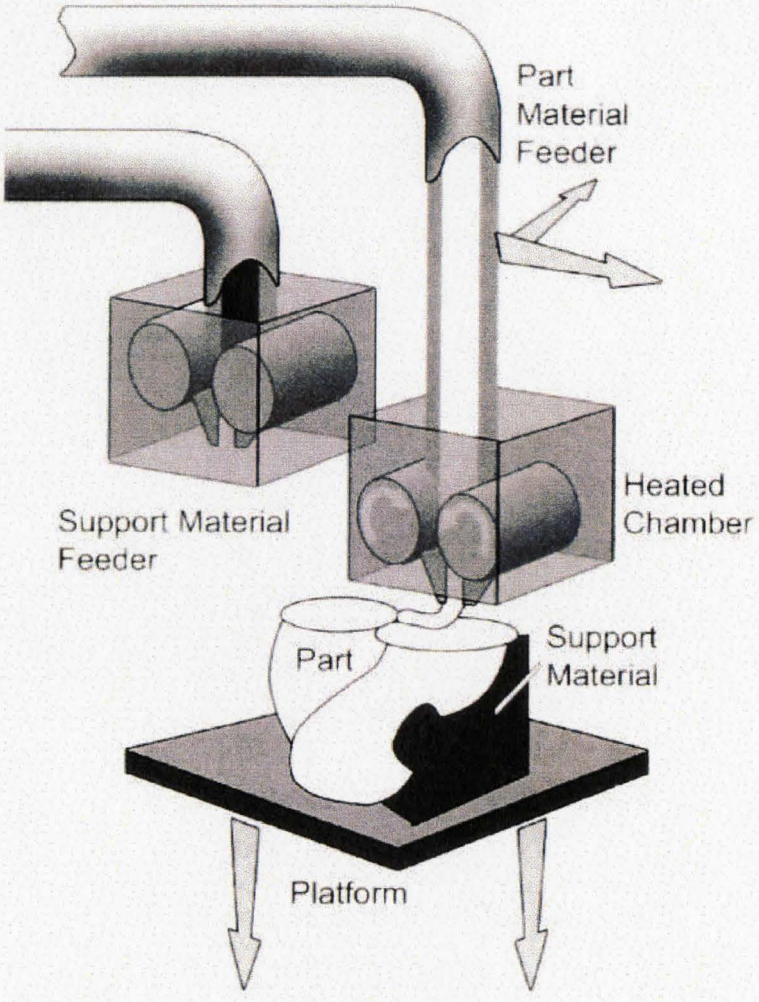


Figure 2.4: FDM System Schematic Drawing [2]

relocation using the spreading blade. Layer by layer, the process is repeated until the part is completed. By simply brushing off the excess powder, the part can be cleaned and made ready for usage. Part cleaning is easier than FDM, as the overhanging geometries are held up by the unneeded powder which can be reused [25, 5, 20].

This process is popular due to its low cost, rapidness, and its full colored part production [20]. However its final parts are not as strong as the parts produced by the previous methods.

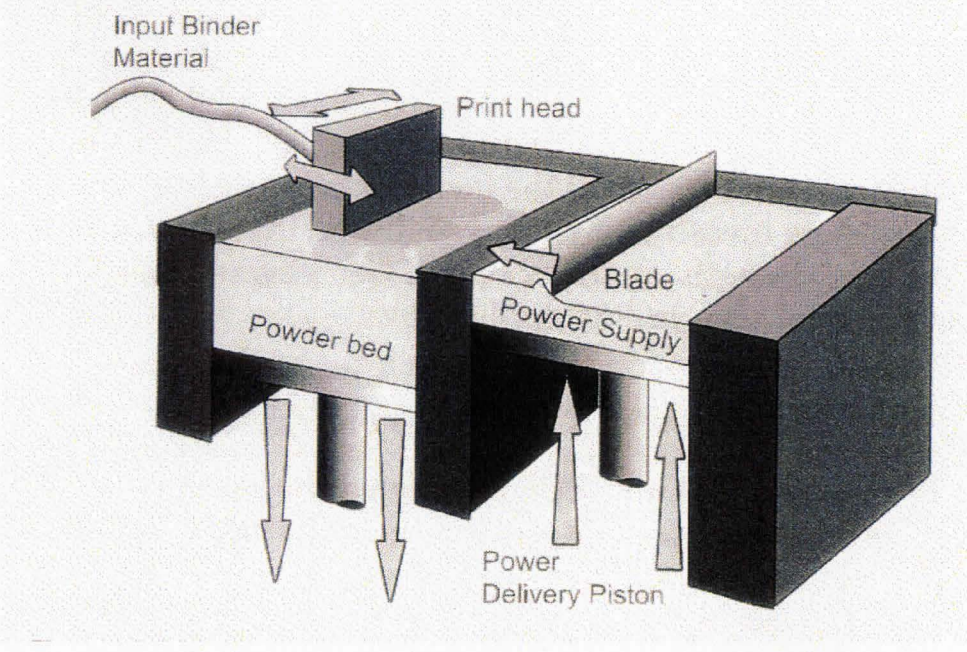


Figure 2.5: 3D Printing System Schematic Drawing [2]

## 2.2 Decoration and Printing Methods

According to Hillestad et al., quality part design process should consider the decoration required at its early stages, where decoration is defined as the application of a finish or graphic that adds value to the final product [26], and the value can be defined as information sent to the user of the product [27]. The decoration/printing

methods or the transfer of 2D images onto 3D surfaces [28] used on plastics, glass, ceramics, metals are numerous, however the most common of these is: pad transfer printing [29]. Each of these methods have its strengths and weaknesses, however all of them share the same weakness in terms of accuracy and the ability to reproduce what the designer of a certain product has envisioned in a CAD model.

## Pad Transfer Printing

Pad Transfer Printing (PTP) is used for decorating products or prototypes in various industries such as: medical, automotive, promotional, apparel, electronics, appliances, sports equipment and toys [28], where such products would be difficult or impossible to decorate [30]. PTP is one of the few technologies that has the ability to print on irregularly shaped parts, and to deposit functional materials such as conductive inks, adhesives, dyes and lubricants, hence its popularity [30, 28]. On the other side, PTP is limited by several constraints such as: the printing designated area, the amount of ink to be absorbed during a stamp [30], the number of colors it can reproduce, and the location accuracy of the print.

PTP has three major components: pad, ink and cliché. The cliché is a $25\mu m$ deep custom etched ink reservoir that is usually made of a hard polymer or steel material where the cliché can represent only one color. The pad, typically made from a silicone rubber, can come in different shapes and sizes according to the product, which acts as the ink transporter. The unique properties of the silicone enable it to pick the design up from a 2D surface transfer it to a 3D one regardless of its complexity. The process as shown in Fig. 2.6 starts by flooding the cliché with ink and then pressing the pad against it. The pad picks up the design and transfers it by pressing against the object [31].

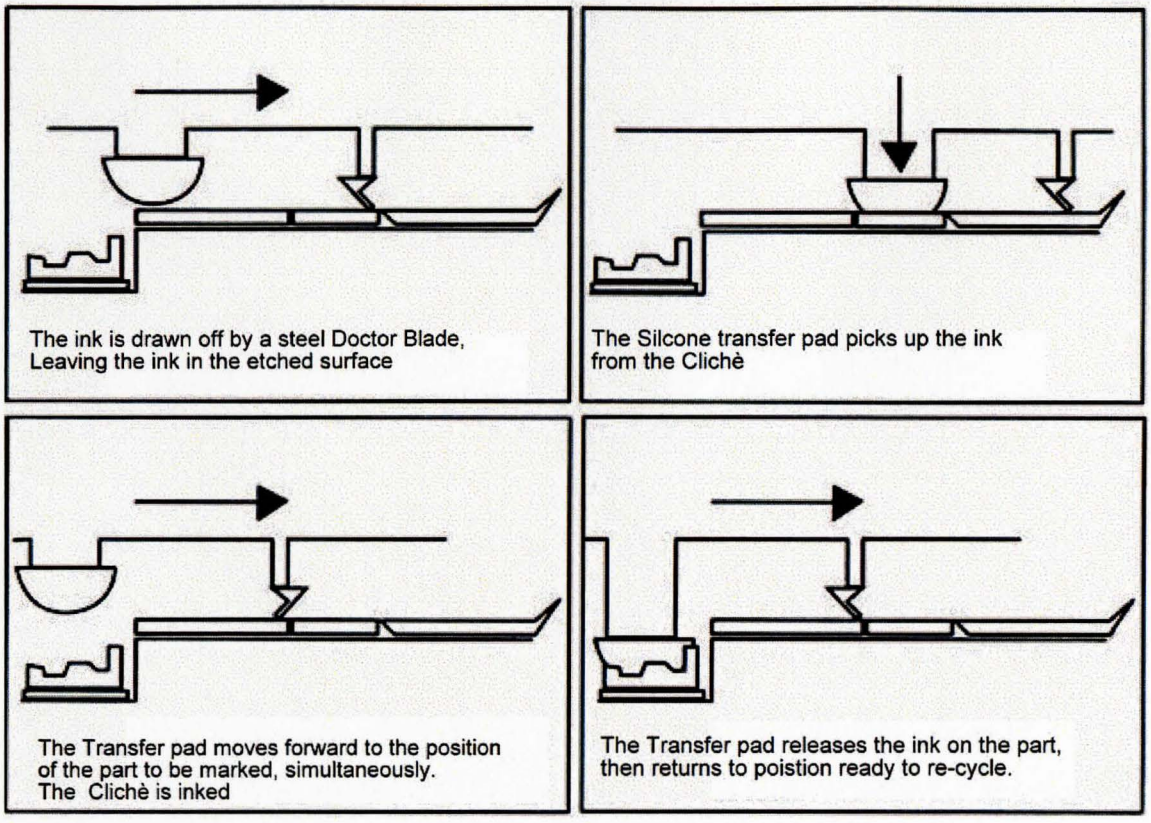


Figure 2.6: Pad Transfer Printing Process Diagram [32]

## 2.3 CAD Systems

In CAD systems there are several techniques to construct a solid model or a closed volume. Techniques such as Constructive Solid Geometry CSG, Boundary Representation (B-Rep), feature based modeling, and boundary modeling determine the method of building the solid and its data tree structure [13]. For example, CSG was used in traditional solid modelers that enabled the modeler to build complex solids by using solid primitives (box, cylinder, sphere, torus, cone, etc.) and using Boolean operators of union, intersection, and difference as tools to combine these primitive as shown in Fig. 2.7 . The CAD system used in the study (Autodesk Inventor) as well as many commercial CAD systems use B-Rep to store their geometry (location

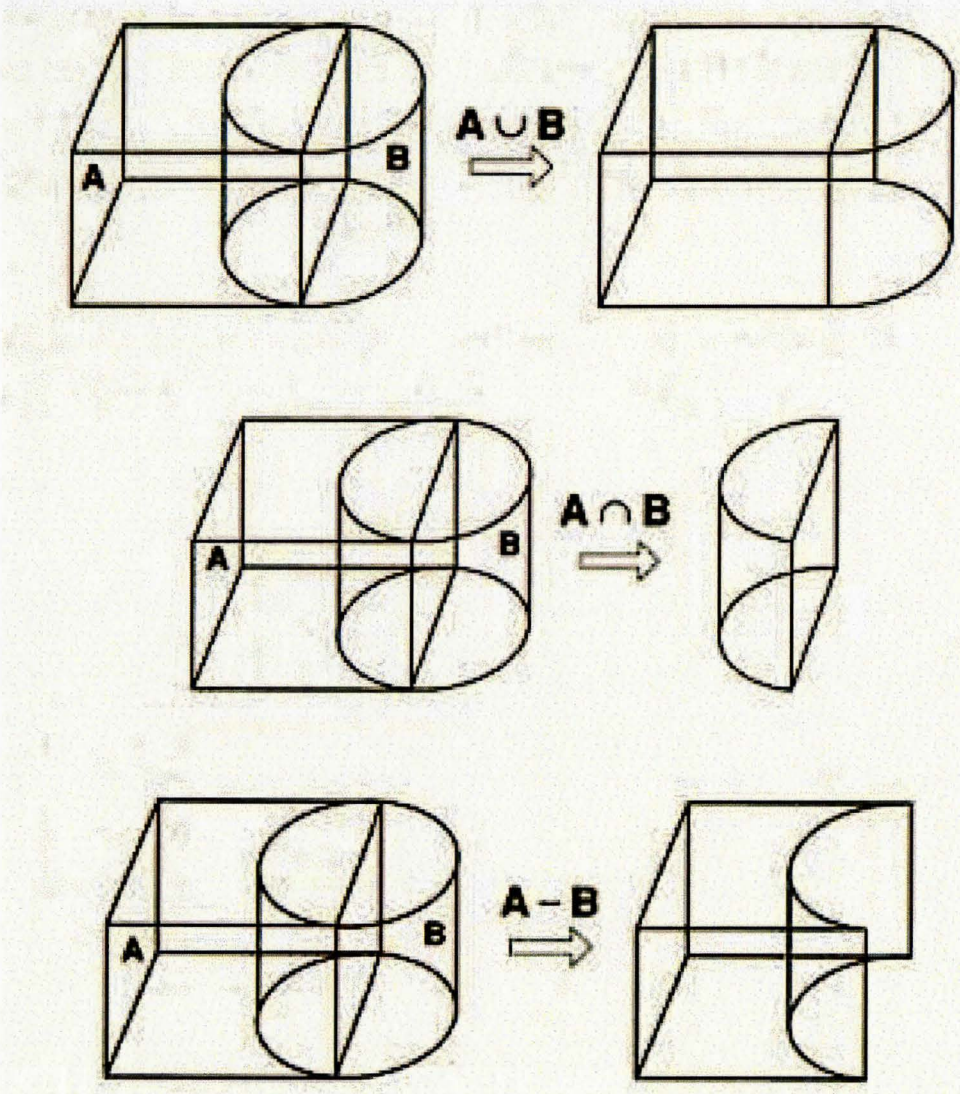


Figure 2.7: CSG Example [13]

and size of entities) and topology (connection among entities). The popularity of B-Rep systems is largely because of its flexibility and the availability of rich and reliable B-Rep kernel systems like ACIS. Exchanging data between B-Rep systems is also feasible using data exchange standards such as the Initial Graphics Exchange Specification (IGES) and the Standard for the Exchange of Product Data (STEP) [13, 33]. A B-Rep object model diagram is shown in Fig. 2.8.

## 2.4 Summary

In this chapter RP technologies, printing technologies, and CAD systems were briefly discussed; in addition, their importance in the product design cycle was emphasized. The advantages of these technologies are numerous, yet they all share one shortcoming: the lack of a bridge between all of them that conveys more information about the product, thus improving the design cycle. For example, RP cannot produce functional parts in color, and when it does produce colored parts, the parts are not functional, PTP is constrained by the very small number of colors it can employ, the shapes it can be applied on, and the lack of accuracy of the RP machine. CAD systems provide a great visualization tool, yet without physical models the sense of scale and aesthetics can be lost. The remainder of this thesis will introduce a new approach that links all these three important components of the product design cycle, it is called Oriented 3D Printing. With oriented 3D printing a product designer can print accurately on functional RP models as many times as desired, without the need to worry about building another RP model.

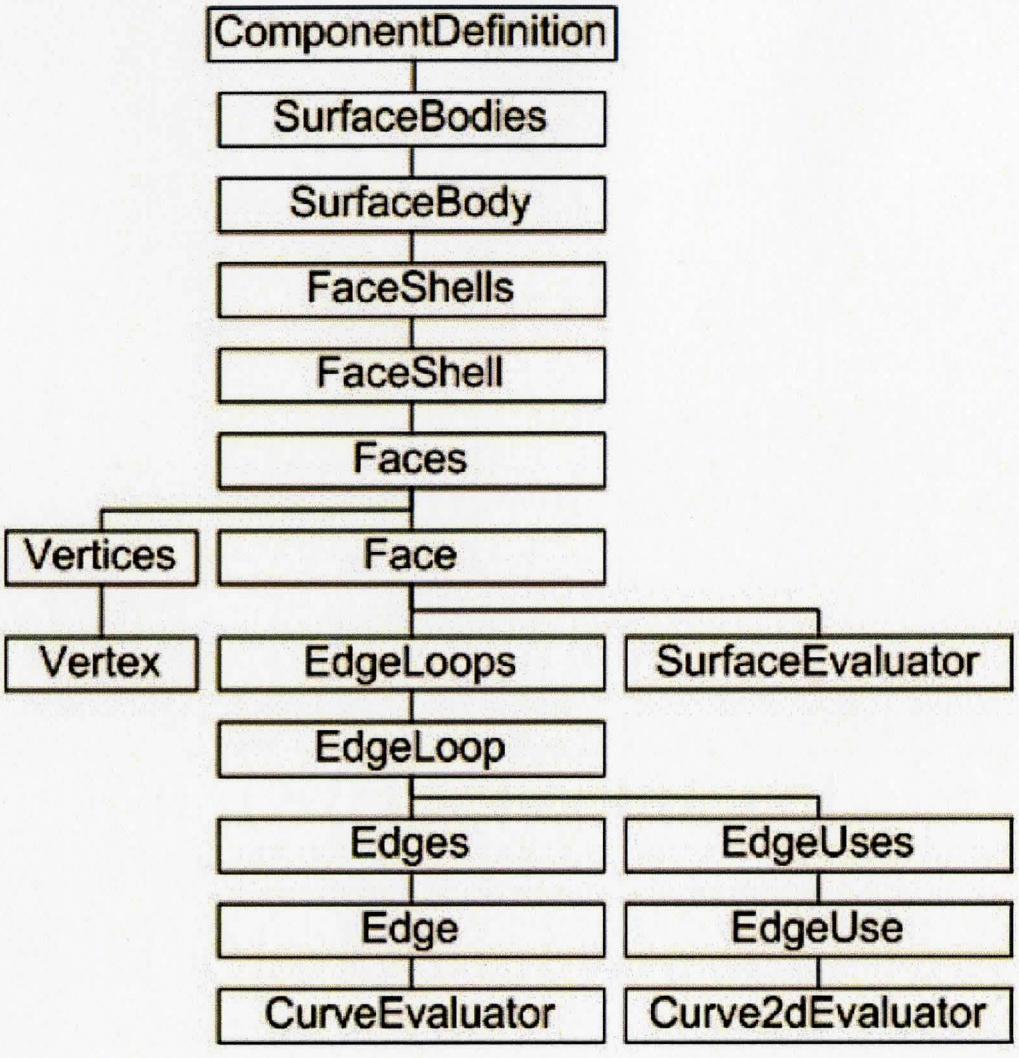


Figure 2.8: B-Rep Object Model Diagram [34]

# Chapter 3

# Hardware Setup

This chapter describes the system architecture and the parts that constitute the oriented 3D printer. In order for an oriented 3D printer to print on non-porous 3D surfaces three tasks need to be completed : ink dispensing, moving the ink dispenser, and accepting the ink dispensed. These tasks can be fulfilled by using a serial ink-jet printer, a 5-axis machine such as: a coordinate measuring machine (CMM), and water soluble ink adhesive coating.

## 3.1 System Architecture

The system architecture for the Oriented 3D Printer shown in Fig. 3.1 is composed of the following parts : workstation, CMM, ink-jet head, and precoatings needed for the samples. The workstation is connected to the CMM controller via an Ethernet cable, and to the ink-jet head through a virtual serial port via a USB cable. The CMM controller has a TTL connection to the ink-jet head. Data is uploaded from the workstation to the ink-jet and the CMM separately, however the ink-jet operation is controlled by the TTL signal that the CMM controller issues at the designated travel

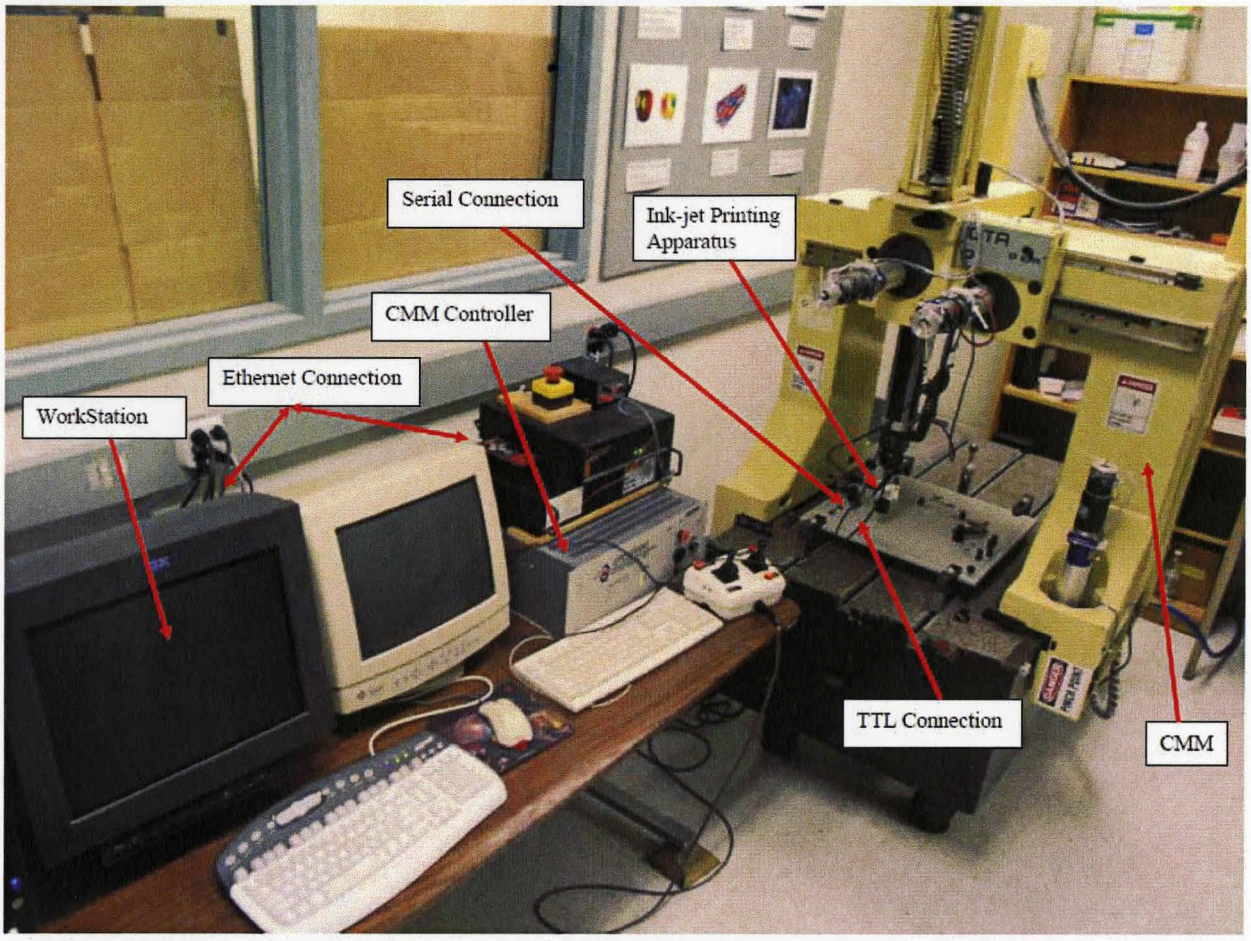


Figure 3.1: Oriented 3D Printing System Architecture

distance.

## 3.2 Ink-jet Printer

The ink-jet printer used in the Oriented 3D printing consists of four major parts: the cartridge, the serial ink-jet printer, the firmware, and the assembly that allows the printer to be mounted in repeatable manner on the CMM.

### 3.2.1 HP 51604 Cartridge

The ink-jet head consists of the HP 51604 thermal ink-jet cartridge shown in Fig. 3.2 and the serial ink-jet printer. According to HP [35] the HP 51604 cartridge was originally designed for the HP ThinkJet and QuietJet printers, and ever-since it became popular in several ink applications across many industries because of its reliability and ease of use. This cartridge is a 96 (Dots Per Inch) DPI monochrome device, and is available in three colors : red, black, and blue. It is also characterized by its robustness, compactness, and printing consistency in different orientations throughout its life. Its non-contact "drop-on-demand" thermal printing is synonymous to quieter printing operations. The ink used in these cartridges is designed for permanence on countless porous surfaces including woods, fabric, paper, card boards, etc. When emptied, they can easily refilled with application based ink using very inexpensive refill kits [36]. The process of ejecting ink from the cartridge is described in [37] as follows: Using capillary action, ink from the sponge bleeds to the nozzle plate where it forms a small pool of ink on each of the twelve nozzles. Small resistors located in each nozzle heat up rapidly when current flows through them and for a short time the resistor gets so hot that the ink vaporizes within the nozzle and flies through the air landing in front of the head.

The non-contact aspect of the cartridge is an important factor, because it allows the printing gap between the cartridge and the media to vary between .5-1.5$mm$ [35, 37] with an optimal printing distance of 1$mm$ while keeping the printing quality intact. Maintaining the non-contact condition is crucial throughout the printing process, because any contact with media could increase the nozzle failure chances dramatically, either through abrasion of the orifice plate or clogging the nozzle. HP recommends that these cartridge be used in either the horizontal or down vertical

firing orientation.

To create characters several nozzles need to be fired at the same time, however this is governed by two conditions to ensure the printing quality. The first condition is not to print more than two droplets at the same instant, and the second condition is to fire from two nozzles that have very low proximity. For example, firing from nozzle #3 and #4 is not recommended because this might cause droplet degradation due to air pressure, while it is acceptable to fire from nozzles #3 and #5 simultaneously, and recommended to fire from #1 and #7. According to the data sheet [35] the voltage required to fire the nozzles is 23.0 *vdc* and the associated pulse width is $4.5\mu s$, with a dead time of $.5\mu s$ and a minimum spacing between firing the nozzles of $800\mu s$. Based on these characteristics all the nozzles can be fired in pairs in $29.5\mu s$. Fig. 3.3 shows the limitations of nozzle firing. The time required to print a row of dots is very important because even-though all 12 nozzles can be printed within $30\mu s$, the wait time to fire them again is $800\mu s$ as shown in Fig. 3.3. If the firing occurs before meeting this condition, the lateral resolution of the printing will decrease if lateral speed is higher than 330 $^{mm}/_{s}$. At this speed the centers of the first and sixth dots will be offseted by $.009735mm$. Fig. 3.4 shows the effect of the lateral velocity on the quality of the printer.

### 3.2.2 Serial Ink-jet Printer

The Parallax Serial Ink-jet printer is a ready-to-run printer shown in Fig. 3.5, where its operation requires only two steps: connecting it to a $5V$ power supply and to the HP 51604 cartridge, and sending the desired text string. This printer is a pre-programmed SX-28AC/SS based micro-controller which interfaces through either a $5V$ logic level UART or USB (virtual COM port) $9600bps$, 8-bit, no parity, true,

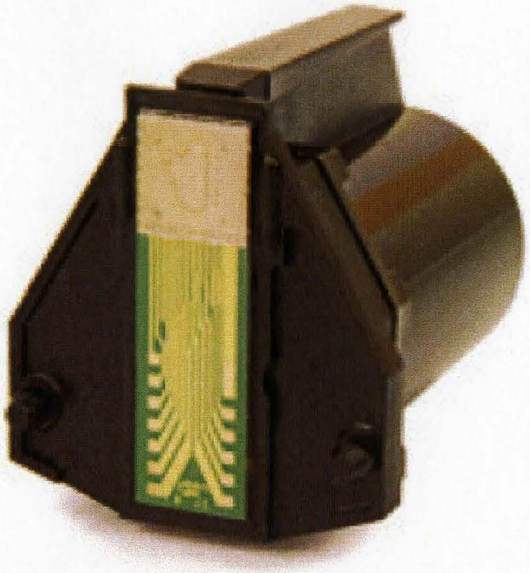

(a) HP 56104

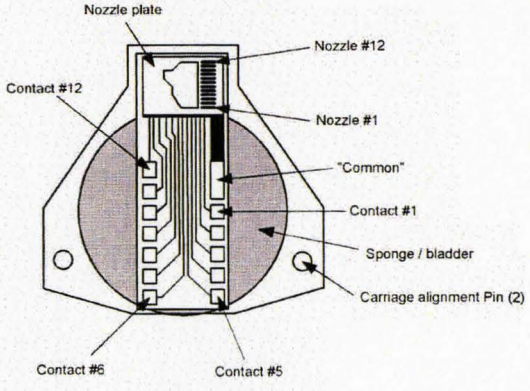


(b) Bussiness End

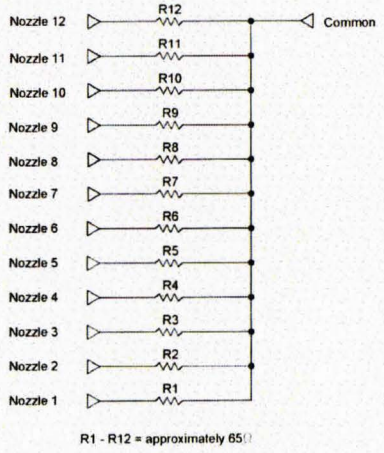


(c) Nozzle Resistors

Figure 3.2: HP 56104 Ink-jet Cartridge [37]

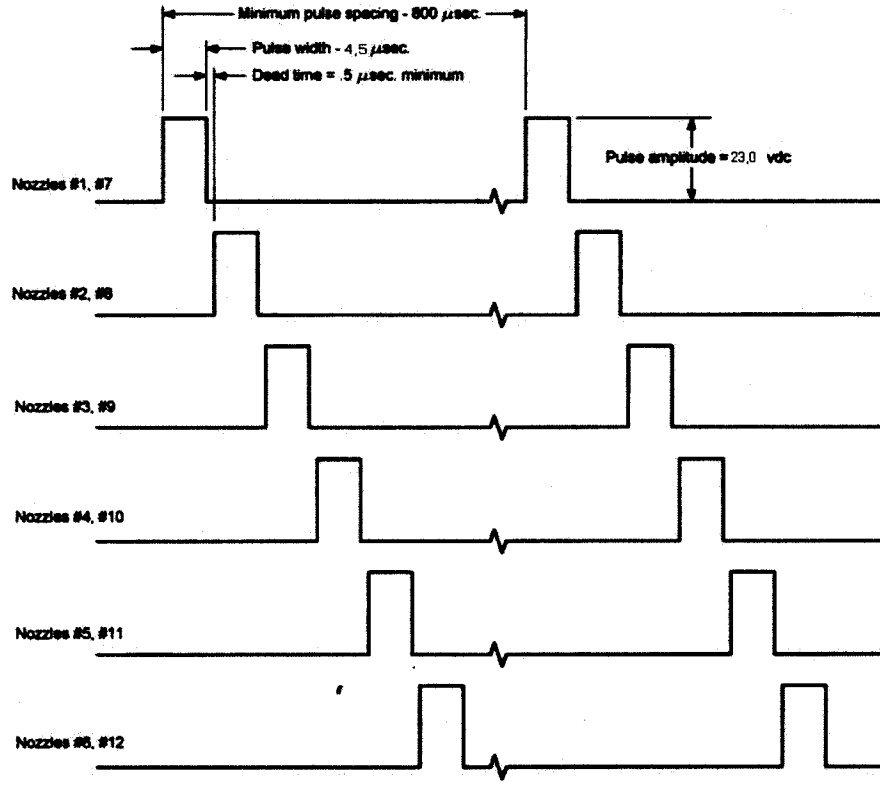


Figure 3.3: HP 56104 Double Nozzle Firing Frequency Limitations [37]

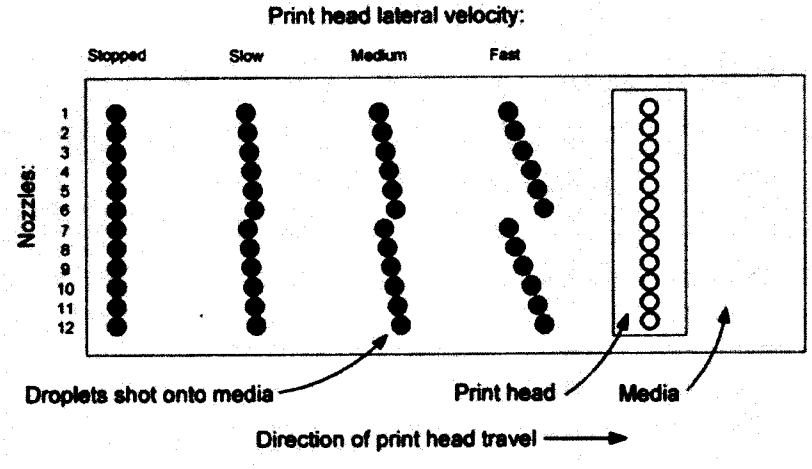


Figure 3.4: Effect of Cartridge Speed on Vertical Line Printing Quality [37]

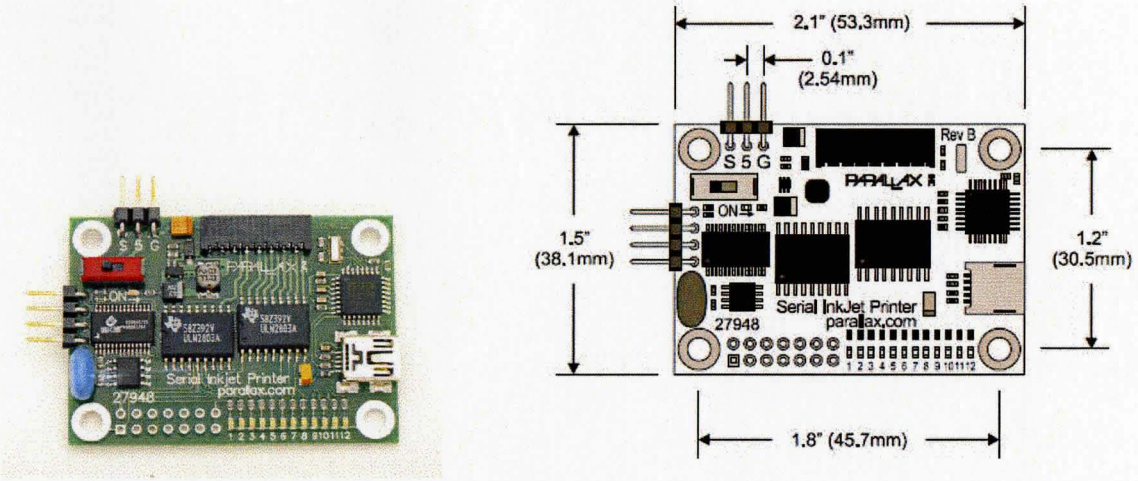


Figure 3.5: Parallax Serial Ink-jet Printer [38]

open baud rate serial connection. A functional diagram of the board is shown in Fig. 3.6.

The main features of the printer are:

- Open-source firmware that can be customized for varying 96 DPI printing products.
- Step-up 6 to 24$VDC$ power supply to provide power for the ink-jet nozzle firing
- Capability to print a 64 character string which at 96 DPI represents 8 inches of print travel
- Font storage up to 64 $Kbyte$ Electrically Erasable Programmable Read-Only Memory EEPROM

### 3.2.3 Firmware

The pre-programmed firmware written in high-level SX/B language can be modified in an external editor and then uploaded to the 20 megahertz SX-28AC/SS micro-

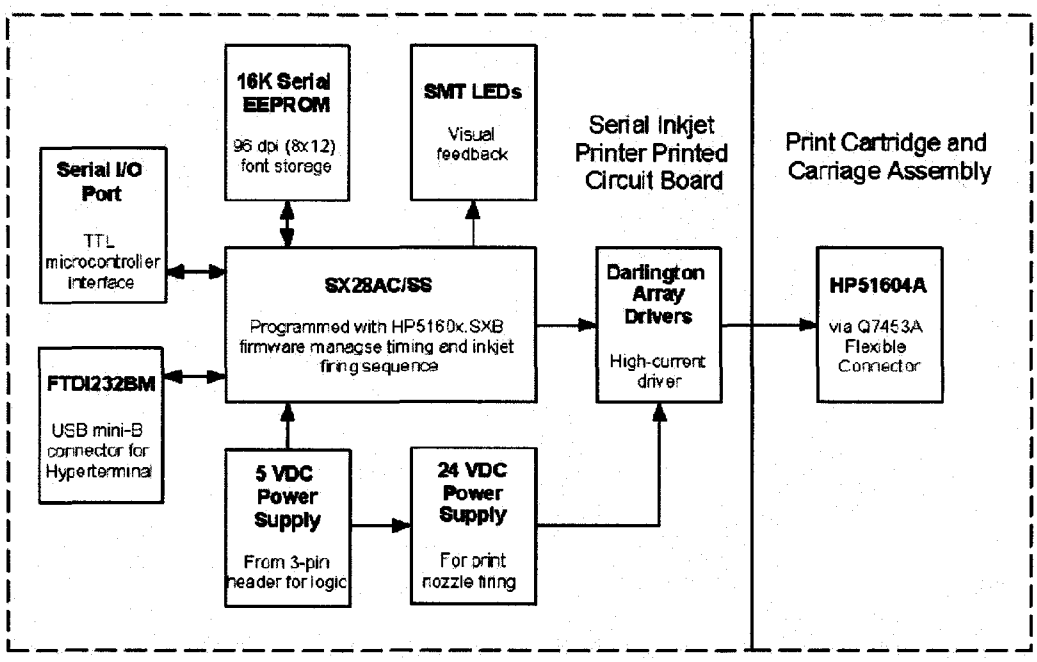


Figure 3.6: Parallax Functional Block Diagram [38]

controller using the Parallax SXKey or SX Blitz through the 4-pin header. The Firmware is used to allow the user to print a string of characters using the embedded font set, and download a new character definition to the on-board EEPROM. It also allows the printer to communicate with the PC through a serial connection, where specific characters are entered to initiate subroutines that perform tasks such as : programming a character font, loading text string, initializing the visual display mode, and a newly added option to print in CMM mode.

To perform the last task, the source code was modified to print a row of data in CMM mode when it receives a TTL logic level signal sent from the CMM motion controller. Algorithm 3.2.3 describes the printing function. This modification in the source code provides independence from CMM acceleration and deceleration, or need to adhere to a constant printing speed, whereby the TTL signal is received when the CMM moves a cumulative distance of $\frac{1}{96}$ inches (0.264 mm), thus ensuring the

**Algorithm 1** Printing in CMM mode

```
Retrieve a character
    Create pointer to character map in EEPROM
    Copy character map  from EEPROM to RAM
    Loop through 12 columns for the character
        Loop through nozzle sequence to print column
        Wait for TTL signal
Loop till the text string ends
```

consistency of the resolution.

### 3.2.4 CMM Mount

The CMM mount uses a Renishaw PAA1 autojoint adapter for repeatable interchange with the touch trigger probe, plus a rapid prototyped plastic adapter that mates with the ink-jet head carrier. Mating the adapter with the printing head had to take into consideration alignments errors resulting from a non-parallelism state between the nozzles and the $x - axis$. After resolving any CMM probe head squaring problems, this issue was addressed by adjusting the probe head mount back using a horizontal level to the horizontal and verifying the answer using calipers by measuring the distance between the standoff and the adapter as shown in Fig. 3.7.

## 3.3 Coordinate Measuring Machines

Coordinate Measuring Machines (CMM) are used to move the printer mount because of their accuracy and their ability to travel in the three major axis in addition to two extra DOF given by a Renishaw PH10 motorized probe head attached to its vertical column.

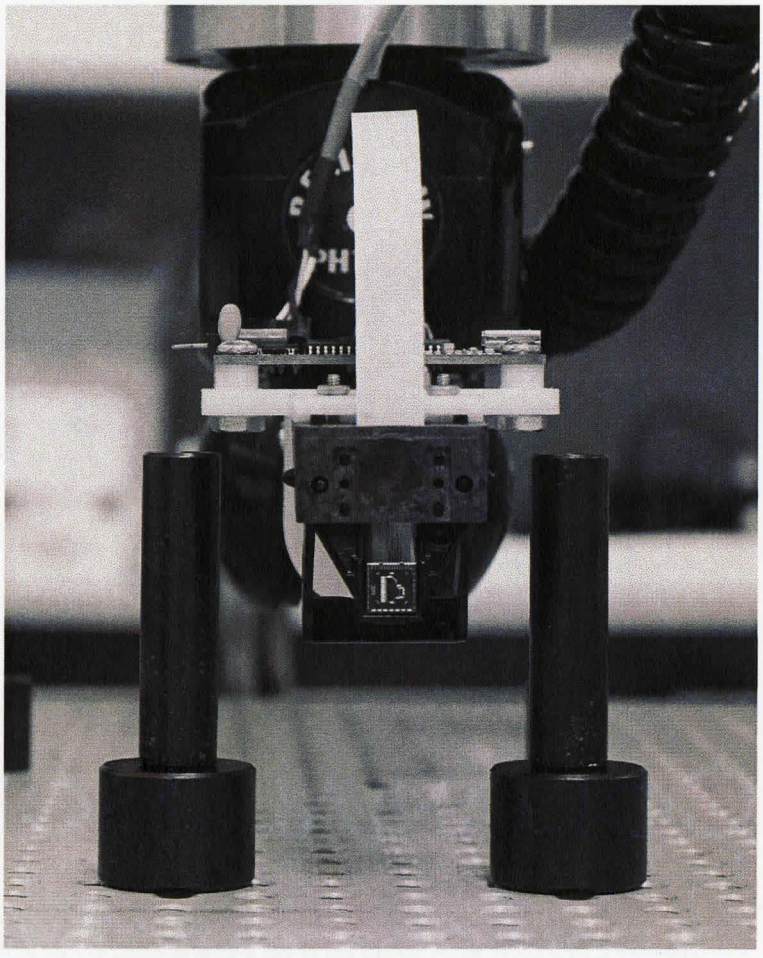

Figure 3.7: Ink-jet Head Mount CMM Adjustment

### 3.3.1 CMM Introduction

Coordinate measuring machines (CMMs) are highly accurate metrology devices normally used for precise, computer aided measurement of three dimensional parts. Quality control purposes and reverse engineering are common uses for CMMs. In the field of quality control, CMMs allow for very high accuracy verification of finished parts, and software is available to automate the comparison of a series of finished parts to the source CAD drawing file [39]. This allows for sample products to be pulled from a production line and tested for product accuracy in terms of shape and dimensions. Another significant area of use of CMMs is in reverse engineering, the process of creating a digital geometric model from an actual part, for which no digital drawing files are available. In this case, rather than simply verifying key dimensions, the entire model is essentially plotted into a grid of data points, called a point cloud, from which software can be used to create a CAD model. The most common type of CMM is the bridge type, which, as its name suggests, consists of a bridge supported by columns on either side. The table is usually made of granite for its dimensional stability, stiffness, and low thermal expansion coefficient. On either side of the bridge are two columns which move front and back, along the $x - axis$. The bridge is a horizontal beam mounted on top of the columns. A vertical column is mounted to the beam in such a way that the entire column can travel from side to side, along the $y - axis$. The probe/digital digitizer/ink-jet head is mounted at the bottom end of this column, and the entire column can move up and down, along the $z - axis$. These are the three degrees of freedom common to a bridge type CMM. Additional degrees of freedom are often gained by wrists used to mount end effectors to the $z - axis$ column. A typical bridge type CMM is the DEA IOTA P CMM shown in Fig. 3.8.

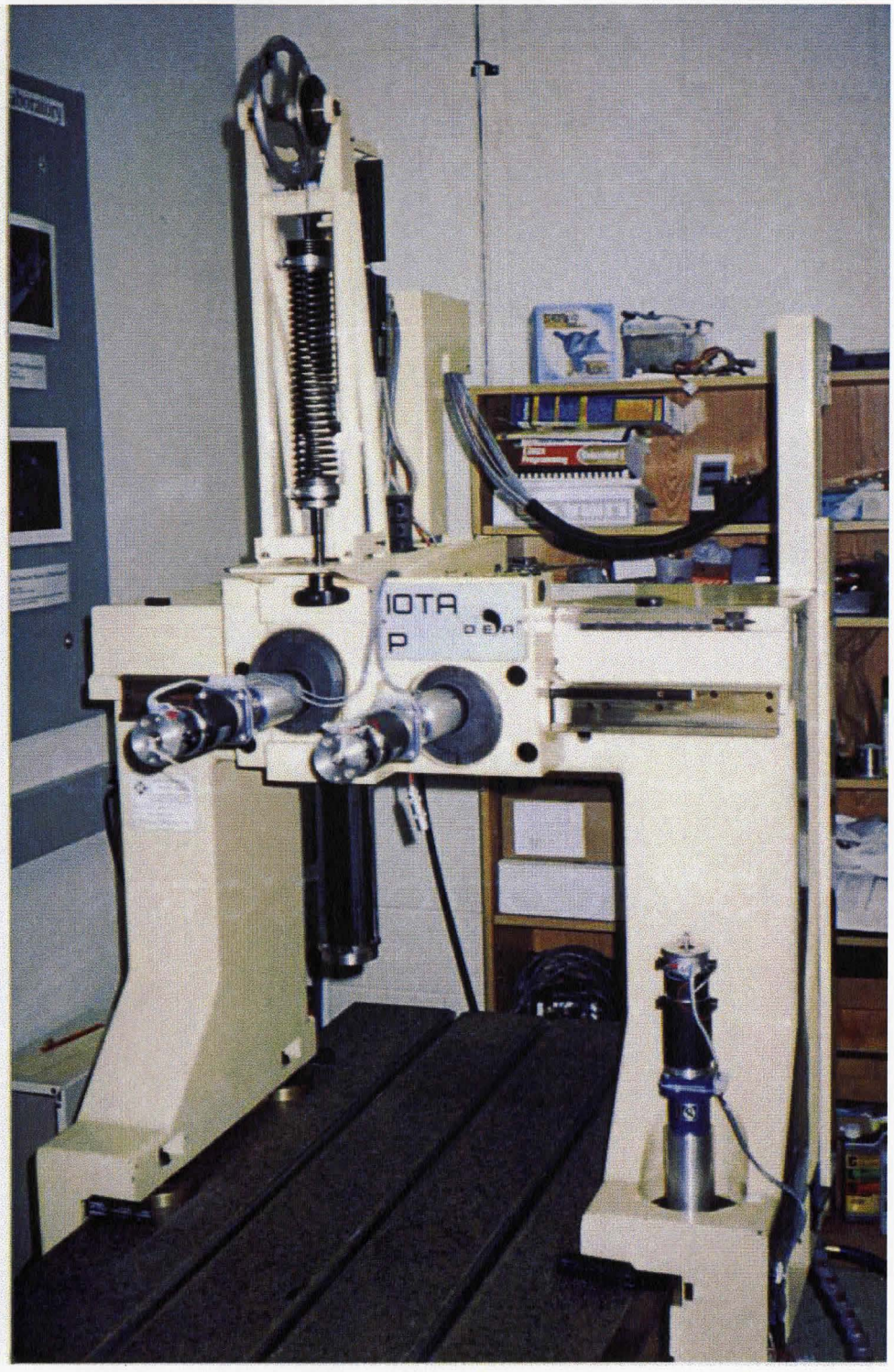


Figure 3.8: DEA IOTA P CMM (McMaster University)

### 3.3.2 Motorized Probe Head and Touch Trigger Probe

The Renishaw PH10M is a motorized probe head shown in Fig. 3.9 is a very reliable head because of it repeatability, where it can achieve 0.5 $\mu m$ repeatability at 62 $mm$ radius, providing accurate positioning even when using long extensions, and because of it accuracy, where it uses six point kinematic location for each of its 720 positions making its locking mechanism extremely repeatable [40].

Ensuring that the probe head is completely square with CMM coordinate system the head shaft had to be adjusted. The PH10M head was rotated to angles $(A = 90, B = -90)$ and then $x - coordinate$ of the standoff was measured, and the same measurements were recorded for angles $(A = 90, B = 90)$. Using these angle combinations the probe head measurement were taken from different sides of the standoff along the $y - axis$, as shown in Fig. 3.10, which accentuated the $x - axis$ error. By adjusting The PH10M head shaft, squaring the head was feasible when the $x - axis$ error was $\leq 10\mu m$ over a distance $\approx 220$ mm .

### 3.3.3 Integrating the Ink-jet head with the CMM

Using a custom program written in MATLAB®, the CMM is controlled using the same CAD computer, with Ethernet connections to the CMM motion controller, and a USB connection to the ink-jet micro-controller. Each dot pattern is printed by executing the following steps:

- The CAD created ink-jet dot pattern for the current ink-jet path is downloaded into the micro-controller font memory.
- The PH10 probe head is rotated to the appropriate angles, and the CMM carriage is translated to the initial position.

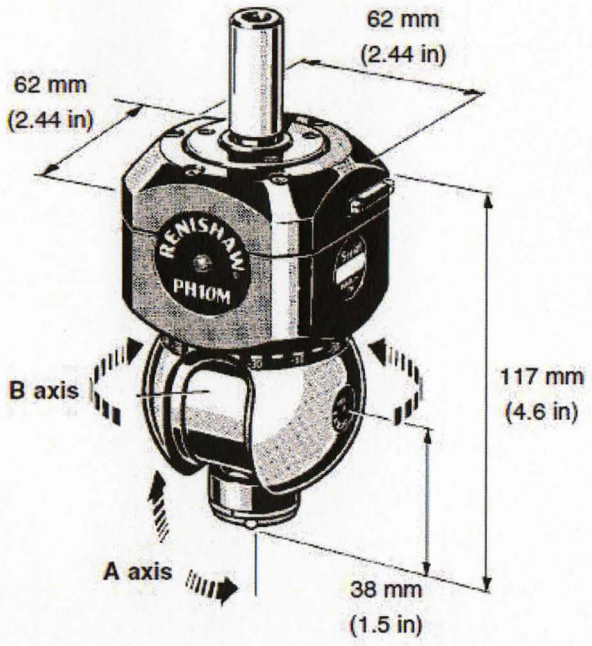


Figure 3.9: Renishaw PH10M Probe Head [40]

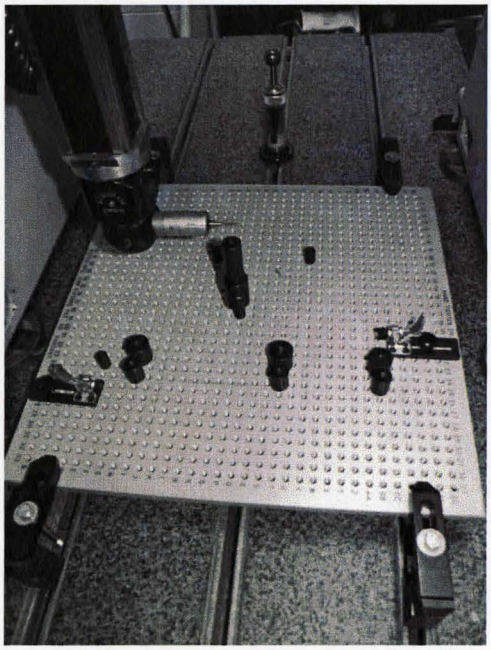

(a) A=90 Degrees, B=90 Degrees

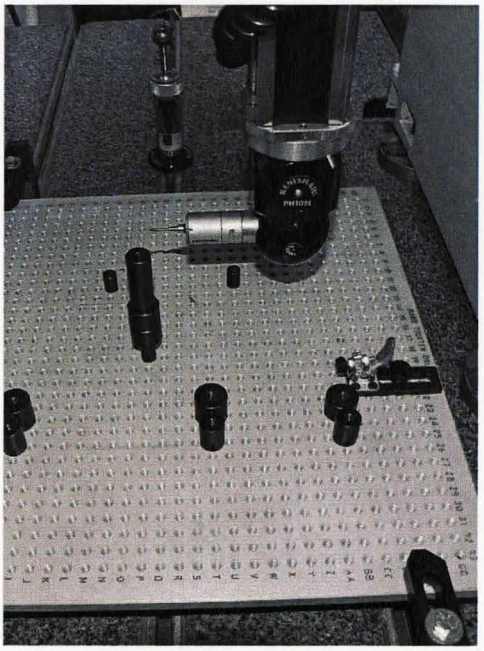

(b) A=90 Degrees, B=-90 Degrees

Figure 3.10: Renishaw PH10M Probe Head Squaring Procedure

- A custom CMM motion command is executed to begin linear motion for the length of the current ink-jet path. Each time a distance of $1/96$ inches has been traveled, the CMM pulses the micro-controller to print the next dot row. For experimental work, a printing speed of 1 $^{mm}/_{s}$ was used.

## 3.4 Ink-Aid Coating

The HP 51604 ink properties doesn't allow it to stick on non-porous surfaces such as glass, aluminum, PVC, or ABS plastic. In order to print on such materials, their surfaces were coated with the water-soluble inkAID [41]. This material eases the procedure of depositing ink on the types of surfaces mentioned without which ink would be easily wiped. The incurred thickness from coating is negligible when compared to the error margin of the ink-jet head ($\pm.5mm$).

### 3.4.1 Transparent Coating

Transparent coating can be applied on materials like ABS plastic and aluminum to prepare them for printing. Printing on aluminum can be used for stress and strain analysis for stamped aluminum sheets or deformed edges [42]. The ability to visualize the individual point would help provide more data about this machining process in a way straight grid lines won't. The individual point would provide more data about rippling and springing during the stamping process. ABS plastic can be coated and then have an image or a grid printed on it, thus providing a new approach to applying images on rapid prototyped solids. The material used is Clear Gloss Precoat Type II which is water soluble and does not need any adhesive when applied to a non-absorbent surface. It is recommended to be applied in two coats, the second applied perpendicularly to the first when it is completely dry [41].

### 3.4.2 Nontransparent Coating

Another non-porous material on which accurate printing is a challenge is glass. The need to print on glass for measurement purposes has been an issue the auto glass industry has been trying to solve for quite a number of years. The material used is White Matte Precoat which is also water soluble.

# Chapter 4

# Image Processing and CAD Implementation

## 4.1 System Workflow

The workflow describing how the images/grids/text are processed and printed is shown in Fig. 4.1. The printing/visualization process starts with an image in any format, and a CAD part. The image is applied to the part in the CAD software, and then the coordinates of this association are retrieved from the CAD system and processed in a Matlab program that converts this association into a point cloud format. The point cloud format can be then used for either visualization or for physical recreation of the image on the part by printing on a blank rapid prototyped model. The point cloud file is processed in Matlab to determine the orientation and location of the probe head. Another Matlab Program uploads the image RGB data onto the ink-jet micro-controller, that awaits a motion triggered TTL signal to dispense ink on the RP model.

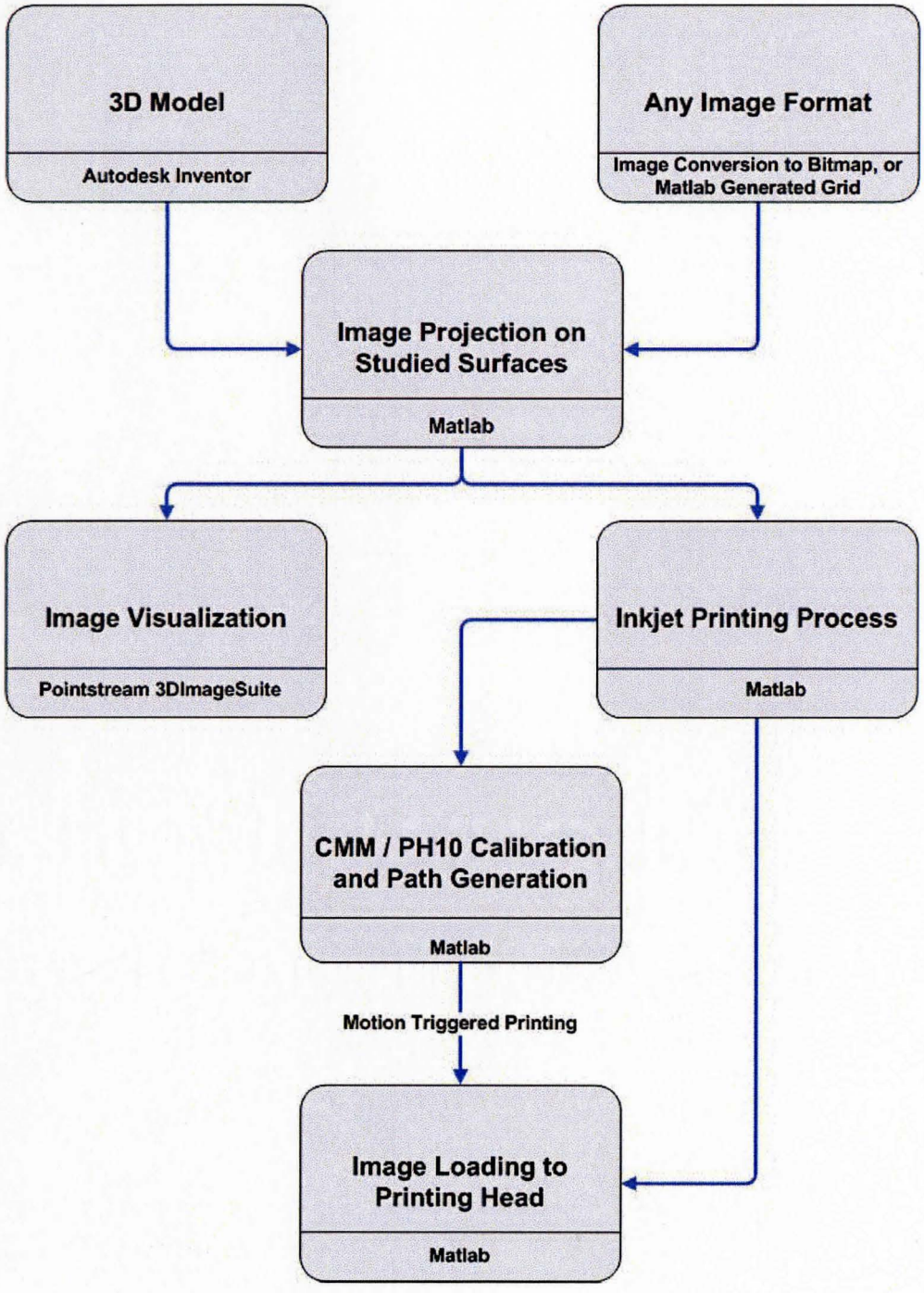


Figure 4.1: Oriented 3D Printing System Workflow

## 4.2 Image Processing

The CAD software used for this study is Autodesk Inventor ®, a 3D parametric solid modeling package produced by Autodesk [34], its image processing method: the decal feature.

### 4.2.1 Autodesk Inventor Processing Of Images

Autodesk Inventor ® uses the operating system DPI settings to scale the input image appropriately and recognize its physical dimensions. Therefore the ink-jet printer, that has an equal printing resolution, will be able to replicate the decal generated in the CAD software in wrapping situations where the pixels are equidistant at 96 DPI.

#### Decal

The Inventor decal feature applies an image such as a logo, label, etc. to a part face. The applicability of decal feature is limited to the formats that Inventor® accepts are: bitmap files, MS word documents, or MS excel spreadsheets, and the geometry of surface that it is required to be applied upon. The decal feature applies images using one of two methods : projection and wrapping as shown in Fig. 4.2. Projecting an image is applicable to all faces regardless of their complexity, but this versatility comes at a price of deforming the image, while wrapping keeps the resolution and physical dimensions of the original image intact, but is limited to planar and cylindrical surfaces.

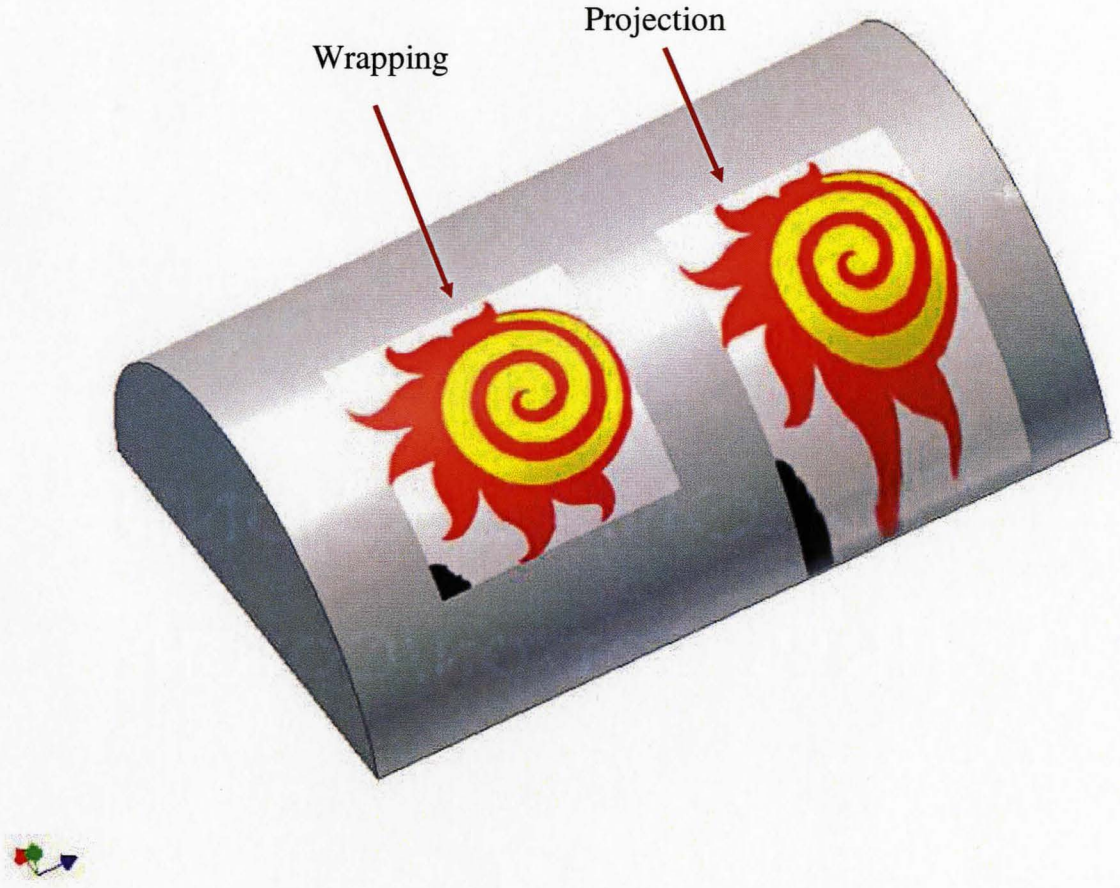


Figure 4.2: Inventor CAD Model Showing Decal Wrapping and Decal Projection

#### Rotation

Inventor uses a mathematical representations called transient geometry to represent the boundaries of the image. The two sides of the control box are always parallel to the Cartesian plane they are included in regardless of its direction, thus when an image is rotated around one of its vertices, the control box changes its dimensions to include the rotated image while keeping its sides parallel to the Cartesian coordinate system of its plane.

### 4.2.2 Grid Generation

Printing grids as points rather than lines can be a matter of extreme importance to deformation measurements in the auto glass manufacturing and sheet metal stamping processes. Measuring individual points using computer vision can generate information to help study the deformation of glass and help generate gradient information for a stamped sheet metal stress and strain analysis. Generating such a grid with resolution of $\frac{1}{96}$ inches, and printing it with the probe head allowable angular increments of 7.5°, would provide such needed a tool for this task. Considering the limitation of the inkjet head to printing in one color offers the flexibility of building the grid as a matrix whose dimensions are to be determined depending on the type of the application. Sample grids generated by matrix patterns 1 and 2 are shown in Fig. 4.4(a) and Fig. 4.4(b).

**Algorithm 2** Grid Generation

```
X_grid;
Y_grid;
Gsize;
size_X=X_grid*Gsize;
size_Y=Y_gird*Gsize;
Grid_Image=zeros(size_X,size_Y);
for i=1:size_X
    for j=1:size_Y
        if mod(i,Gsize)==0
            Grid_Image(i,j)=1;
            elseif mod(j,Gsize)== 0
            Grid_Image(i,j)=1;
        end
    end
end
[m,n]=size(Grid_Image);
Final_Grid_Image=(Grid_Image(Grid_size:m,Grid_size:n));
Final_Grid_Image(1,:)=1;
Final_Grid_Image(:,1)=1;
```

To generate these matrix patterns algorithm 4.2.2 was used. The X_grid and Y_grid variables define the number of grids needed to be generated in the X and Y directions respectively, and the Gsize variable is the variable responsible for the resolution of the grid. The examples shown in Fig. 4.4 are generated with Gsize 2 and 12 respectively.

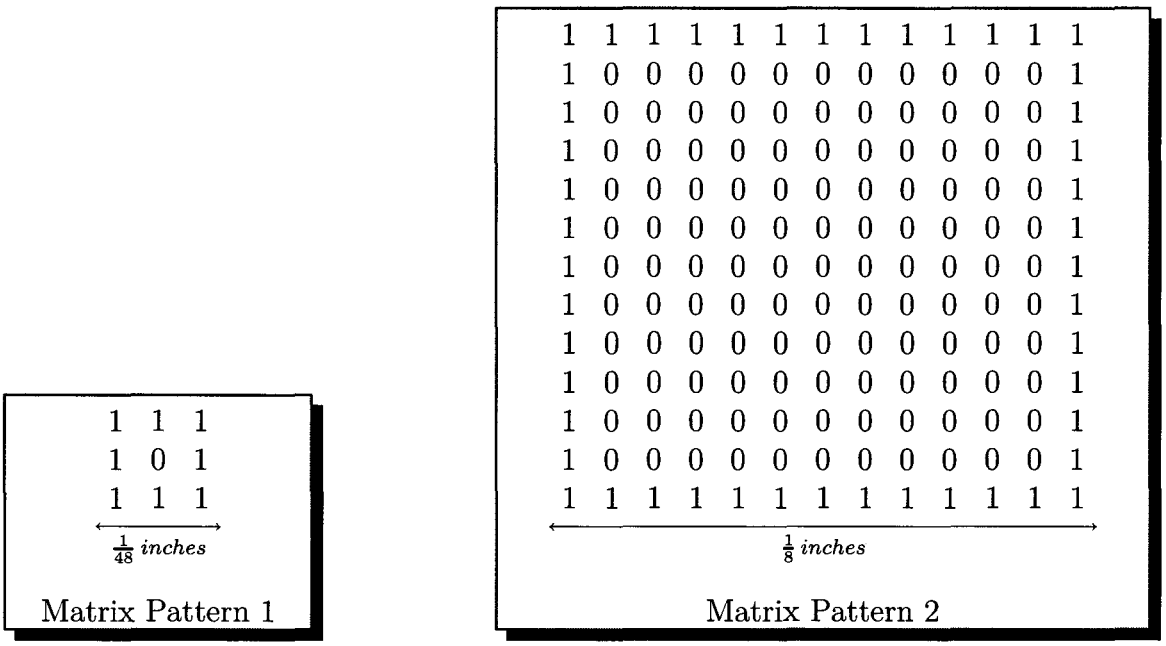


Figure 4.3: Matrix Patterns for Grid Generation

Since Matlab produces images with DPI properties that are equal to those of the system, each member of this matrix will be spaced at a distance of $\frac{1}{96}$ inches when shown as an image, thus complementing the CMM distance pre-determined triggers to print at a resolution of 96 DPI.

### 4.2.3 Binary Conversion

Converting RGB or grayscale images into binary ones is a necessary stage because of the inkjet limitation to printing in one color. Pixels in binary images are to have only one of two values 0 (off switch or black) or 1 (on switch or white), thus rendering a binary image into a logical array of zeros or ones. Converting to a binary image is done using a Matlab® function called `im2bw` which employs Otsu thresholding algorithm to perform this task [43]. Images with large and uniform clusters of pixels seem to work properly with this method as shown in Fig. 4.5.

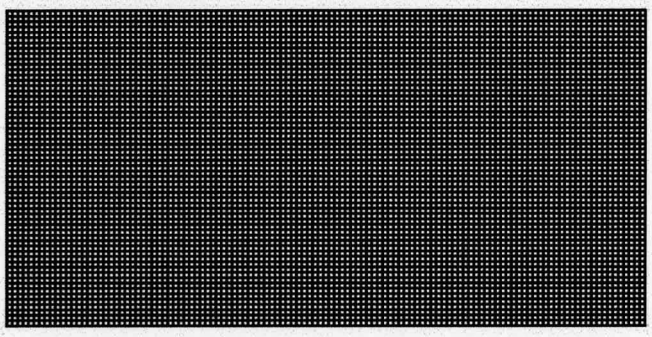

(a) Size 2

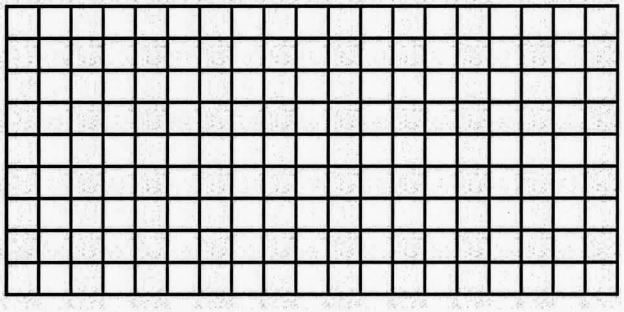

(b) Size 12

Figure 4.4: Actual Size Grid Size $\frac{1}{48}$ Inches Vs. Size $\frac{1}{8}$ Inches

(a) Binary Image

(b) RGB Image

Figure 4.5: Images Showing Large Uniform Clusters of Pixels

### 4.2.4 Images And Text Rotation

Rotation of images is of particular importance because it allows the user to have the flexibility of the CAD software. Matlab has two functions that perform the same task `imrotate` and `imtransform` using different pivoting points. `imrotate` rotates an image counterclockwise around its center point, while `imtransform` applies a 2D spatial transformation around the $z-axis$ passing through any point. Both functions were tested and there was no difference in the pixels generated after the rotation - subtraction of the matrices generated yielded a zero answer, thus the pivoting point became a non issue when choosing the image rotating function. `imrotate` was chosen to perform this task, because of the simplicity of its use. The coordinates of the control box produced as in Fig. 4.6 are taken as the image two defining range box points from the CAD software and imported to Matlab where the dimensions of the control box are calculated while keeping the coordinates of the rotated image with respect to its local coordinate system.

#### Results For Text And Images

Text images and regular images contain large clusters of pixels. As shown in Fig. 4.6 the rotated images and text demonstrate that rotation has minimal effect on the

overall shape of these clusters. This software rotation slightly impacts the quality of the pixels; however, it can be of a great benefit for images rotated by an angle that is not a multiple of 7.5°. These minimal effects can be eliminated if the rotation is performed by the hardware, where the probe head can be rotated and calibrated to print a straight and un-manipulated image at the desired angle. In the case of software rotation, the control box containing the rotated image becomes the "straight" image that ought to be printed at probe angle 0°. The rotation function optimization is not an important issue, thus trying to find a combination of hardware and software angles is not considered. The image seen in Fig. 4.6 is a rotated image with its control box, it contains pixels that are not supposed to be printed. To remove these pixels a logical matrix of ones with the same dimensions of the original unrotated image is created, rotated, and then its values are inverted to zeros. This matrix is added to the control box image and the results is then inverted to end up with a rotated image that only contains the big clusters of pixels as shown in Fig. 4.7.

### Problems With Grid

Grid images are a set of one pixel aligned in rows and in columns that cannot be considered as big clusters of pixels and cannot be rotated without major distortion. Since these lines should be printed as a collinear set of points the major distortions shown in Fig. 4.8 are not acceptable. The only rotation applicable to grids without compromising the quality of the dotted lines is the hardware rotation.

(a) Unrotated Image

(b) 15 degrees CounterClockWise Rotation

McMaster University

DMSL

(c) Unrotated Text


(d) 15 degrees CounterClockWise Rotation

Figure 4.6: Software Rotation for Images and Text

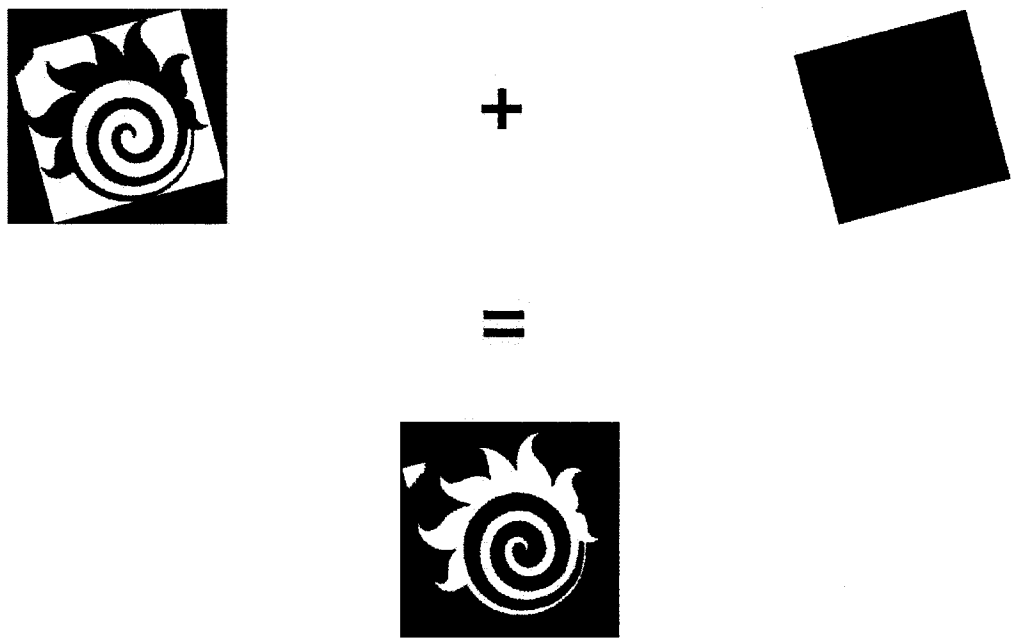

Figure 4.7: Image Processing "Cleaning" for Printing

(a) 0 degrees (b) 15 degrees

Figure 4.8: Grid Rotation Problems

### 4.2.5 Preparing Image For Printing

Processing images as described in the preceding steps yields a set of binary matrices that can be sent through the serial port to the ink-jet micro-controller. Since only six nozzles can be operated simultaneously, six rows of the matrix can be chosen

to be sent to the ink-jet printer. Due to the limitation of probe head angle A of the probe to a range of $(0°-105°)$, rotation of probe head angle B by $(\pm 180°)$ might be required, thus 2 scenarios for printing the same 6 rows exist where the angle B can be either( 0°or $\pm 180°$). The approach to sending images to the micro-controller is done by reprogramming the existing letters. As mentioned in the previous chapter each letter is a set represented by an array of $(12\times 12)$ bits. These bits are divided into 2 sets of $(6\times 12)$ that accept the decimal equivalent for each column. In the example discussed below, the first $(6\times 12)$ matrix is to be printed at angle $B = 0°$, therefore the array is multiplied by the binary-to-decimal conversion array $bD_1$ which converts $(6\times 12)$ array of interest ($UpVal$ for example) into a decimal value accepted by the micro-controller. The micro-controller needs the second $(6\times 12)$ array to complete reprogramming the values of the letter of interest and this can be done by sending an array $LowVal$ of 12 zeros. If printing is required at angle B $\pm 180°$ the corresponding $(6\times 12)$ array is multiplied by the binary-to-decimal conversion array $bD_2$.

**Example 4.1**

$$bD_1=\begin{bmatrix} 2^5 & 2^4 & 2^3 & 2^2 & 2^1 & 2^0 \end{bmatrix}, bD_2=\begin{bmatrix} 2^0 & 2^1 & 2^2 & 2^3 & 2^4 & 2^5 \end{bmatrix}$$

$$UpVal = \begin{bmatrix} 0 & 0 & 0 & 0 & 0 & 1 & 0 & 0 & 0 & 0 & 0 & 0 \\ 0 & 0 & 0 & 0 & 1 & 0 & 1 & 0 & 0 & 0 & 0 & 0 \\ 0 & 0 & 0 & 1 & 1 & 0 & 1 & 1 & 0 & 0 & 0 & 0 \\ 0 & 0 & 0 & 1 & 1 & 1 & 1 & 1 & 1 & 0 & 0 & 0 \\ 0 & 0 & 1 & 1 & 1 & 1 & 1 & 1 & 1 & 1 & 0 & 0 \\ 1 & 1 & 1 & 1 & 1 & 1 & 1 & 1 & 1 & 1 & 1 & 1 \end{bmatrix}$$

$$bD_1 \times UpVal = \begin{bmatrix} 1 & 1 & 3 & 15 & 31 & 39 & 31 & 15 & 7 & 3 & 1 & 1 \end{bmatrix}$$

$$bD_2 \times UpVal = \begin{bmatrix} 32 & 32 & 48 & 60 & 62 & 57 & 62 & 60 & 56 & 48 & 32 & 32 \end{bmatrix}$$

$$LowVal = \begin{bmatrix} 0 & 0 & 0 & 0 & 0 & 0 & 0 & 0 & 0 & 0 & 0 & 0 \end{bmatrix}$$

The values are sent to the micro-controller where one is taken from $bD_1 \times UpVal$ or $bD_2 \times UpVal$ depending on the angle of printing and the next is taken from $LowVal$. The sending process is repeated until all the values are sent. Listening to the port to check for errors is done after data transmission to verify that no data corruption has occurred.

### 4.2.6 Point Cloud Visualization and Generation

Image point cloud generation is the process of adding coordinates to a binary image to match the wrapping coordinate conditions of the CAD software. Such process allows the image to be viewed in 3D as point cloud that resembles the output of the

decal feature. The purpose of the visualization is to add more details to parametric point clouds as an extra step forward in visualizing surfaces as a set of true points with coordinates and colors. In order to achieve this it is critical to to understand the how the CAD software parametrizes the surface this section discusses. Autodesk Inventor® surface description employs parametric representation where each surface point is expressed as a function of the parameters $(u, v)$.

$$P(u,v) = [x_{(1^{st}Dimension)}(u,v), y_{(2^{nd}Dimension)}(u,v), z_{(3^{rd}Dimension)}(u,v)] \tag{4.1}$$

where

$$u_{\min} \leqq u \leqq u_{\max}$$

$$v_{\min} \leqq v \leqq v_{\max}$$

### Deformation of Projected Image in Decal Feature

To apply images to surfaces the decal feature employs two methods: projection and wrapping as shown in Fig. 4.2. Fig. 4.9 shows how the number pixels in the perspective projection plane changes when applied onto a geometrically different surface, which means that the projection of image is treated as wrapping of a deformed image Fig. 4.10, thus making the point cloud visualization method image dependent. Generating these deformed images is done by splitting the original image into $\frac{1}{96}$ inch sections which are then stretched individually by a scale factor of the arc of length where they are applied. This stretching creates a new image that can be as wrapped one and then converted into a point cloud, using the methods discussed in the following sections.

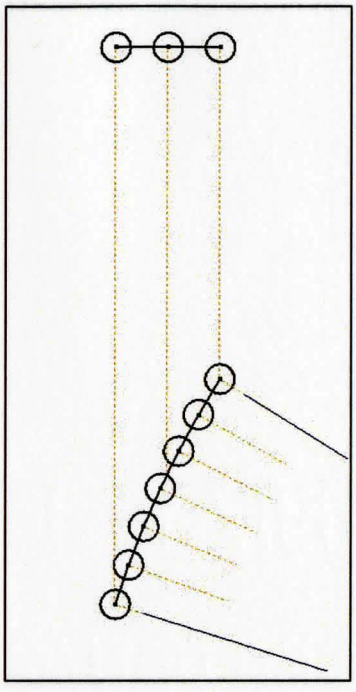

Figure 4.9: Pixel Projection and Deformation on Arcs

### Half Cylinder

The CAD parametrization of a any point on a cylindrical surface of radius $R$ and height $h$ can be expressed in the form of equation 4.2

$$P(u) = \begin{cases} x = R\cos(u) \\ y = R\sin(u) \\ z = Rv \end{cases} \tag{4.2}$$

where

$$u \in [u_{min}, (u_{min} + 2\pi)] \text{ and } v \in [v_{min}, (v_{min} + \tfrac{h}{R})]$$

A point cloud of a 96 *dpi* image wrapped around a cylinder is generated using the parametric Equation 4.2. For successful employment of this equation, its defining parameters $u_{min}$ and $v_{min}$ must be found in order to calculate the starting wrapping

Figure 4.10: Image Deformation Processing Samples

point as generated by the CAD software.

**Wrapping** To calculate wrapping starting points coordinates the CAD software analyzes the location of the image control box on its plane with respect to the center of the cylinder and based on that it determines where the wrapping should start.

The $3^{rd}$ Dimension or $z$ in this study represents the axis of wrapping, and the image control box width $w$ will be the wrapped side. To minimize the computation processes $w$ is located in the $xy$ plane where its Cartesian equation $y = constant$ between $[x_{min}, x_{max}]$.

As can be seen in Figures 4.11, 4.12, and 4.13, there are 3 cases that govern the location of the starting point while wrapping an image around a half cylinder.

- Case (1): Image overlapping over 2 Quadrants

  If $w$ is divided between 2 quadrants, Inventor finds the the location of its end points and projects the one closest to the center of the cylinder $x$ coordinate and then considers that point as the start wrapping point as shown in Fig. 4.11(a) and (b) where the condition for wrapping around half cylinders is:

$$\left|\frac{w}{R}\right| \leq \pi$$

- Case (2): Image overlapping over one Quadrant

  If $w$ end points [$C$ (close to the center) and $F$ (far from the center)] are located entirely in one quadrant, wrapping start point is the one closest to the center of the cylinder, the same as in case (1) as shown in Fig. 4.12(a) and (b). However since wrapping is limited to one quadrant only, the far end from the center cannot be wrapped in the$-y$ direction, therefore the following conditions should be met.

1. $\left|\frac{w}{R}\right| \leq \frac{\pi}{2}$

2. $x_C$ should exist in the following $x$ range:

$$x_C \in [0, \pm R\cos(\frac{w}{R})]$$

- Case (3): $w$ midpoint projection is the center of the circle

  As shown in 4.13(a) $C$ and $F$ are equidistant the center of the circle, thus the closest point formula for projection cannot be applied in this situation. The equation used to determine the location of either end points is

$$\pm R\cos(\frac{\pi}{2} - \frac{w/2}{R}) \tag{4.3}$$

  where

$$\left|\frac{w}{R}\right| \leq \pi$$

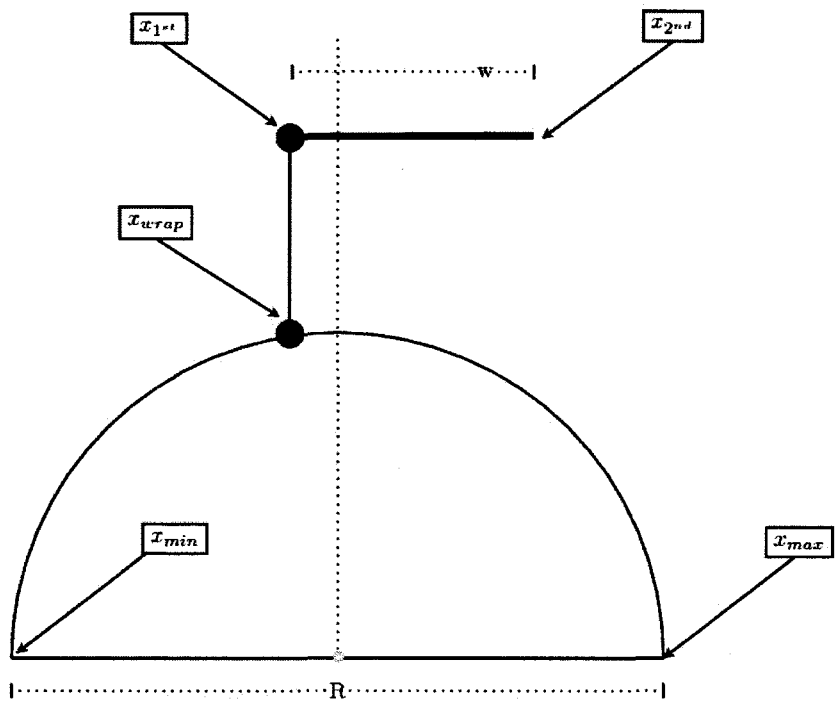


(a) Image in 2 Quadrants

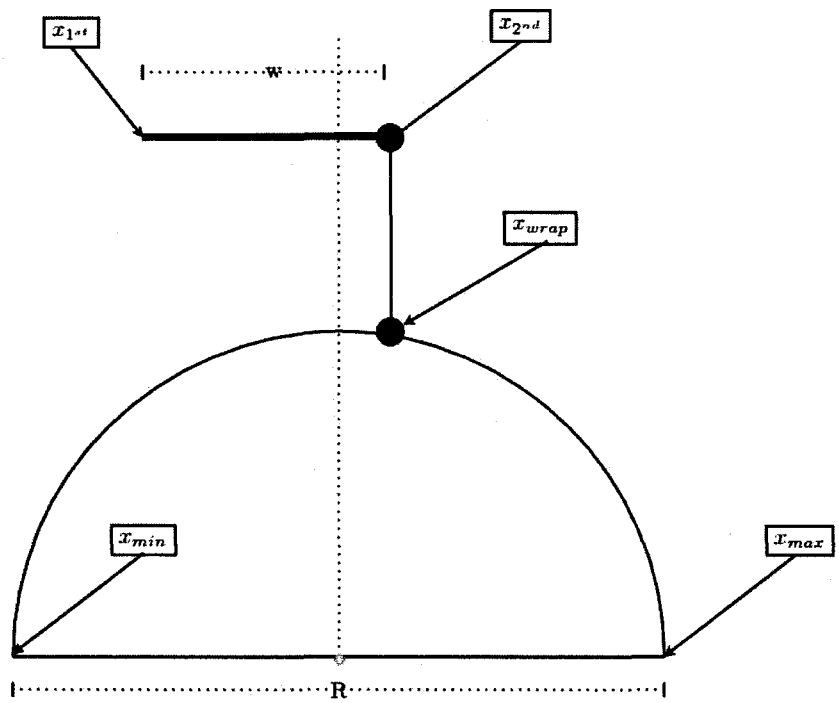


(b) Image in 2 Quadrants

Figure 4.11: Cylindrical Wrapping: Case 1

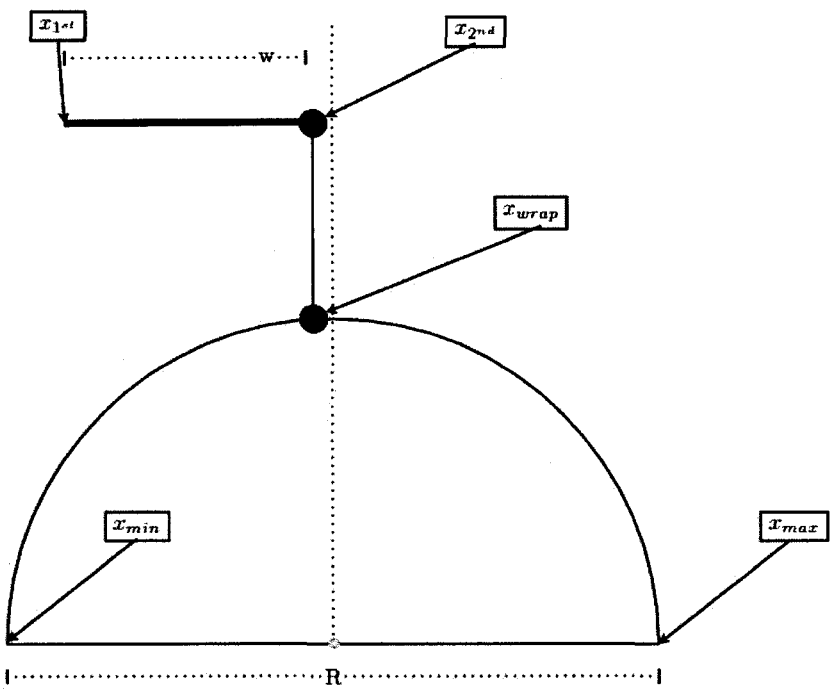


(a) Image in 1 Quadrant

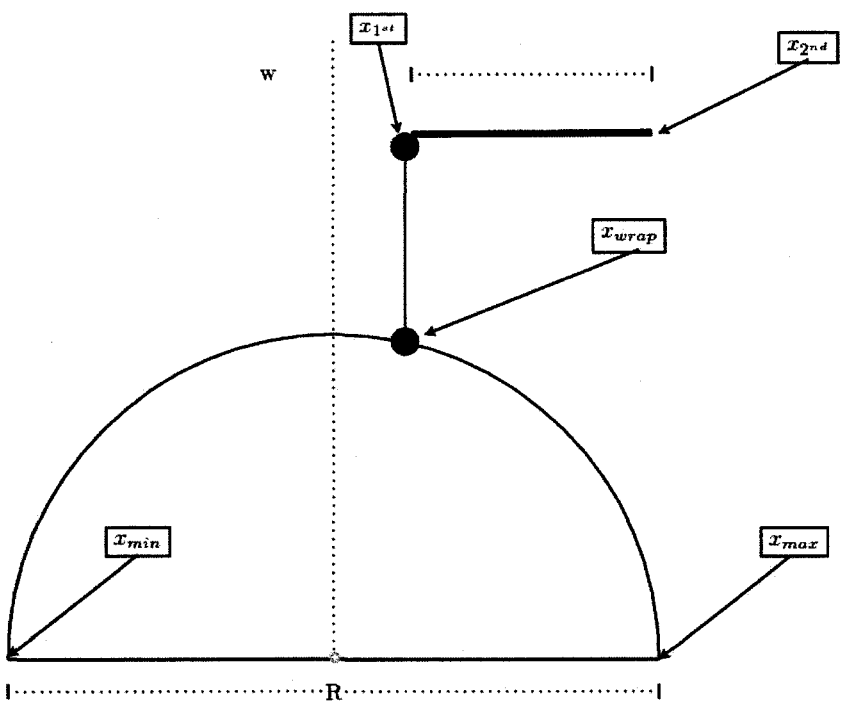


(b) Image in 1 Quadrant (Maximum Allowable for printing purpose)

Figure 4.12: Cylindrical Wrapping: Case 2

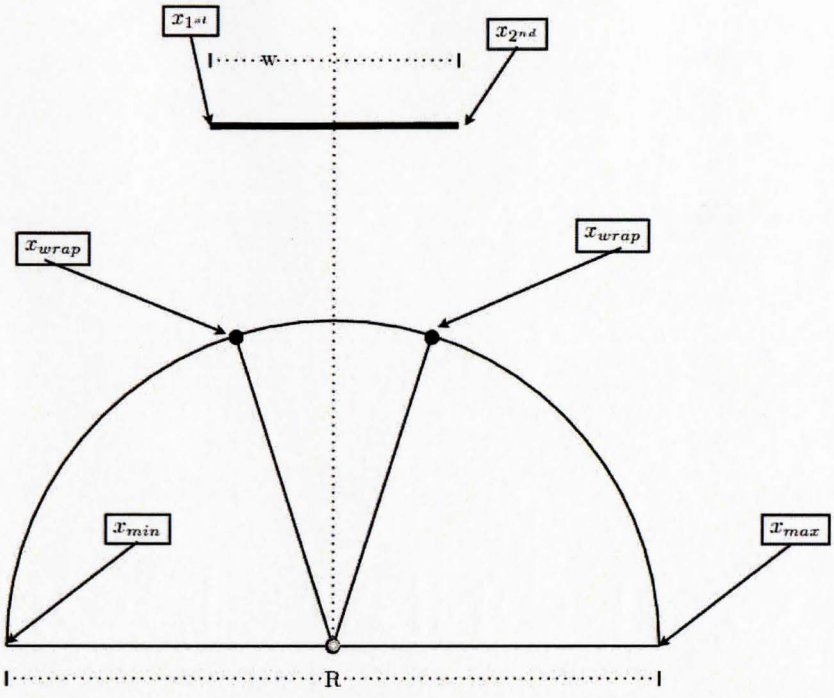


(a) Image Vertices are equidistant from the Center

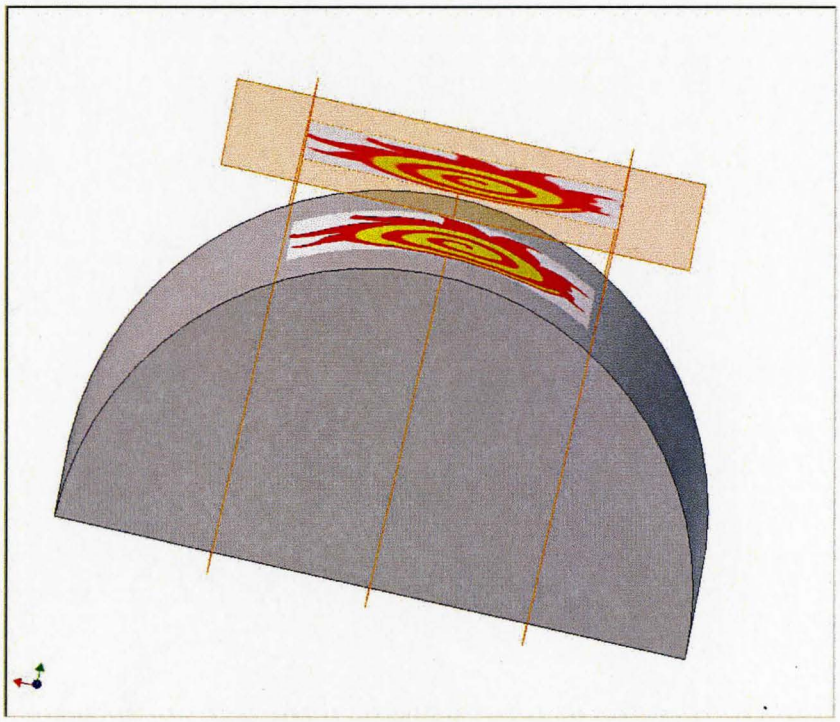

(b) CAD Visualization of Case 3

Figure 4.13: Cylindrical Wrapping: Case 3

After calculating the wrapping start point the generation of the point cloud file can be initiated. The point cloud file is an ASCII text file, and is visualized using Pointstream 3DImageSuite® [44]. A typical file would include the coordinates, RGB, and normal, data for each displayable point . A typical line in this file appears as follows:

$$\underbrace{-17.333414 \quad 11.921250 \quad 7.118998}_{(x,y,z)} \qquad \underbrace{255 \quad 0 \quad 0}_{(r,g,b)} \qquad \underbrace{0 \quad 0.980905 \quad -0.194489}_{(i,j,k)}$$

where

- $(x, y, z)$ represent the coordinates
- $(i, j, k)$ represent the normal $(i, j, k) \in [(0, 0, 0), \pm(1, 1, 1)]$
- $(r, g, b)$ represent the color $(r, g, b) \in [(0, 0, 0), (255, 255, 255)]$

RGB values for the pixels in RGB images require no calculation where their values can be read for each individual pixel.

The normal in this case study is always located in the $xy$ plane, which means that $x$ and $y$ are the only coordinates of interest for calculating the normal for any specific point. The normal is the unit vector of the line connecting the center of the cylinder $O(x_O, y_O, z_O)$ to the pixel $P(x_P, y_P, z_P)$, therefore $(i, j, k)$ of the any specific `ON` pixel point cloud is

$$\frac{\overrightarrow{N}_{OP}}{\left|\overrightarrow{N}_{OP}\right|} \tag{4.4}$$

where

$$\left|\overrightarrow{N}_{OP}\right| = \sqrt{x_P^2 + y_P^2} \text{ and } \overrightarrow{N}_{OP} = [\overrightarrow{x}_P, \overrightarrow{y}_P, \overrightarrow{o}]$$

To populate the cylindrical image point cloud in a counterclockwise fashion around $+z$ axis the wrapping point that has the highest $x$ value needs to be found. To achieve this the following these cases are considered:

- If Case (1) is applicable and the image length is smaller than half circular arc length i.e. wrappable

  then the angle of projection $\theta = \arccos(\frac{x}{R})$

  - If $x_{1^{st}} < x_{2^{nd}}$ then $x_{1^{st}} = x_{wrap} = R\cos(\theta)$
  - If $x_{1^{st}} > x_{2^{nd}}$ then $x_{2^{nd}} = x_{wrap}$ and $x_{1^{st}} = R\cos(\frac{w}{R} - \arccos(\left|\frac{x_{wrap}}{R}\right|))$

- If Case (2) is applicable and the image is wrappable

  then the angle of projection $\theta = \arccos(\frac{x}{R})$

  - if $x_{1^{st}} < x_{2^{nd}}$ then $x_{1^{st}} = x_{wrap}$
  - if $x_{1^{st}} > x_{2^{nd}}$ then $x_{1^{st}} = x_{1^{st}} = R\cos(\frac{\pi}{2} - (\frac{w}{R} + \arccos(\left|\frac{x_{wrap}}{R}\right|)))$

- If Case (3) is applicable and the image is wrappable

  $x_{1^{st}} = x_{wrap} = R \times \cos(\frac{\pi}{2} - \frac{w/2}{R})$

After determining $x_{1^{st}}$and its angle $\theta_{1^{st}} = \arccos(\frac{x_{1st}}{R})$ generating the point cloud can be done by a $for$ loop that checks the values of each row of the final image $I$ where the increments of $row(I)$ translate to $\left(\frac{1/96}{R}\right)$ degrees. $(x, y, z)$ are in inches.

$$x = R\cos\left(row(I)\left(\frac{1}{96R}\right) + \theta_{1^{st}}\right) \text{ where } col \in [0, round(96w)]$$

$$y = R\sin\left(row(I)\left(\frac{1}{96R}\right) + \theta_{1^{st}}\right)$$

$$z = z_0 \pm \left(col(I) \times \frac{1}{96}in\right) \text{ where } col \in [0, round(96l)]$$

**Projection** Image projection is applicable on a half cylinder from perspective planes parallel to the $xy$ plane, if its width $w \leq 2R$. Generating this point cloud can be done by using the deformed image as the one to be wrapped around the half cylinder using the method discussed in in the previous section, where the starting point $x_{1^{st}}$ can be either edge of its control box and its angle $\theta_{1^{st}} = \arccos(\frac{x_{1^{st}}}{R})$.

Fig. 4.14 shows a point cloud of projection and wrapping of the same image around a half cylinder.

### Half Ellipse

The CAD parametrization of a any point on a elliptical cylinder of major axis $a$, minor axis $b$, and height $h$ can be expressed in the form of Equation 4.5

$$\begin{cases} x = a\cos(u) \\ y = b\sin(u) \\ z = av \end{cases} \tag{4.5}$$

where

$$u \in [u_{min}, (u_{min} + 2\pi)] \ , \ v \in [v_{min}, (v_{min} + \tfrac{h}{a})] \ , \text{ and } a \geq b$$

When the Inventor decal feature is used on ellipses the wrap option becomes inapplicable, even though the parametric equations used to represent the ellipse in the software can produce such wrapping as this section will show. Generating an elliptical point cloud of wrapped images is quite a challenge because of the complexity of the geometrical shape of the ellipse. Unlike circular cylinders, performing this task for ellipses had to overcome two main obstacles:

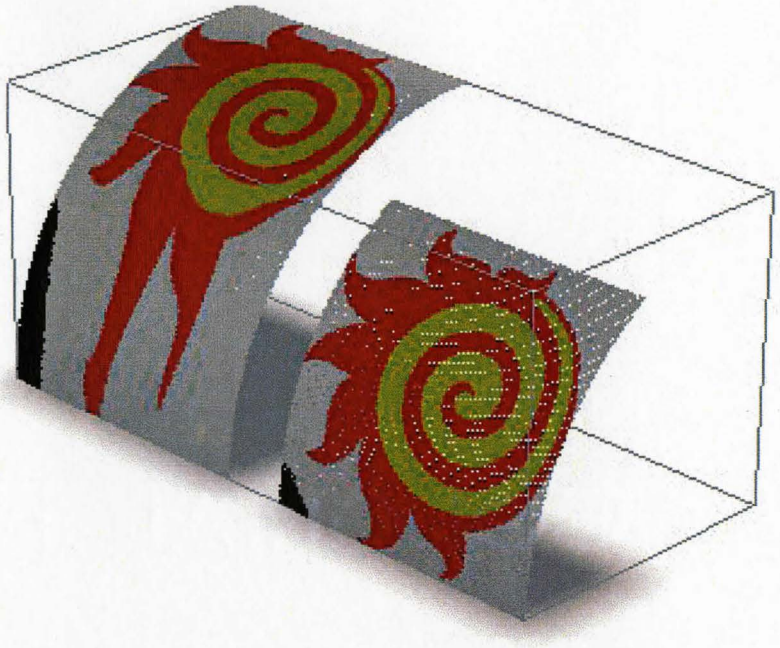

(a) Isometric View

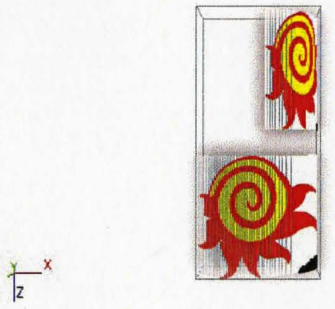

(b) Top View

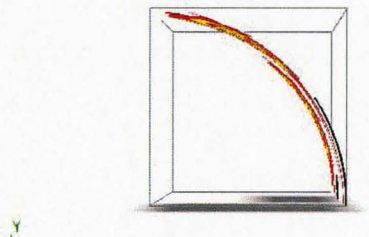

(c) Front View

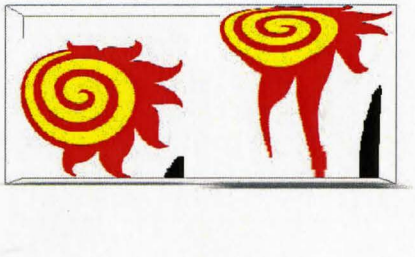

(d) Right View

Figure 4.14: Half Cylinder Image Point Cloud Visualization in Pointstream Pointstream 3Dsuite (Wrapped and Projected)

- Calculating the angle of a fixed elliptical arc length .

  In circles this can be easily solved by dividing the desired arc length -$\frac{1^{th}}{96}in$ in this study- over the radius which yields uniform angular sections, yet in ellipses this angular section is dependent on the location of the arc length which is determined by $a$ and $b$, and the complexity of solving inverse elliptical integrals of the $2^{nd}$ order. The issue of inverse elliptical integrals and their solution will be addressed in the following chapter.

- Rotation around the Ellipse center.

  In circles there exists no such thing as change of circular form if the circle is rotated around its center, while a rotated ellipse changes the conditions for the wrapping, and angular sections used in the parametric solution.

The wrapping starting point will be the projection of the image control box side $w$ furthest point in the $+x$ direction, because of the counterclockwise direction of the wrapping.

Wrapping around an ellipse should meet this condition:

$$w_{max} \lessapprox \int_0^{\pi} \sqrt{(-a\sin(\theta))^2 + (b\cos(\theta))^2)}d\theta \tag{4.6}$$

The projection of point located in the $xy$ plane along the side $w$ where its Cartesian equation $y = cst$ between $[x_{far}, x_{close}]$ where $x_{far} > x_{close}$can be achieved by choosing $x_{far}$and finding the angle $\theta_1$where its projection $x_1$is located.

$x_{far} = x_1 \Rightarrow \theta_1 = \arccos(\frac{x_1}{a})$ where $\theta_1$ should meet the following condition

$0 \leq \theta_1 \leq \theta_{max}$

$\theta_{max}$ refers to the angle where the projection may not surpass, $\theta_{max}$ can be found from the following integral $w \cong \int_{\theta_{max}}^{\pi} \sqrt{(x'^2 + y'^2)}$ where $w$ is the width of the side to be projected, after finding $\theta_{max}$ it is converted into a coordinate value $x_{max}$, thus creating this condition.

$$0 \leq x_1 \leq x_{max}$$

If the image meets the mentioned conditions the generating the .asc file can proceed where $(i, j, k)$ can be generated by finding the unit vector of the normal to the ellipse at point $(x, y, z)$ and angle $\theta$.

$$\overrightarrow{T} = \frac{d\vec{P}}{d\theta} = \begin{cases} \frac{d\vec{x}}{d\theta} = x' = -a\sin(\theta) \\ \frac{d\vec{y}}{d\theta} = y' = b\cos(\theta) \\ \frac{d\vec{z}}{d\theta} = 0 \end{cases}$$

$$\overrightarrow{N} = \frac{d\vec{T}}{d\theta} = \begin{cases} \frac{d\vec{x\prime}}{d\theta} = -a\cos(\theta) \\ \frac{d\vec{y\prime}}{d\theta} = -b\sin(\theta) \\ \frac{d\vec{z\prime}}{d\theta} = 0 \end{cases}$$

$$\left|\overrightarrow{N}\right| = \sqrt{(-a\cos(\theta))^2 + (-b\sin(\theta))^2}$$

$$(i, j, k) = \frac{\vec{N}}{\left|\vec{N}\right|}$$

After determining $x_1$and its angle $\theta_1 = \arccos(\frac{x_1}{a})$ generating the point cloud can be done by the method used for the circle i.e. using a $for$ loop that checks the values of each row of the final image $I$ where the increments of $row(I)$ translate to elliptical angular increment $\Delta\theta$ °.

If the value of the $I_{(row,col)} = 0$ then nothing is done

If $I_{(row,col)} = 1$ then

$$x = R\cos\left(row(I)\Delta\theta + \theta_1\right) \text{ where } col \in [0, round(96w)]$$

$$y = R\sin\left(row(I)\Delta\theta + \theta_1\right)$$

$$z = z_0 \pm \left(col(I)\tfrac{1}{96}{}^{th} in\right) \text{ where } col \in [0, round(96l)]$$

### Projection

Image projection is applicable on half ellipses from perspective planes parallel to the $xy - plane$, if its width $w \leq 2a$ where the starting point $x_{1^{st}}$ can be either edge of its control box and its angle $\theta_{1^{st}} = \arccos(\frac{x_{1st}}{a})$.

Fig. 4.15 shows a point cloud of projection and wrapping of the same image around half ellipse.

### Half Rotated Ellipses

If an ellipse is rotated by an angle $\alpha$ where $0 < \alpha < \frac{\pi}{2}$ around its center as shown in Fig. 4.16 the parametric equations of $(x,y)$ become $(X,Y)$. The new equations can be calculated using the following equation.

$$\begin{bmatrix} X \\ Y \end{bmatrix} = \begin{bmatrix} \cos(\alpha) & -\sin(\alpha) \\ \sin(\alpha) & \cos(\alpha) \end{bmatrix} \times \begin{bmatrix} x \\ y \end{bmatrix} \tag{4.7}$$

$$\begin{bmatrix} X \\ Y \end{bmatrix} = \begin{cases} x\cos(\alpha) - y\sin(\alpha) = a\cos(\theta)\cos(\alpha) - b\sin(\theta)\sin(\alpha) \\ x\sin(\alpha) + y\cos(\alpha) = a\cos(\theta)\sin(\alpha) + b\sin(\theta)\cos(\alpha) \end{cases}$$

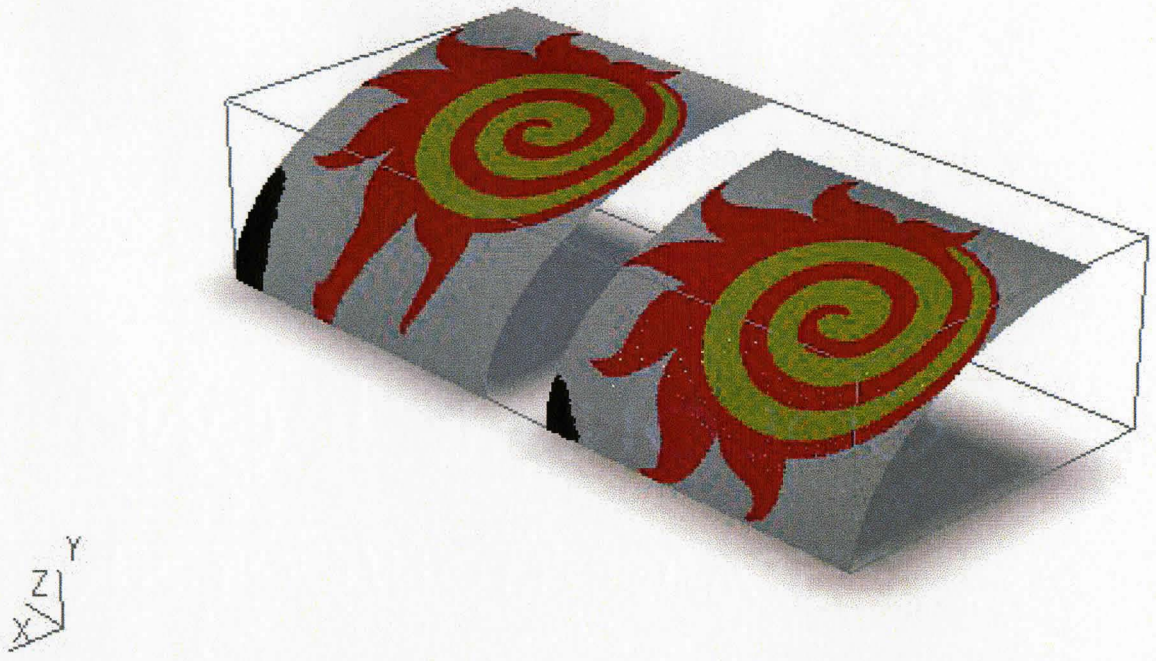


(a) Isometric View

(b) Top View

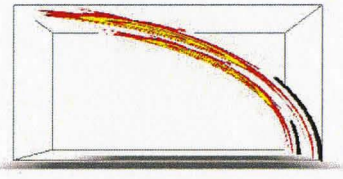

(c) Front View


(d) Right View

Figure 4.15: Half Ellipse Image Point Cloud Visualization in Pointstream Pointstream 3Dsuite (Wrapped and Projected)

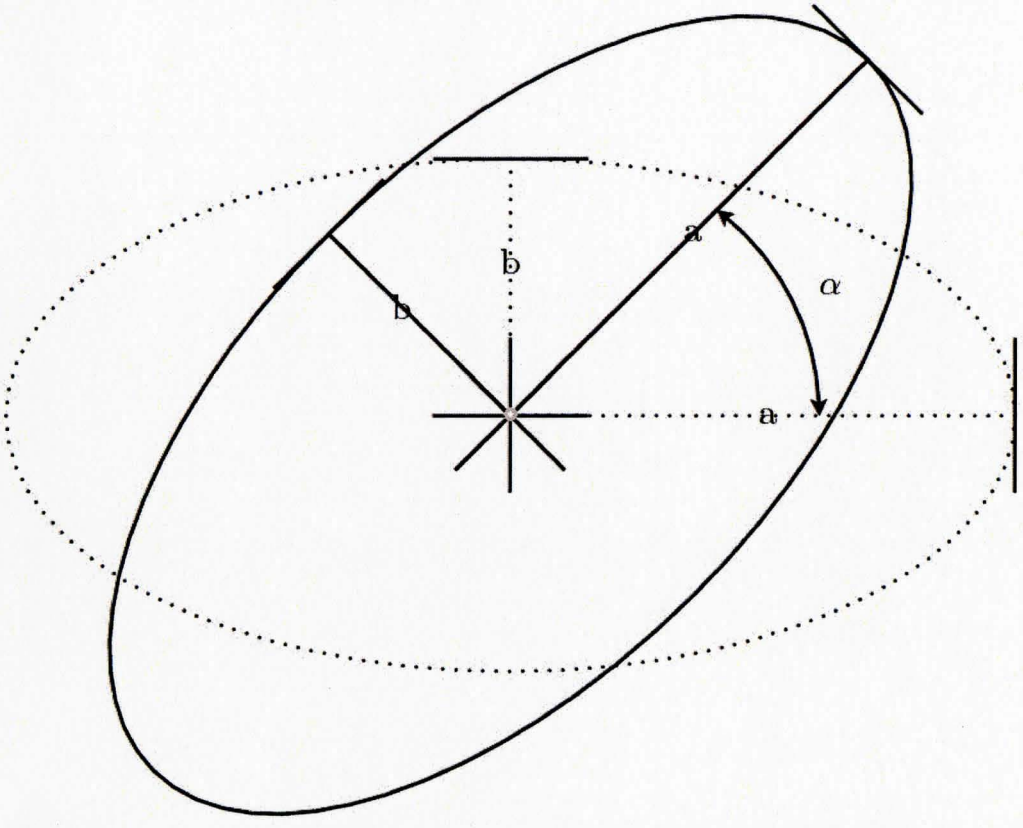


Figure 4.16: Half Rotated Ellipse Geometry

Wrapping starts by finding the starting point $P$ on the side $w$ that has an $x$ value = $x_1$,since the point $P$ is projected along the parametric line $L=\begin{cases} x = x_1 \\ y = t \end{cases}$

where any value of $t$ can fit the above equation the only solvable equation to find the value of $\theta$ is $X = x_1$.

$$x_1 = a\cos(\theta_1)\cos(\alpha) - b\sin(\theta_1)\sin(\alpha)$$

let

$$a\cos(\alpha) = mandb\sin(\alpha) = n$$

$$x_1 - m\cos(\theta_1) = n\sin(\theta_1)$$

square both sides

$$x_1^2 + m^2\cos^2(\theta_1) - 2x_1 m\cos(\theta_1) = n^2 - n^2\cos^2(\theta_1)$$

Collecting terms gives:

$$(n^2 + m^2)\cos^2(\theta_1) - 2x_1 m\cos(\theta_1) + (x_1^2 - n^2) = 0 \tag{4.8}$$

the roots of this quadratic equation are:

$$\sin(\theta_1) = \frac{-2x_1 n \pm \sqrt{4x_1^2 n^2 - 4(n^2+m^2)(x_1^2-m^2)}}{2(n^2+m^2)}, \text{ or } \cos(\theta_1) = \frac{2x_1 m \pm \sqrt{4x_1^2 m^2 - 4(n^2+m^2)(x_1^2-n^2)}}{2(n^2+m^2)}$$

$$\Longrightarrow \theta_1 = \arcsin\left(\frac{-2x_1 n \pm \sqrt{4x_1^2 n^2 - 4(n^2+m^2)(x_1^2-m^2)}}{2(n^2+m^2)}\right), \text{ or } \theta_1 = \arccos\left(\frac{2x_1 m \pm \sqrt{4x_1^2 m^2 - 4(n^2+m^2)(x_1^2-n^2)}}{2(n^2+m^2)}\right)$$

Finding the correct root is done by finding its corresponding largest $Y$ value.

Checking the applicability of wrapping in this situation can be achieved by finding the tangent perpendicular to the $x - axis$ where

$$x_{max} = cst$$

$x_{max}$ can be found when roots of the quadratic equation 4.8 are equal, then

$$x_{max} = +\sqrt{(n^2 + m^2)} \tag{4.9}$$

and its angle $\theta_{max}$ can be found using equation 4.8.

To find $x_{end}$ where $y_1 = 0$

$$\implies a\cos(\theta)\sin(\alpha) + b\sin(\theta)\cos(\alpha) = 0$$

$$\text{and } \theta_{end} = \pi + \arctan\left(-\tfrac{b}{a}\tan(\alpha)\right) \text{ since } \tan(\pi - \alpha) = \tan(-\alpha)$$

To calculate the image width acceptable for this the arc length the following condition condition should be met

$$w_{max} \approxeq \int_{\theta_{max}}^{\theta_{end}} \sqrt{(X'^2 + Y'^2)}d\theta$$

If the condition is met, then the range where the wrapping can start at can be be calculated by $w \approxeq \int_{\theta_{min}}^{\theta_{end}} \sqrt{(X'^2 + Y'^2)}d\theta$ where $\theta_{min}$ is found and converted into a coordinate value $x_{min}$.

After determining angle $\theta_1$ generating the point cloud starts by applying a $for$ loop that checks the values of each row of the final image $I$ where the increments of $row(I)$ translate to rotated elliptical angular increment $\Delta\theta$ °.

If the value of the $I_{(row,col)} = 0$ then nothing is done

If $I_{(row,col)} = 1$ then

$X = a\cos(row(I)\Delta\theta+\theta_1)\cos(\alpha)-b\sin(row(I)\Delta\theta+\theta_1)\sin(\alpha)$ where $col \in [0, round(96w)]$

$Y = a\cos(row(I)\Delta\theta+\theta_1)\sin(\alpha)+b\sin(row(I)\Delta\theta+\theta_1)\cos(\alpha)$

$Z = Z_0 \pm \left(col(I) \times \frac{1}{96}^{th} in\right)$ where $col \in [0, round(96l)]$

and

$X' = -a\sin(row(I)\Delta\theta+\theta_1)\cos(\alpha)-b\cos(row(I)\Delta\theta+\theta_1)\sin(\alpha)$

$Y' = -a\sin(row(I)\Delta\theta+\theta_1)\sin(\alpha)+b\cos(row(I)\Delta\theta+\theta_1)\cos(\alpha)$

As for the values of $(i, j, k)$ they can be generated by finding the normal at the points generated

$$\overrightarrow{N} = \frac{d\vec{T}}{d\theta} = \begin{cases} \frac{d\vec{X}_I}{d\theta} = -a\cos(row(I)\Delta\theta+\theta_1)\cos(\alpha)+b\sin(row(I)\Delta\theta+\theta_1)\sin(\alpha) \\ \frac{d\vec{Y}_I}{d\theta} = -a\cos(row(I)\Delta\theta+\theta_1)\sin(\alpha)-b\sin(row(I)\Delta\theta+\theta_1)\cos(\alpha) \\ \frac{d\vec{Z}_I}{d\theta} = 0 \end{cases}$$

$$\left|\overrightarrow{N}\right| = \sqrt{(X')^2+(Y')^2}$$

$$(i, j, k) = \frac{\vec{N}}{\left|\vec{N}\right|}$$

Image projection is applicable on ellipses from perspective planes parallel to the $xy-plane$, if its width $w \leq |x_{max}|+|x_{end}|$ where the starting point $x_{1^{st}}$ can be either edge of its control box..

Fig. 4.15 shows a point cloud of projection and wrapping of the same image around rotated half ellipse.

### Bsplines

A Bspline curve is defined as $C(u) = \sum_{i=0}^{n} N_{i,k}(u)P_i$ where $P_i = [x_i(u), y_i(u), z_i(u)]^T$ are the $(n+1)$ control points, and $N_{i,k}(u)$ are the basis functions of degree $k$ [33, 45]. This kind of parametric curves is used in CAD softwares to allow the construction of


(a) Isometric View


(b) Top View

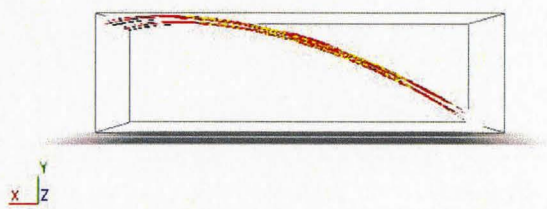


(c) Front View

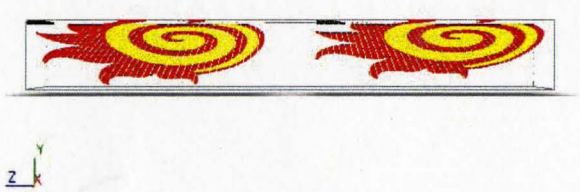


(d) Right View

Figure 4.17: Rotated Half Ellipse Image Point Cloud Visualization in Pointstream Pointstream 3Dsuite (Wrapped and Projected)

complex surfaces. The degree $k$ is what determines the smoothness and continuity of the curve, however increasing the degree complicates the calculation.

Autodesk Inventor represents Bsplines with a cubic degree, which means $k = 4$. In order to find a point along Bspline path at a certain $u$ then the following equation is used.

$$C(u_i) = P_i N_{i,4} + P_{i+1} N_{i+1,4} + P_{i+2} N_{i+2,4} + P_{i+3} N_{i+3,4}$$

Decaling images on Bspline surfaces in Inventor can only be done by projecting them onto the surface, which as mentioned earlier deforms them. In order to visualize wrapped image around Bspline extrusions a Visual Basic (VB) macro was written to utilize the curvature evaluator that Inventor uses. These extrusions can be viewed as 2D Bsplines where the values of the parameter $u$ only affect two coordinates.

This macro as shown in Fig. 4.18 finds the arc length of the whole Bspline and then displays it to let the users know the allowable width of an image that can be wrapped, when users enter the width of the image in $mm$ the program calculates the range where the user is allowed to create the wrapping starting point. This range is chosen to be on the first quadrant side. After entering a valid starting point in one dimension the macro determines where is located on the curve by interesting a line parallel to the $y - axis$ with the Bspline. With the starting point found the macro calculates an array of equidistant points where they are located at a distance of $\frac{1}{96}$ inches from each other along the Bspline. For each point in the array the tangent is also calculated. These values are then stored in a text file to be processed in Matlab.

In Matlab a program was written to read the values of the two used coordinates and then map the image values to their corresponding coordinates. To do this operation a $for$ loop is used to check the values of each row of the final image $I$ and create

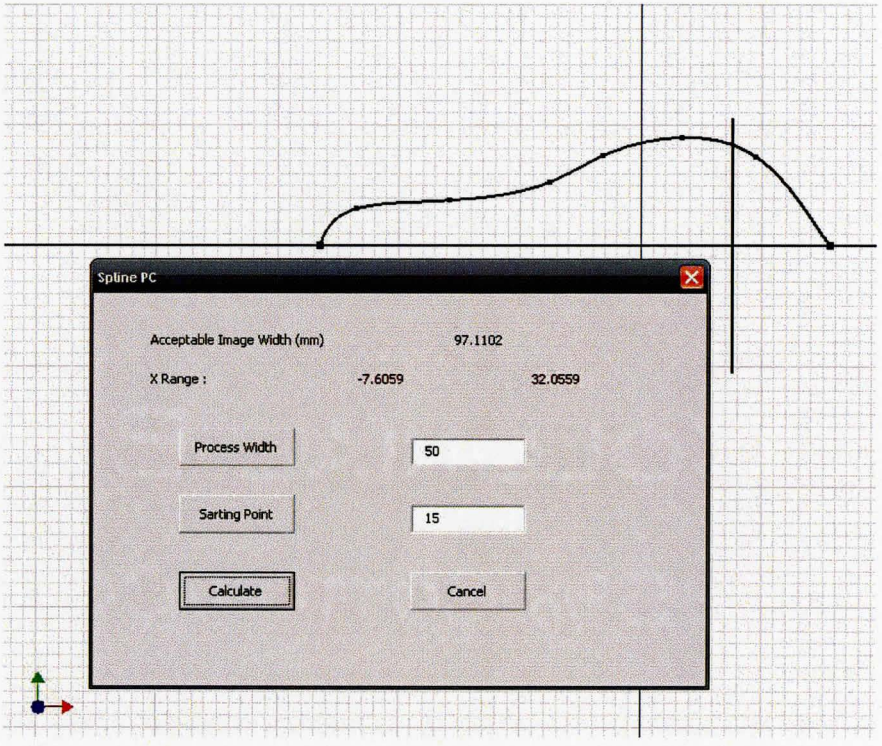


Figure 4.18: Bspline VBA Macro was Used in Geneating Bspline Coordinates and Normals

the Bspline point cloud .asc file.

If the value of the $I_{(row,col)} = 0$ then nothing is done

If $I_{(row,col)} = 1$ then

$x = x_{Row-macro}$

$y = y_{Row-macro}$

$z = Z_0 \pm \left(col(I) \times \frac{1}{96}^{th} in\right)$ where $col \in [0, round(96l)]$

and $(i, j, k) = \frac{\overrightarrow{(x,y,0)}}{\left|\sqrt{x^2+y^2}\right|}$

Fig. 4.19 shows a Bspline point cloud.

## 4.3 CAD Implementation

In this section implementing oriented 3D printing on various geometric surfaces and materials, generating paths for planes, inclined planes, cylinders, ellipses, and the calibration processes involved will be discussed. The examples follow the progression of application, where subsequent examples discuss new problems, and improve on the solution of previous problems at the same time.

### 4.3.1 CMM Environment Setup

Planes can be defined by using only three points. To set up the $xy$ plane accurately on the CMM granite foundation, the CMM fixture plates and standoffs are used because of their repeatability. Standoffs are attached to the CMM fixture in order to give it elevation, then measurements of the plate fixture are taken along the $x - axis$ at both ends of the plate. When the difference between the $x$ measurements of these ends becomes $\leq 30\mu m$, the plate is clamped as shown in Fig. 4.20 The importance

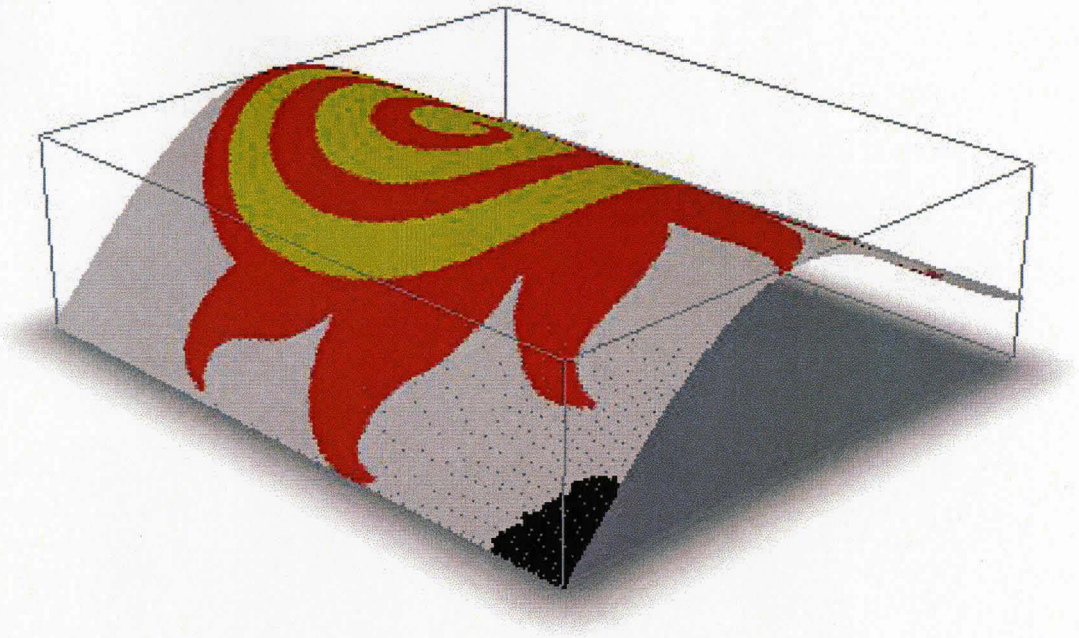

(a) Isometric View

(b) Top View

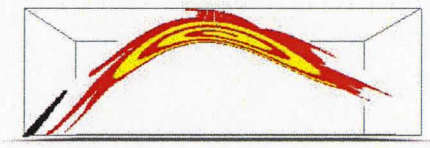

(c) Front View

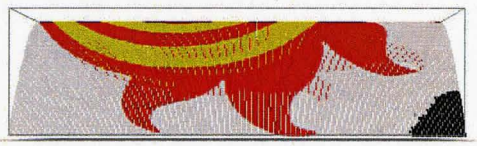

(d) Right View

Figure 4.19: Bspline Image Point Cloud Visualization in Pointstream Pointstream 3Dsuite

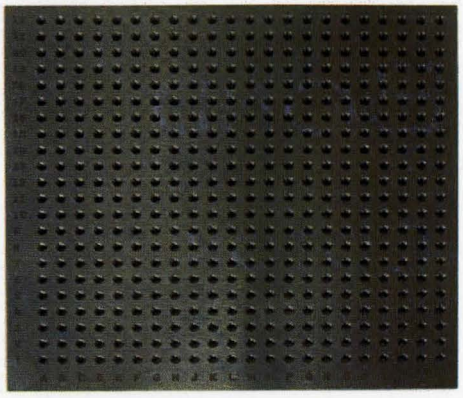

(a) Aluminum Fixture Plates

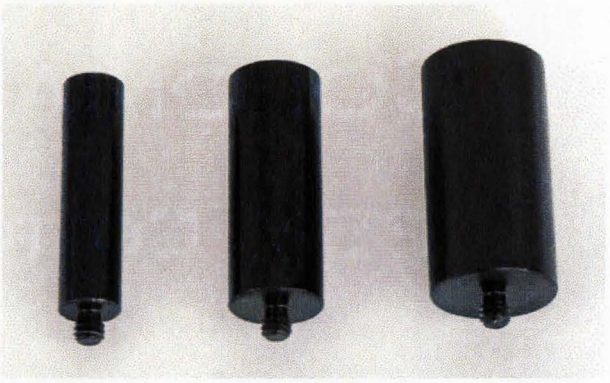

(b) Standoff

Figure 4.20: CMM $xy$ Plane Setup Tools [46, 47]

of having such a plane is to establish the $xy$ plane and determine the coordinates of its normal, the $z - axis$.

### 4.3.2 Planes

Plane printing was performed on the $xy$ plane established by the fixture plate. Numerous planar applications make use of this printing method including: printing on glass and metal sheets. The relative ease of calibrating in 2D can be extended to any geometrical surface which adds to its appeal.

### 4.3.3 Creating Relevant Coordinate Systems

Creating local coordinate systems for planar applications can be established by positioning three standoffs on the fixture plate : two along the $x - axis$ and one along the $y - axis$ where the combination of the plane, and the three standoffs, eliminates the six degrees of freedom of any placed object. The Elimination of the DOF is detailed in Table 4.1.

Determining the plane can be done by probing three random points on the flat

| | $1^{st}$ axis | | $2^{nd}$ axis | | $3^{rd}$ axis | |
|---|---|---|---|---|---|---|
| | Rotation | Translation | Rotation | Translation | Rotation | Translation |
| Plane (Datum A) | ✘ | | ✘ | | | ✘ |
| 2 Standoffs (Datum B) | | | | ✘ | ✘ | |
| 1 Standoffs (Datum C) | | ✘ | | | | |

Table 4.1: 3-2-1 DOF Elimination

areas of the fixture plate located in the region bounded by the standoffs. These points generate a plane whose coordinates and direction are calculated by the Mitutoyo GeoMeasure® [48] measuring software. The cylindrical standoffs are then measured and their centers and radii calculated.

The averaging of the $X$ coordinates of the standoff, located on the $x - axis$, are used to determine the $x$ coordinate of the coordinate system center, while the $y$ coordinate of the $Y$ standoff is used to calculate the its y coordinate. The averaging of the radii of $X$ standoff is used to find the offset in the $X$ direction, while the measured value is used for the Y one.

After calculating the centre coordinates, a transformation matrix is constructed in order to convert between the part and the machine coordinate system PCS and MCS respectively.

$$M_P = \begin{bmatrix} \cos(0) & -\sin(0) & 0 & x_{center} \\ \sin(0) & \cos(0) & 0 & y_{center} \\ 0 & 0 & 1 & z_{center} \\ 0 & 0 & 0 & 1 \end{bmatrix}$$

The theoretical values of the rotation part of $M_P$ were verified by processing the

measurements obtained in GeoMeasure.

$$M_P(calculated) = \begin{bmatrix} \hat{i}_{1c} & \hat{i}_{3c} & \hat{i}_{(1c\times 3c)} & x_{center} \\ \hat{j}_{1c} & \hat{j}_{3c} & \hat{j}_{(1c\times 3c)} & y_{center} \\ 0 & 0 & 1 & z_{center} \\ 0 & 0 & 0 & 1 \end{bmatrix}$$

The conversion from PCS to MCS can be done using the following formulas

$$P_{MCS} = M_P(P_{PCS})$$

and

$$P_{PCS} = M_P^{-1}(P_{MCS})$$

### 4.3.4 Calibration In $xy$ Plane

Several steps must be taken to ensure that printing is accurate and aligned properly. Several assumptions have to be taken into consideration:

- The imperfection of the head mount

  Since the head mount was rapid prototyped, the flatness of the surface, where it mates with the Renishaw adapter, generates undesired angular gaps. For the same reason, inaccuracies with the screw threading that holds the printer mount would create a problem of parallelism. These factors combined would easily create an Abbe error where the angular error amplifies the axial displacement of the centre of rotation as shown in Fig. 4.21.

- The inconclusive resolution of the calibrating test scan

  To accurately determine the distances from the centre of rotation and the edges of the different angles shown in Fig. 4.22 a print out of these edges is performed

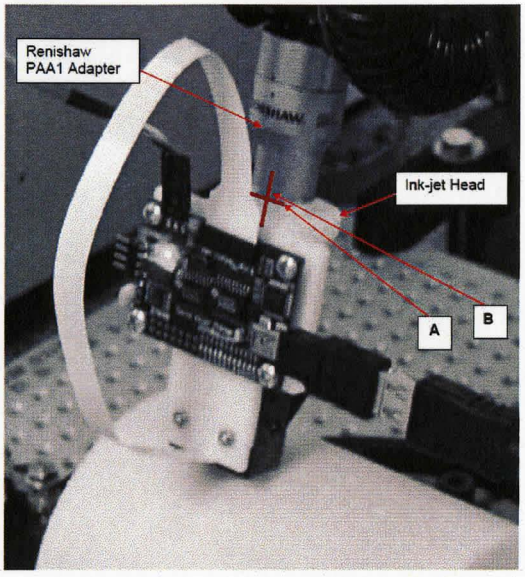


(a) Ink-jet Head Mounted on CMM

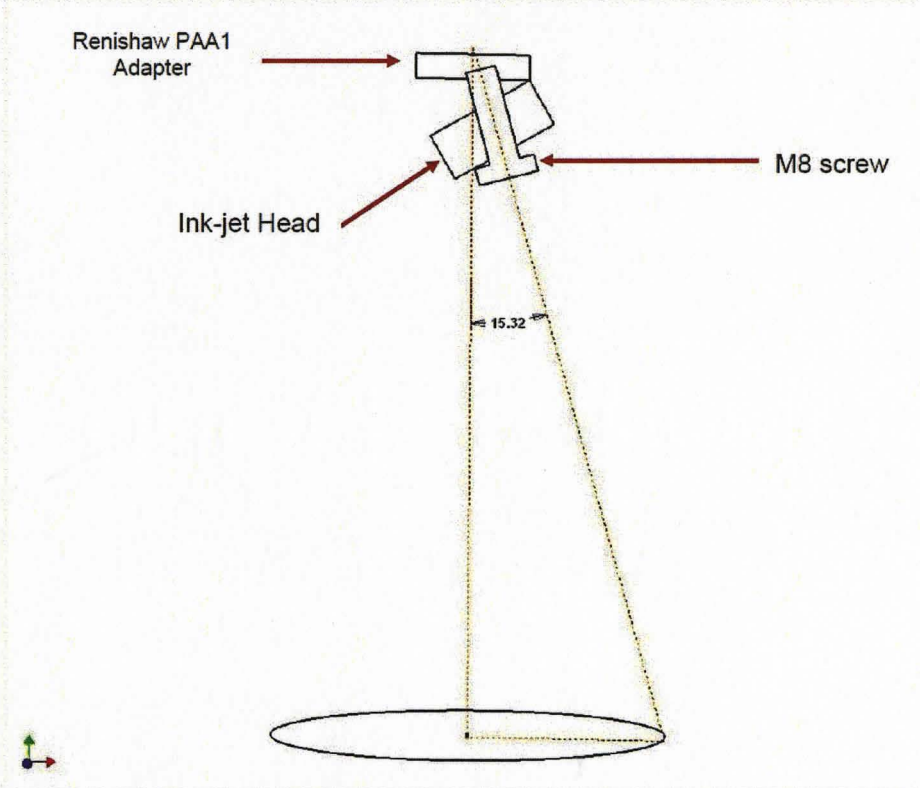


(b) Exaggeration of the Angular Error to Demonstrate the Effect of Abbe Error

Imperfection in the quality of the holder creates problems in A (where the ink-jet head mates with the adapter) and B where the screw meets the adapter. These angular errors create a displacement error that expands with height.

Figure 4.21: Abbe Error Effect

at different B angles. This sample print was then scanned with a resolution of 300 DPI, then the scanned image was scaled down to 96 DPI to maintain the physical dimensions of the printout. With its resolution matching the resolution of the printer, this image was viewed as a point cloud in Pointstream 3Dsuite and measurements between the relevant edges were taken. These measurements served only as a starting point where several printing tests were performed to hone the calibration. It is also important to note that the Abbe error factor was eliminated by adding it to the total $x$ and $y$ offsets. As shown in Fig. 4.22 the tips of the edge or the points of interest were connected and their centre of rotation found.

- Results for the first nozzle offsets are added to the original offsets of the PCS (refer to Page 74). With the Printer Calibrated at Angle $B = 0$, calibrating at different angles can be done using the translation required from the location at $B_1 = 0$ to $B_2 = B_2$

  if the $z - axis$ passes through the center of the calibrating coordinate system, then the upper first nozzle coordinates are $(-x_{offset}, -y_{offset})$ and following transformation matrix is applied.

$$R_{xy} = \begin{bmatrix} \cos(B_2) & -\sin(B_2) & 0 \\ \sin(B_2) & \cos(B_2) & 0 \\ 0 & 0 & 1 \end{bmatrix}$$

$$L_{B_1} = \begin{Bmatrix} -x_{offset} \\ -y_{offset} \\ z \end{Bmatrix}$$

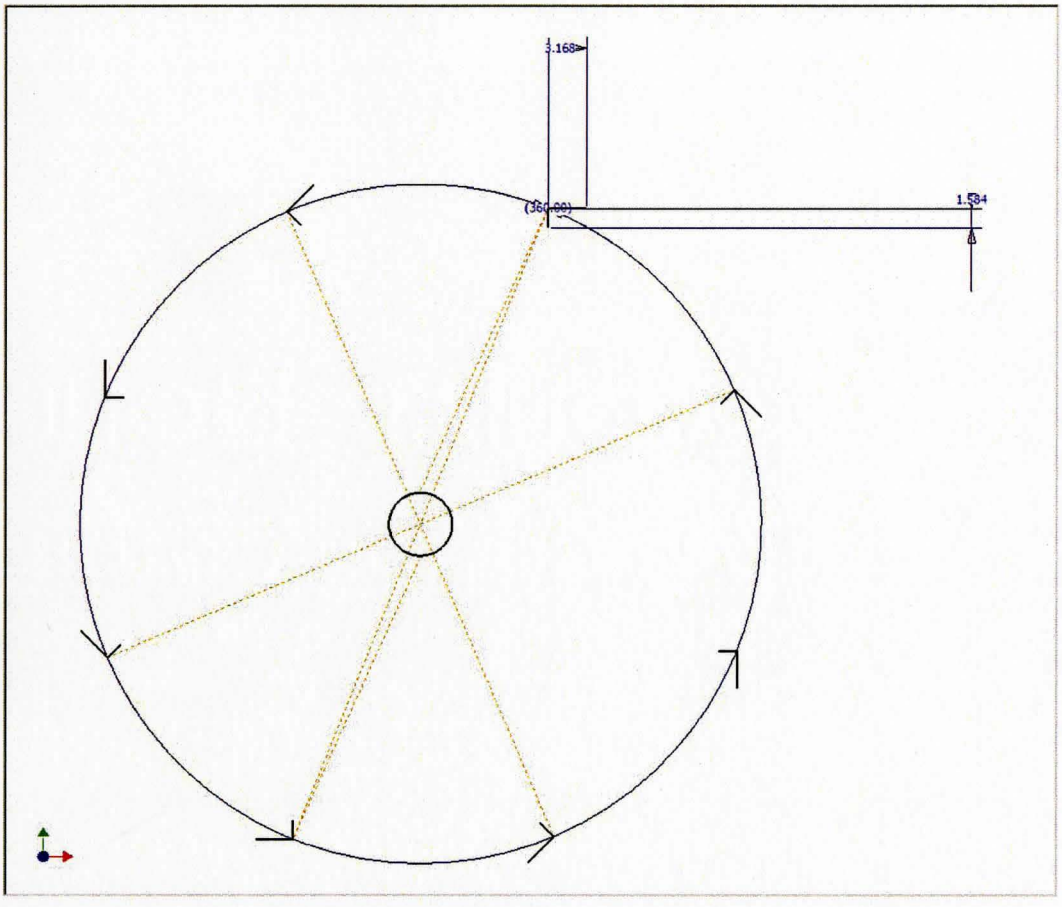


Figure 4.22: Grid Calibration: Printing Grid Edges at Certain Angles Helps Find the Center of Rotation, Hence the Coordinates of the Upper Nozzle.

$$L_{B_2} = R_{xy}(L_{B_1})$$

$$\therefore \text{translation } T_{(L_{B_1} \rightarrow L_{B_2})} = L_{B_1} - L_{B_2}$$

If $B_1 \neq 0$ the same process is applied and two translation are found for $0 \rightarrow B_1$ and $0 \rightarrow B_2$ and $T_{(L_{B_1} \rightarrow L_{B_2})} = T_{(0 \rightarrow L_{B_1})} - T_{(0 \rightarrow L_{B_2})}$ follows.

- To calibrate the $z$ direction the head holder needs to touch the fixture plate and record that elevation.

### 4.3.5 Planar Printing

Planar printing is done by driving the CMM along one axis $(y - axis)$ where it prints a $\frac{1}{8}$ inches strip of a of 8 inches maximum distance[38], which is the memory maximum limit of the micro-controller buffer. After reprogramming the characters that start at (ASCII 65 A) and could end at (ASCII 126 ~), these characters are then loaded to printing buffer and printed as a text string where each column of each character is printed when it receives a TTL signal issued by the CMM controller. These signals are issued when the CMM moves $\frac{1}{96}$ inches in all directions combined, thus printing using one axis is very important to ensure the resolution quality. After printing this string buffer, the head moves back to its originating $y$ coordinate and $\frac{1}{8}$ inches in the $x$ direction and starts another strip.

### 4.3.6 Inclined Planes

Inclined planes constitute the second level of geometrical complexity. Inclined printing is important to verify the accuracy and to refine the printing process at an inclined angle. For this case study the angle of inclination $\beta$ was chosen to be 11° to avoid using a multiple of 7.5° and because there are two probe angles A applicable to

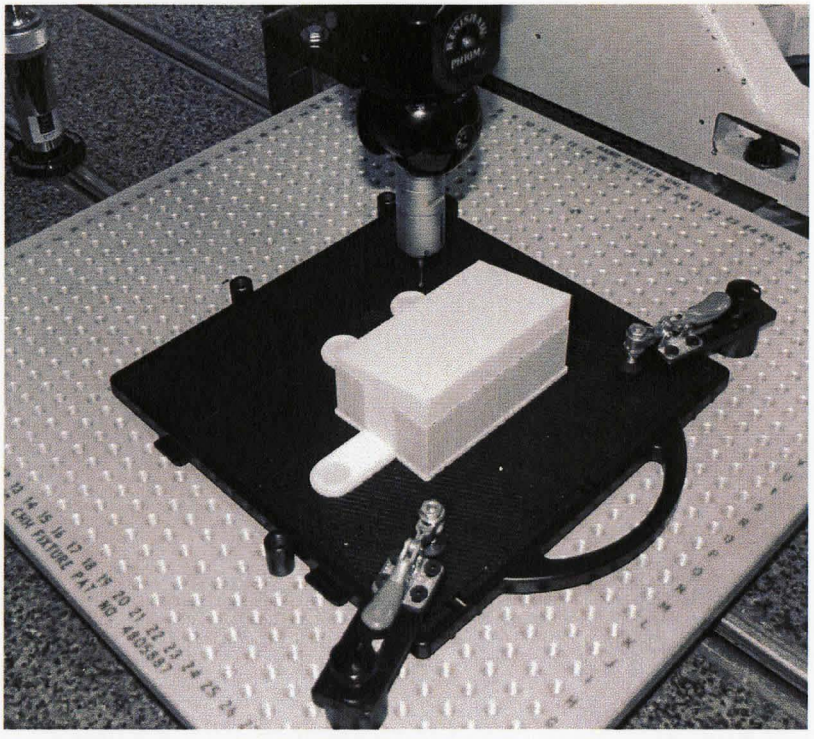

Figure 4.23: Inclined Plane LCS Creation

it : 7.5° and 15°. In the inclined printing experiments the choice of angles yielded no difference, and the $\frac{1}{8}$ inches grid printed was accurate, however the width of the printer along the $(x - axis)$ made the clearance gap at the back of the printer very small at the smaller angle, while the larger angle created a larger gap at the back than the front, as a result the larger angle was chosen to avoid touching the plane.

### Establishing Relevant Coordinate Systems

The Inclined plane used is rapid prototyped using Dimension BST rapid prototyping machine. Since the built solid is attached to the flat base plate by breakable plastic, keeping the solid attached provides the ease of repeatably replicating the position of plate using the existing $3 - 2 - 1$ datum structure as shown in Fig. 4.23. The center of the coordinate system can be found by probing the $xz$ plane, $yz$ plane,

and the inclined plane.

### Moving in Position

Printing on inclined planes require two calibrations: the $xy$ with the $z-axis$ as the axis of rotation, and the $xz$ with the $y-axis$ as the axis of rotation. Since the first calibration was already performed for the $xy$ plane, it can be carried over to inclined planes, however the $xz$ calibration requires locating the upper nozzle with respect to the $y-axis$. These coordinates are easily found since the $x$ coordinate is shared with the $xy$ calibration, and the $z$ coordinate can be found by measuring the distance from the PAA1 adapter to the nozzle plate, and adding it to the PH10M measurements [40] provided by Renishaw.

Moving to a certain point requires two location transformations, the first of which is the planar one described on page 77, while the second one used considers the $y-axis$ passing through the second center of the calibrating coordinate system, with respect to which the upper first nozzle coordinates are $(-x_{offset_1},\ z_{offset_1})$ and the following transformation matrix is applied.

$$R_{xz} = \begin{bmatrix} \cos(A_2) & 0 & \sin(A_2) \\ 0 & 1 & 0 \\ -\sin(A_2) & 0 & \cos(A_2) \end{bmatrix}$$

$$L_{A_1} = \begin{Bmatrix} -x_{offset_1} \\ y \\ z_{offset_1} \end{Bmatrix} \text{ where } A_1 = 0$$

$$L_{A_2} = R_{xy}(L_{A_1})$$

$$\therefore \text{translation } T_{(L_{A_1} \to L_{A_2})} = L_{A_1} + L_{A_2}$$

**Printing**

Grids were chosen for this printing experiment, and the results shown in Fig. 5.3 show the accuracy of the operation on inclined rapid prototyped surface. The printing process is similar to planar surfaces, but after printing the loaded text buffer the printer head returns to its originating $y$ coordinate and $\frac{1}{8}$ $in$ in both $x$ and $z$ directions, where:

$$x_{increment} = \frac{\cos(\beta)}{8}$$
$$z_{increment} = \frac{\sin(\beta)}{8}$$

### 4.3.7 Analysis Of Angular Sectioned Trajectory VS. Parametric Trajectory

Renishaw PH10M probe moves in angular increments of 7.5°, thus rendering any path from a continuous smooth one into a set of connected line one that follows the tangent of the surface. Since the optimal printing distance of the HP ink-jet head is $1 \pm .5$ mm, and since the rapid prototyped surfaces are confined by a $(8 \times 8 \times 12)$ inches envelope, analysis of surfaces and 7.5° increment tangents would assess whether these trajectory lines are within the accepted tolerance.

As shown in Figures 4.24, 4.25, and 4.26 the gap between the tangent and the surface where the printing is applied is $< 1mm$.

### 4.3.8 Half Cylinders

Half Cylinders are the natural progression from inclined planes because the CMM treats them as set of connected inclined planes. The range of $(0, \pi)$ was chosen because of the range of angle $A$ $(0, 105)°$ and because the gravitational resistance

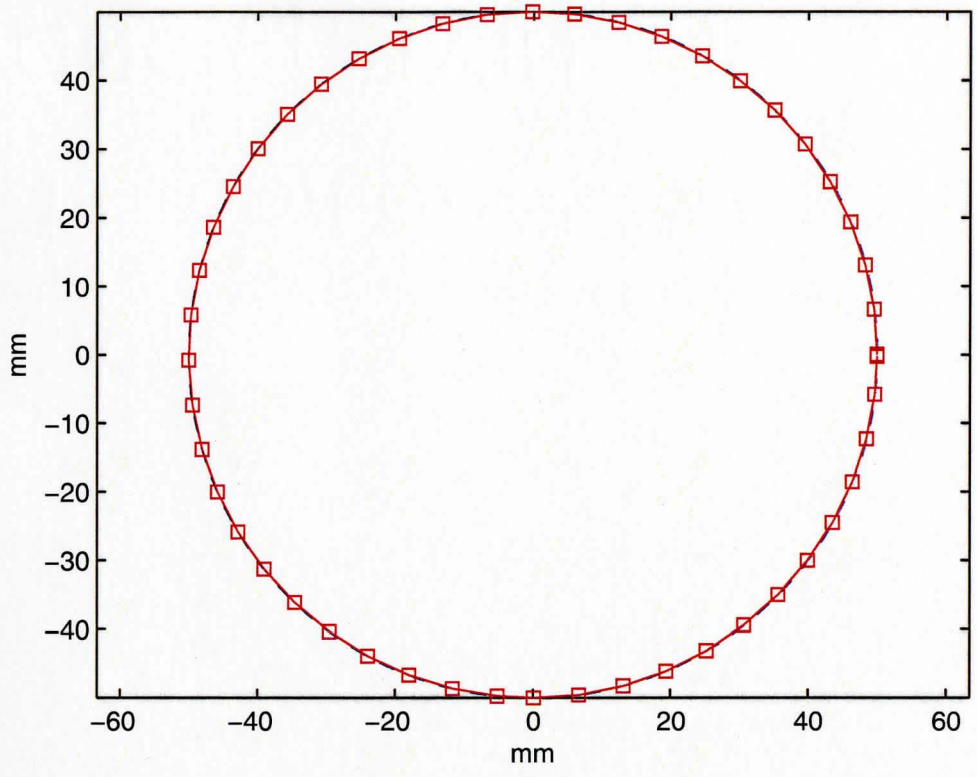


(a) Circular Tangents

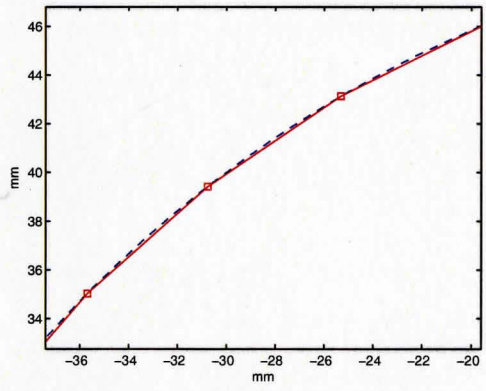


(b) Closeup Region

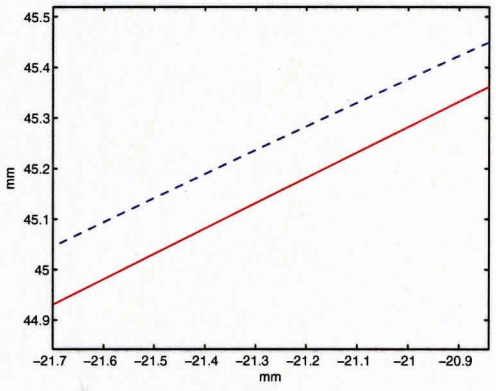


(c) Closeup Region Enlargement

Figure 4.24: Cylindrical Tangents Vs. 7.5° Line Segments

could affect the quality of printing if the ink-jet head is tipped above the horizontal as recommended by HP [35].

### Image Sectioning

Wrapping images is required in order to print them around cylindrical paths, thus after finding the wrapping starting point, as discussed in the previous chapter, this point $x$ *coordinate* is compared with displacement angular span to find the region to which it belongs. The displacement angular span is an array of $x$ *coordinate* of all the angles between $[0,\pi]$ with an increment of 7.5°. If the cases for wrapping an image are met, then the sectioning has two formats.

- Format 1 : One Quadrant

  If the image wraps completely in one quadrant, then the region where the wrapping starting point must be found in the array, thus determining $A$ rotation, and determining the arc length of the first strip located between the angle of wrapping start and the next 7.5° increment. This arc is then divided by the resolution (96 DPI), and rounded down to determine the width of the starting strip. The remaining unprinted portion of the image is then divided into uniform 7.5° arcs which are rounded down to ensure that there is no pixel loss and assigned to their respective angle $A$. After the uniform sectioning stage, there might remain some rows of pixels that can be considered the final strip.

- Format 1 : Two Quadrants

  If the image wraps in two quadrants, which translates into two $B$ angles, the image is divided into two separate images, where the first starts wrapping in the first quadrant and ends at the tip of the cylinder, and the second one starts

wrapping at angle $\frac{\pi}{2}$. The sectioning for each of the two images is then processed using Format 1.

### Printing

Printing along circular tangent path is similar to printing on inclined planes, where the ink-jet head moves back to its originating *ycoordinate* and follows the path in the $xz$ plane; however, since the length of the strip is a variable, the increments of path are dependent on its width $w_{strip}$. The increments are calculated by the following formulas

$$x_{increment} = \frac{w_{strip}\cos(A)}{96}$$
$$z_{increment} = \frac{w_{strip}\sin(A)}{96}$$

Unlike inclined planes where $B$ doesn't change, $B$ is dependent on the region of printing, whether it is in the first quadrant or the second quadrant.

- First Quadrant

  If the printing is located in the first quadrant, regardless whether the wrapped image is sectioned or not, the $1^{st}$ nozzle is then considered the point of interest where the calibration occurs.

- Second Quadrant

  If the printing is located in the second quadrant, the sixth nozzle is then considered the point of interest where the calibration occurs. At this point the offset from the $z-axis$ changes by the distance separating 6 nozzles $(6\times\frac{1}{96})in$, which requires changing the rotation parameters for $A$ and $B$ calibration functions. In addition the strip needs to be flipped around the $y-axis$ which is done by multiplying its columns by a different binary conversion array.

### Moving in Place

Calibrations on cylinders is done by creating a new coordinate system CS, where this system is used to verity the calibration results obtained on the cylinder. Construction of CCS can be done by wrapping a paper on the half cylinder where where its $y-axis$ coincides with PCS $y-axis$, and its $x-axis$ is parallel to the $xz-plane$ along the edge of the cylinder. The conversion between PCS and CCS can be calculated using these formulae:

$$\begin{aligned} x_{PCS} &= R(1-\cos(\tfrac{x_{CCS}}{R})) \\ y_{PCS} &= t \\ z_{PCS} &= R(1-\sin(\tfrac{z_{CCS}}{R})) \end{aligned} \tag{4.10}$$

where $0 \leq t \leq e$ the width of the extrusion.

A grid edge whose CCS coordinates (1,1,1) cm is printed on the wrapped paper in PCS at the relevant A angle where a rotation matrix transforms the PCS point to its equivalent at the desired angle, and the results are then compared. The calibration point can be chosen to be (1,1,1) either in cm or in inches, where these dimensions can be easily measured on the test paper. Since the first calibration was already performed for the $xy$ plane, it can be carried over to inclined planes, however the $xz$ calibration requires the locating the upper nozzle with respect to the $y-axis$. These coordinates are easily found since the $x$ coordinate is shared with the $xy$ calibration, and the $z$ coordinate can be found by measuring the distance from the Renishaw PAA1 adapter to the nozzle plate, and adding it to the PH10M measurements [40] provided by Renishaw.

Moving to a certain point requires two location transformations, the first of which is the planar one described on page 77, while the second one considers the $y - axis$ passing through the second center of the calibrating coordinate system, with respect to which the upper first nozzle coordinates are $(-x_{offset}, z_{offset})$ and the following transformation matrix is applied.

$$R_{xz} = \begin{bmatrix} \cos(A_2) & 0 & \sin(A_2) \\ 0 & 1 & 0 \\ -\sin(A_2) & 0 & \cos(A_2) \end{bmatrix}$$

$$L_{A_1} = \begin{Bmatrix} -x_{offset_1} \\ y \\ z_{offset_1} \end{Bmatrix} \text{ where } A_1 = 0$$

$$L_{A_2} = R_{xz}(L_{A_1})$$

$$\therefore \text{translation } T_{(L_{A_1} \to L_{A_2})} = L_{A_1} + L_{A_2}$$

If $A_1 \neq 0$ the same process is applied and two translation are found for $0 \to A_1$ and $0 \to A_2$ and $T_{(L_{A_1} \to L_{A_2})} = T_{(0 \to L_{A_1})} + T_{(0 \to L_{A2})}$ follows.

When printing in the second quadrant is required, the printer head is turned 180° and the sixth nozzle becomes the point of interest for printing because of the flipping the printed strips as discussed on page 4.2.5. Finding the location $L_{B_2}$ can be done using the following formula

$$L_{B_2} = R_{xy}(L_{B_1}) \text{ where } B_1 = 0$$

$$\therefore \text{translation } T_{(L_{B_1} \to L_{B_2})} = L_{B_1} - L_{B_2} - \frac{1^{th}}{16}$$

and then rotating the new location using the following transformation.

$$L_{A_1} = \begin{Bmatrix} x_{offset_1} - \frac{1^{th}}{16} \\ y \\ z_{offset_1} \end{Bmatrix}$$

$$L_{A_2} = R_{xz}(L_{A_1})$$

### 4.3.9 Ellipses

Ellipses were chosen for printing on because they are a geometric case where image sectioning width is dependent on the tangent of the ellipse. This dependency is due to the variance in the elliptical arc length for the same angle at different location.

### 4.3.10 Elliptical Arc Length

Elliptical arc length can be calculated using the following equation

$$S_E = \int_{\theta_1}^{\theta_2} f(\theta) d\theta \tag{4.11}$$

where

$f(\theta) = \sqrt{(-a\sin(\theta)\cos(\alpha) - b\cos(\theta)\sin(\alpha))^2 + (a\sin(\theta)\sin(\alpha) - b\cos(\theta)\cos(\alpha))^2)}$,

and

$$0 < \alpha < \tfrac{\pi}{2}$$

An integral of this form shown in equation 4.11 is called an elliptic integral. This type of integrals cannot be solved by using ordinary terms [49]. Since there is no mathematical way of finding its inverse where $S_E$ and $\theta_1$ are known, numerical integration is used.

The numerical method used to estimate the angle increments where the arc length value is $\frac{1}{96}$ inches is Simpson's rule.

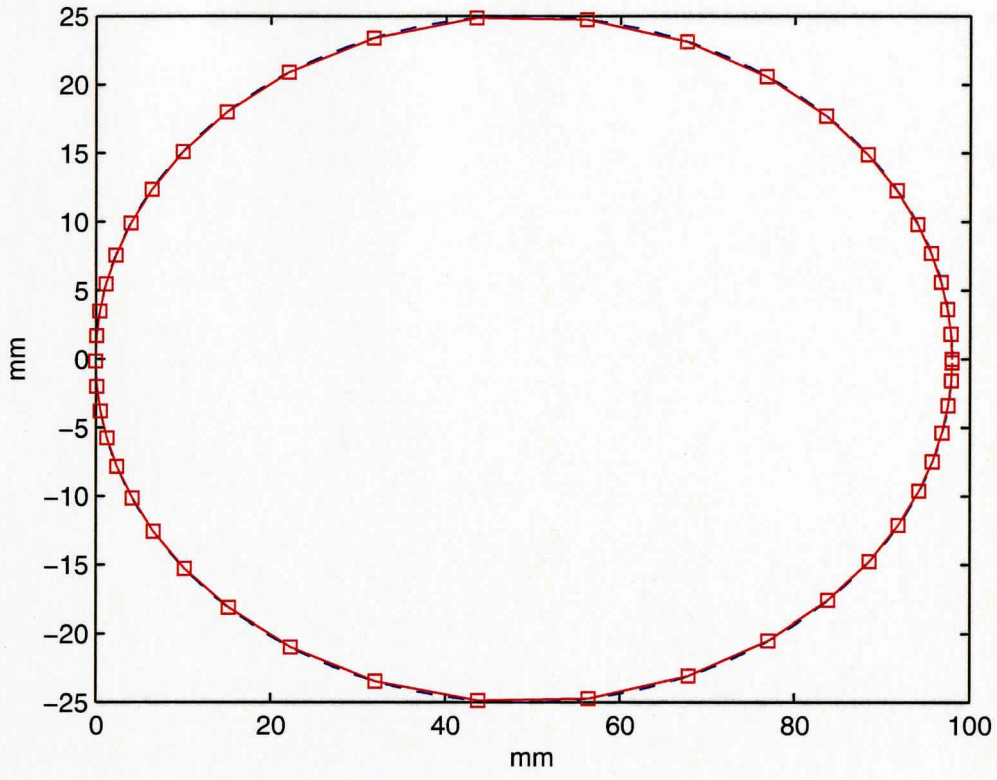


(a) Ellipse and Elliptical Tangents at 7.5 Degrees

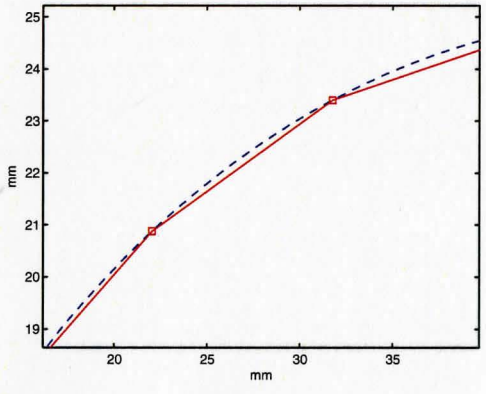


(b) Closeup Region

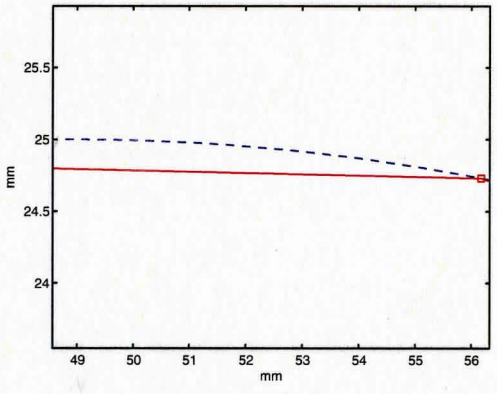


(c) Closeup Region Enlargement

Figure 4.25: Elliptical Tangents Vs. 7.5° Line Segments

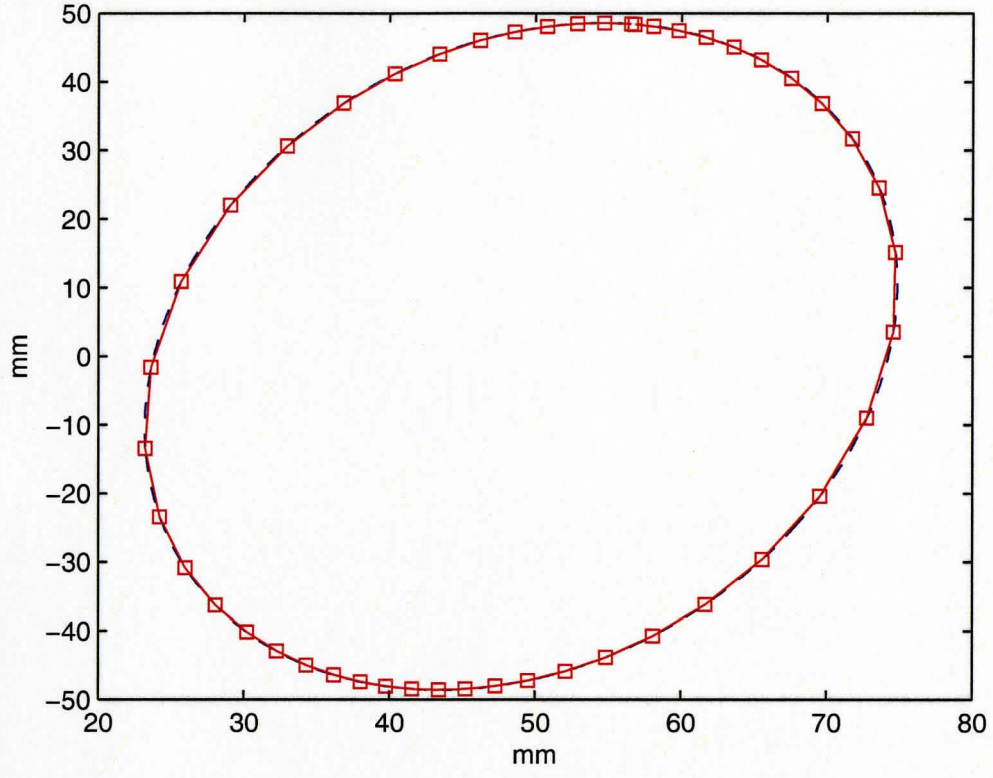


(a) Rotated Ellipse and Elliptical Tangents at 7.5 Degrees

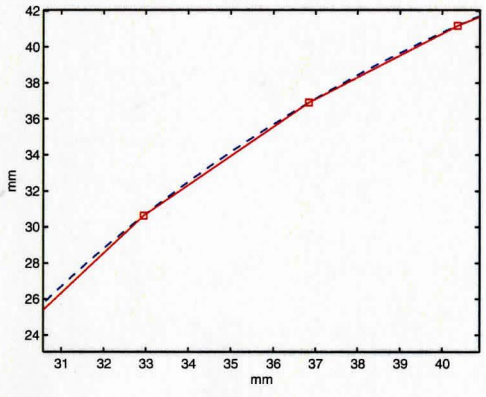


(b) Closeup Region

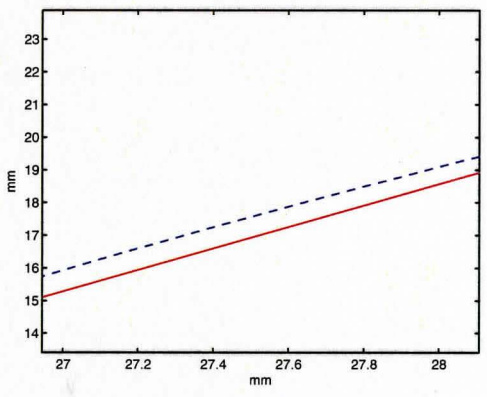


(c) Closeup Region Enlargement

Figure 4.26: Rotated Elliptical Tangents Vs. 7.5° Line Segments

$$S_E \approx \frac{\theta_2-\theta_1}{6}\left[f(\theta_1)+4f\left(\frac{\theta_1+\theta_2}{2}\right)+f(\theta_2)\right]$$

The value calculation starts by integrating from $\theta_1$ to $\theta_1 + \delta\theta$ where $\delta\theta = 10^{-6}$. When the integration yields a result of $\frac{1}{96}$ inches with a margin of error of $\pm 10^{-4}$, the result value is considered the new starting angle and the process is repeated for a number of steps equal to the number of pixels of the wrapped side of the image. This procedure will create an array of angles where the arc length between any consecutive two members is $\frac{1}{96}$ inches. The tangent value $t$ is then calc ulated at each of these angles and stored in a new array.

$$t = -\frac{b^2}{a^2}\left(\frac{a\cos(\theta)\cos(\alpha) - b\sin(\theta)\sin(\alpha)}{a\cos(\theta)\sin(\alpha) + b\sin(\theta)\cos(\alpha)}\right) \tag{4.12}$$

The tangent array members are compared to check where the difference between members is greater than 7.5°, the indices of these members become the map of how the image is to be sectioned as shown in Fig. 4.27 . When the slope changes signs, the image is partitioned to be printed at different angle $B$ which is either 0°or 180°. Generating the printing path as similar to cylinder with only one difference: the varying image section size. The paths for ellipses are shown in Fig. 4.25 and Fig. 4.26.

### 4.3.11 BSplines

Generating the path for Bspline paths depends on the coordinate and tangent file generated using the VB Inventor macro. The same process used for the ellipse tangent array is used for the Bspline tangents where the tangent array members are compared with each other to check where the difference is greater than 7.5°as shown in Fig. 4.28, the indices of these members become the map of how the image is to be sectioned with their corresponding angles $A$. The only addition to the ellipse path is

Figure 4.27: Elliptical Image Angular Sectioning

the possibility of change in the slope sign more than once, thus requiring the partition of the image accordingly.

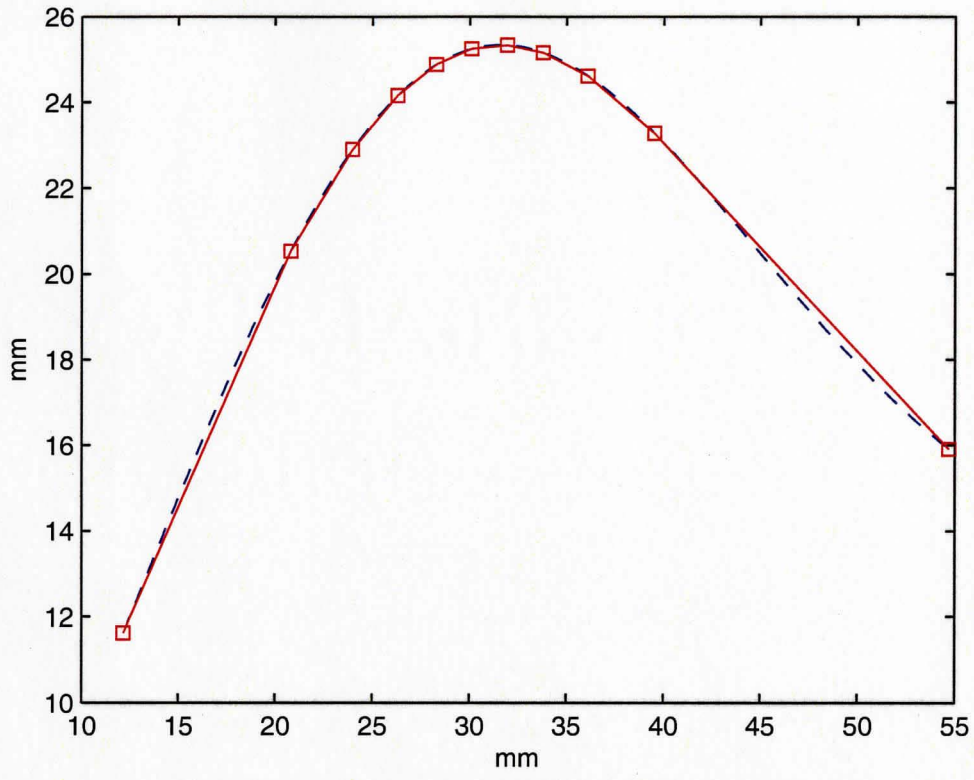


(a) Spline

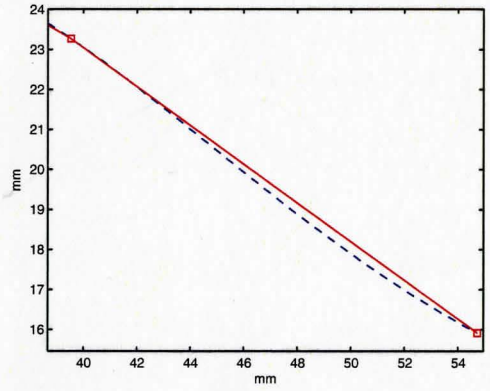


(b) Closeup Region

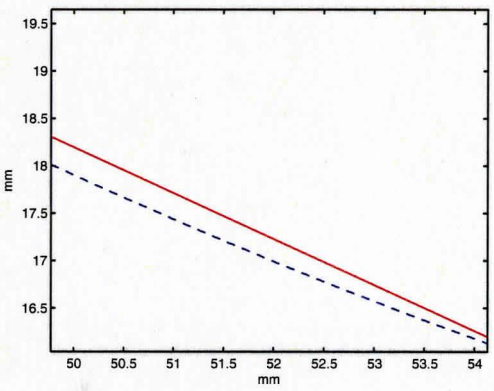


(c) Closeup Region Rnlargement

Figure 4.28: Spline Tangents Vs. 7.5° Line Segments

# Chapter 5

# Test Cases and Results

Oriented 3D printing results can be divided in two categories: geometry and materials. In the geometry section, only parts made with Dimension BST machine were used. The following solids were used: flat plane, inclined plane, half cylinder, and elliptical cylinder, and 2D Bspline extrusion. In the materials sections, flat sheets of glass, and aluminum were used. All of the samples were coated with InkAID precoat, to allow the ink to stick on the surfaces. The washability of the ink allowed the test to be repeated several times, without the need to discard any of the sample parts.

## 5.1 Geometry

Printing on the RP parts was a challenge in terms of verifying the alignment of the image segments. The roughness of the surface was an obstacle to seeing whether or not printing is accurate. Since all the samples used are wrappable, a white piece of paper was taped on their surfaces allowing the calibration and the measuring of some preliminary sample grids. Since these grids are of a known size, measuring them on a flat paper was a sufficient evidence that the calibration of the printer, and the

alignment of the image segments are right as shown in Fig. 5.1

Figure 5.1: Photocopy of a Test Printout on Paper: The Paper Sheet was Wrapped around the Cylinder for Quality Checks

The following images show the samples printed on, which under magnification

show printed dots can be separated each other.

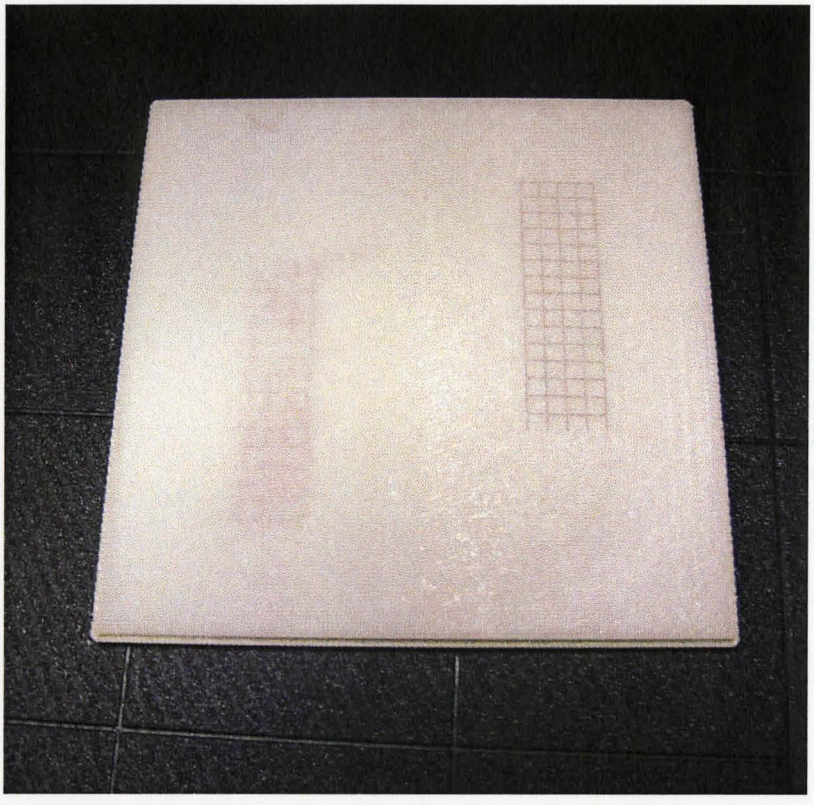

Figure 5.2: Printing on RP Flat Planes: Grid Quality Varied Dramatically Between the Un-coated Side (Right) and the Coated Side (Left)

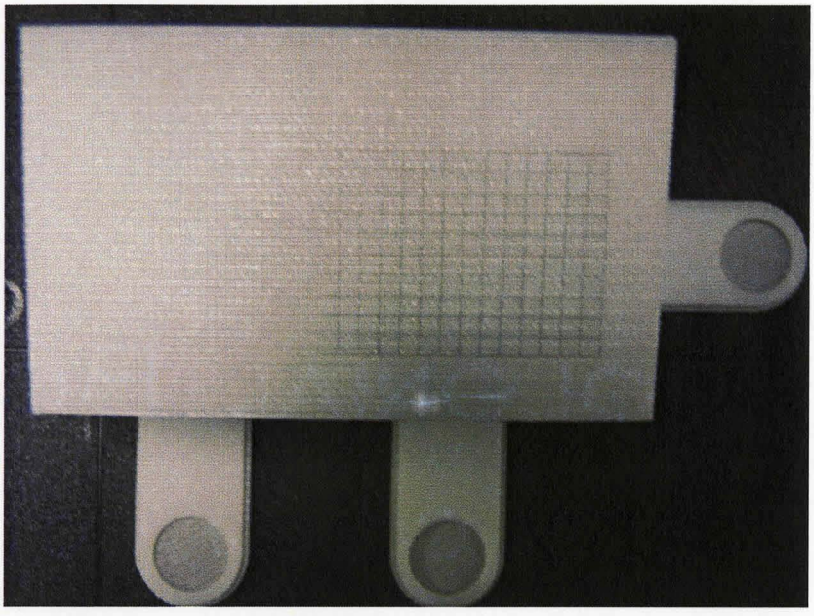

(a) Grid Printout

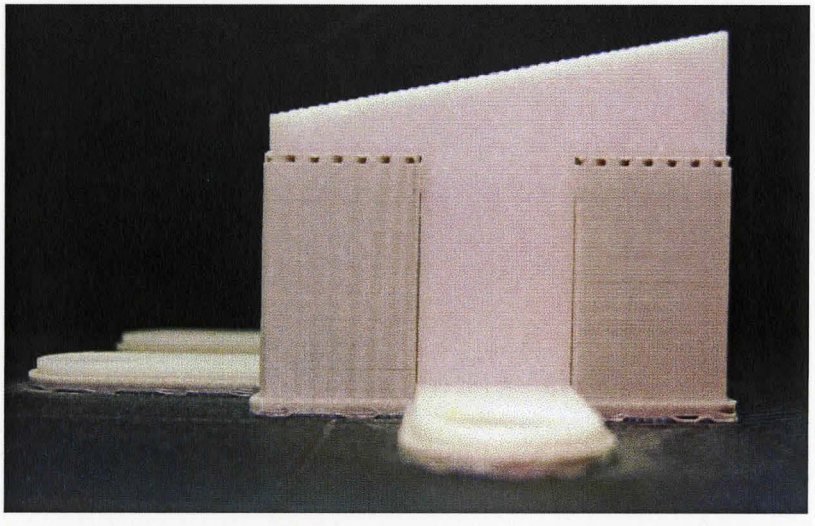

(b) Profile Picture Showing the Solid's Stepped Form

Figure 5.3: Printing on RP Inclined Planes: $\frac{1}{8}$ Inches

(a) Printing In Both Quadrants

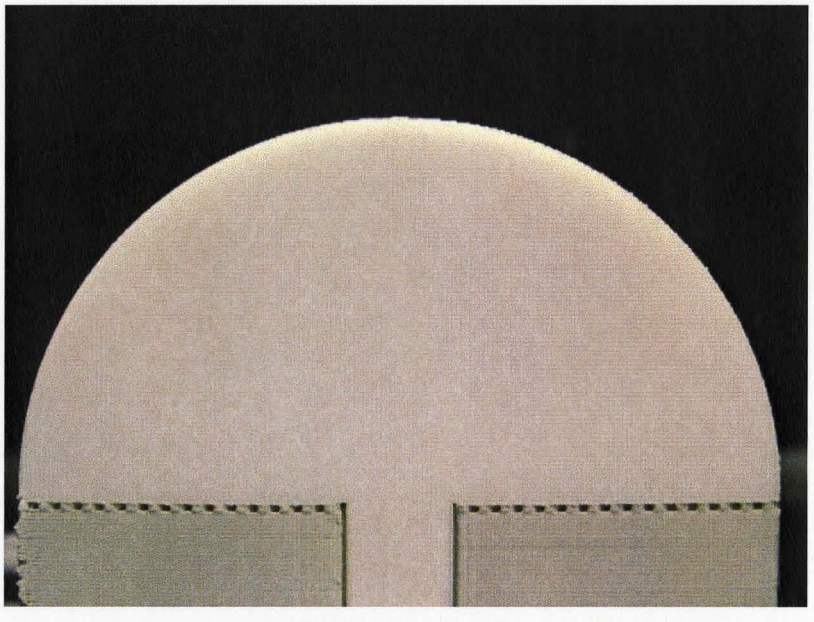

(b) Stepped Profile

Figure 5.4: Printing on RP Half Cylinder

(a) Printing in Both "Quadrants"

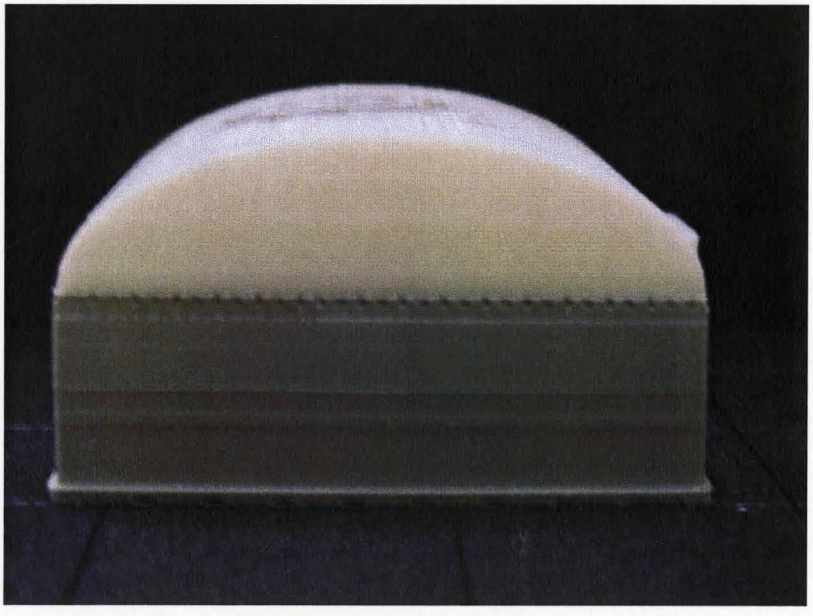

(b) Stepped Profile

Figure 5.5: Printing on RP Elliptical Cylinder

(a) Printing in Only Two "Quadrants"

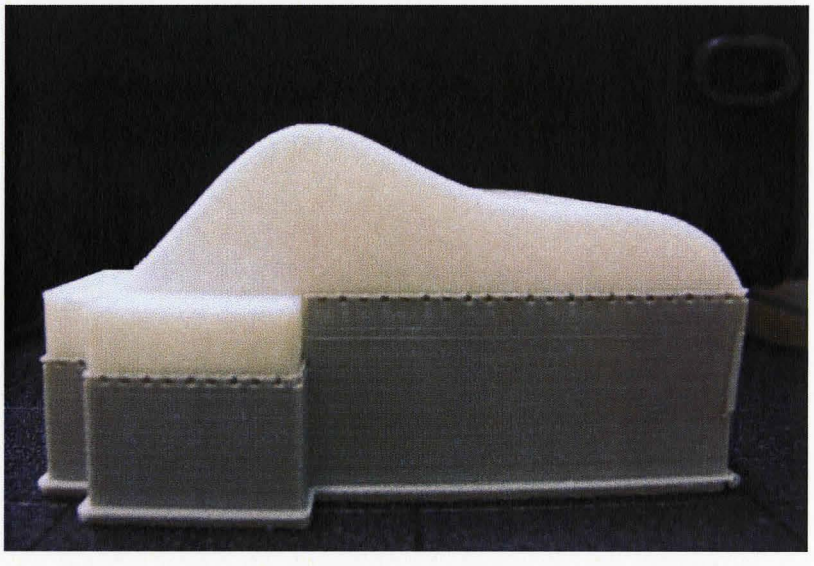

(b) Bspline Profile

Figure 5.6: Printing on RP 2D Bspline Extrusion

## 5.2 Materials

Materials of interest used in this study were: aluminum sheets and glass sheets. Wipeable printing on glass could provide the auto glass industry a tool which by they can print accurately on glass when in a certain orientation, and then measure it at different one, thus giving them better insight into the deformation of glass. For this purpose two different coatings were applied, a transparent one and a white one as shown in Fig. 5.7. The transparent approach was discarded because of the inability of the computer vision camera to detect the grid, and the white coating shows the dots clearly separated although with a minor loss to their shape.

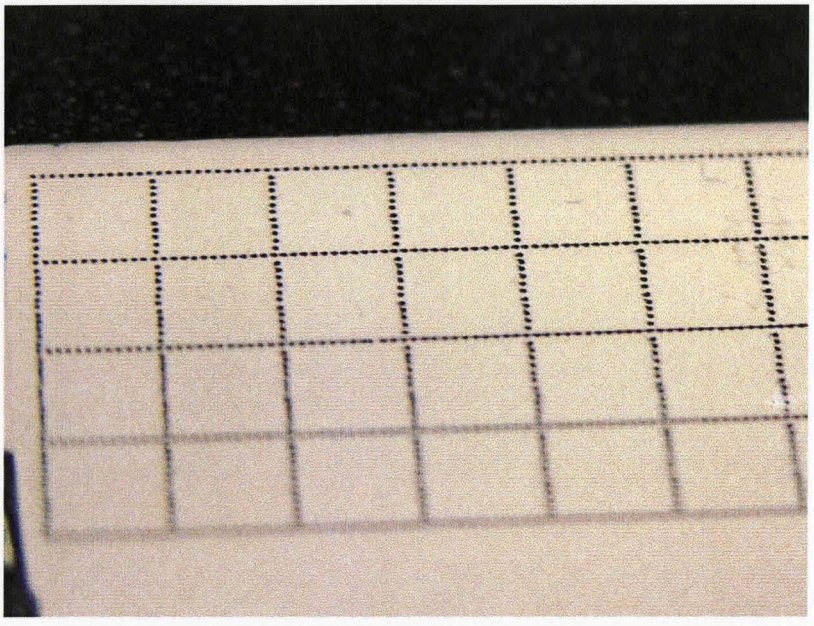

(a) Glass Coated with InkAID White Matte Precoat

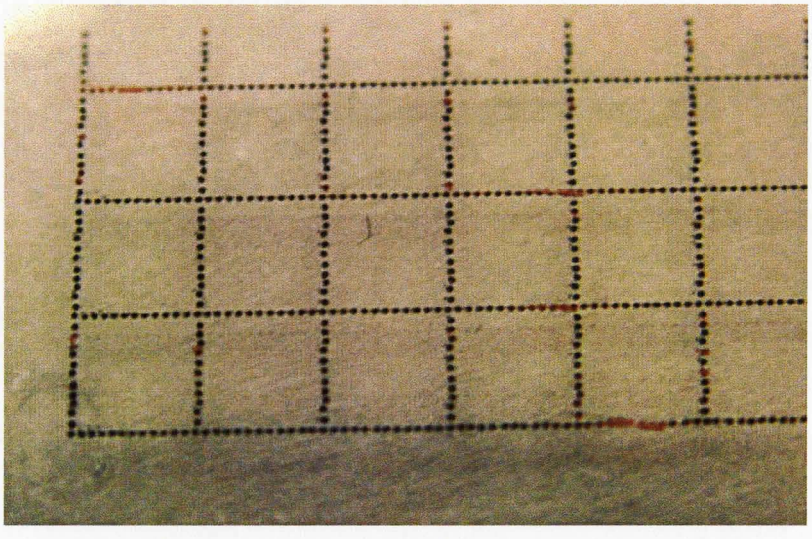

(b) Glass Coated with InkAID Clear Gloss Precoat Type II

Figure 5.7: Printing on Glass Sheets: (a)White (b)Transparent

Aluminum on the other hand, as the representative of metal sheets, can be grid-printed at a higher resolution than anything available right now, and a stress analysis can be performed on both its face and edge by analyzing the grid locations.

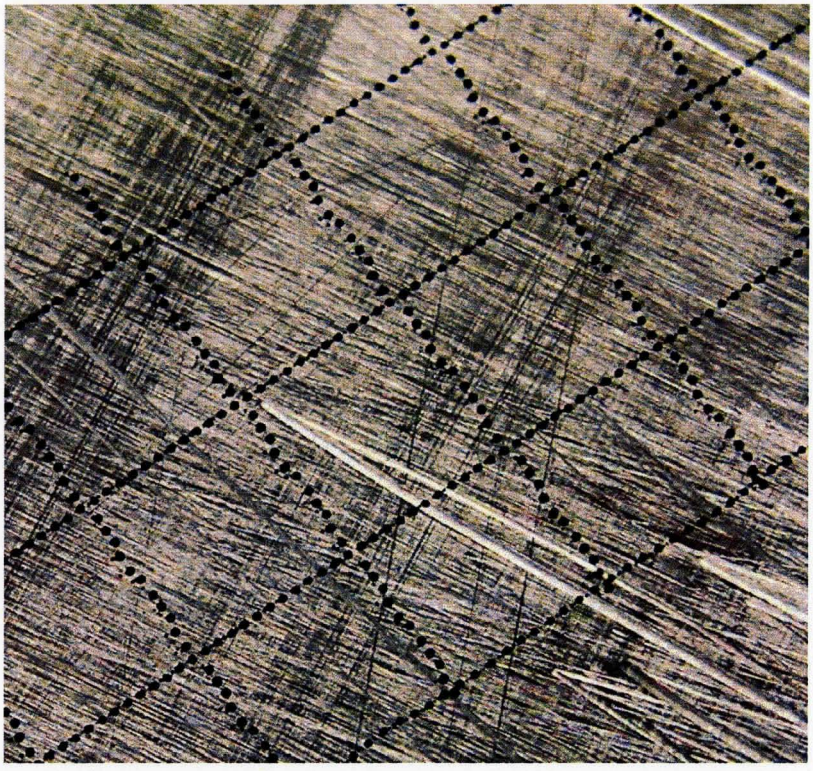

Figure 5.8: Printing on Aluminum Sheets: Transparent Coating (InkAID Clear Gloss Precoat Type II)

# Chapter 6

# Conclusions and Recommendations

## 6.1 Conclusions

Oriented three dimensional printing was presented in this thesis, where a custom built printing apparatus was used to investigate the approach of moving an ink-jet head in 3D on a 5-axis machine. This work has successfully addressed the following issues: decal images on solid models conversion to colored point clouds, printing monochrome images on the following rapid prototyped solids (flat planes, inclined planes, cylinders, elliptical cylinders, and 2D Bspline extrusions), and printing grids on different material surfaces (aluminum sheets, glass, and ABS plastic).

Image conversion into point clouds for the solids mentioned above allowed the visualization and wrapping of images on surfaces where the used CAD system is not equipped to perform such a task, thus enabling the image storage into a format that can be integrated with the printing apparatus. Printing on or decoration of the RP model was achieved in monochrome and at 96 DPI resolution due to the limited capabilities of the printing head, however printing produced consistent results on these surfaces during the runs when the RP model was covered with paper. When printing

directly on the RP models, after coating them with the ink aid, the quality of the print decreased due to the roughness of the surface, regardless of the geometry. This issue can be attributed to the resolution of the RP machine (0.01 inches per layer). The achieved printing results are more than adequate for a prototype, where the purpose of printing is to attempt to replicate what was created in the CAD system, or what an artist has envisioned and reverse engineered and then rapid prototyped. Coating proved to be a critical factor, because of the properties of the off-the-shelf ink used. Using the coating helped the ink stick on the surfaces and materials used and helped keep the integrity of the dots created. Although the dots had a minor loss of the circularity, they stayed separated with very little ink noise from splatter in between them. These results allow grids printed in this manner to increase the resolution of metal sheets square grids and be printed with sizes as low as $1/48$ inches. Coated printing on different surfaces opens the way for researchers to study the properties of materials such as: aluminum and glass, where deformation can be studied more accurately and examined more closely.

## 6.2 Future Work

There are several improvements that can be added to this system: printing performance to decrease the printing time, moving from monochrome to full color, using different types of inks that can suit different applications, printer head size reduction, printing on parametric surfaces with 2 parameters $(u, v)$, and computer aided tissue engineering where living tissues are created by spraying living cells [50, 51].

Color printing would the next step after monochrome, a step that would make this approach as the a viable approach for consumers who would reap the benefits from the color printing without the shortcomings of the only color RP approach in the

market provided by ZCorp [20]. This improvement is feasible, because the RGB data is stored in the point cloud file, and could be accessed and used with the appropriate hardware.

Another issue is the printer head size reduction which would be a great advancement because of the maneuverability it can provide in terms of its ability to print on surfaces where the radius of curvature is too small for the current system.

The final issue that needs to be dealt with is the applicability of the printer head on complex surfaces. Achieving this goal requires printing along the curvature of the surface in the $yz$ plane as well as the $xz$ plane, where segmentation of the image needs to be done along the $y - axis$ as well as the $x - axis$. Fortunately, with the printing gap tolerance allowed this should be a reachable goal.

# References


[1] Ling Wai Ming and Ian Gibson. Possibility of colouring sls prototypes using the ink-jet method. *Rapid Prototyping Journal*, 5(4):152 – 153, 1999. Available from: http://dx.doi.org/10.1108/13552549910295460.

[2] N. Hopkinson R.J.M Hague P.M Dickens, editor. *Rapid Manufacturing: An Industrial Revolution For The Digital Age.* Wiley, Chichester, West Sussex, England, 2006.

[3] Mahtun H. Khalid and G.M. Helander. Customer emotional needs in product design. *Concurrent Engineering Research and Applications*, 14(3):197 – 206, 2006. Available from: http://dx.doi.org/10.1177/1063293X06068387.

[4] Donald A. Norman. *Emotional Design: Why We Love (Or Hate) Everyday Things.* Basic Books.

[5] S.O. Onuh and Y.Y. Yusuf. Rapid prototyping technology: Applications and benefits for rapid product development. *Journal of Intelligent Manufacturing*, 10(3):301 – 311, 1999. Available from: http://dx.doi.org/10.1023/A:1008956126775.

[6] L.K. Cheung, M.C.M. Wong, and L.L.S. Wong. The applications of stereolithography in facial reconstructive surgery. pages 10 – 15, Shatin, Hong Kong, China, 2001. Available from: http://dx.doi.org/10.1109/MIAR.2001.930257.

[7] Richard Bibb, Dominic Eggbeer, and Robert Williams. Rapid manufacture of removable partial denture frameworks. *Rapid Prototyping Journal*, 12(2):95 – 99, 2006. Available from: http://dx.doi.org/10.1108/13552540610652438.

[8] 3D Art To Part.: Santa Clara, CA, USA. http://www.3darttopart.com.

[9] The art of 3d printing - 2008-04-28 00:00:00 - design news [online]. Available from: http://www.designnews.com/article/6315-The_Art_of_3D_Printing.php.

[10] Wohlers Associates, Inc.: Fort Collins, Colorado USA. http://wohlersassociates.com/.

[11] Jeffrey P. Jarosz and Ilene J. Busch-Vishniac. A topical analysis of mechanical engineering curricula. *Journal of Engineering Education*, 95(3):241 – 242, 2006.

[12] PolyU Industrial Centre. Rapid product development resource centre [online]. Available from: http://rpdrc.ic.polyu.edu.hk/content/rp_for_arch_short_guide.htm.

[13] Kunwoo Lee. *Principles of CAD/CAM/CAE Systems*. Addison-Wesley Longman Publishing Co., Inc., Boston, MA, USA, 1999.

[14] Stratasys, Inc. Eden Prairie, MN, USA. http://www.dimensionprinting.com.

[15] Solido Ltd. Yehud, Israel. http://www.solidimension.com.

[16] 3D Systems, Rock Hill, SC, USA. http://www.3dsystems.com.

[17] Objet Geometries Ltd. Rehovot ,Israel. http://www.objet.com.

[18] envisionTEC Gladbeck Germany. http://www.envisiontec.com.

[19] EOS GmbH Electro Optical Systems Munich Germany. http://www.eos.info.

[20] Z Corporation Burlington, MA USA. http://www.zcorp.com.

[21] Castle Island Co. Rapid prototyping and solid freeform fabrication - the world-wide guide [online]. Available from: http://home.att.net/~castleisland/ [cited 2008.07.04].

[22] Tom Mueller. Stereolithography-based prototyping: case histories of applications in product development. pages 305 – 309, Portland, OR, USA, 1995. Available from: http://dx.doi.org/10.1109/NORTHC.1995.485087.

[23] Wikipedia. Stereolithography [online]. Available from: http://en.wikipedia.org/wiki/Stereolithography [cited 2008.09.22].

[24] Wikipedia. Fused deposition modeling [online]. Available from: http://en.wikipedia.org/wiki/Fused_deposition_modeling.

[25] Rapid prototyping, plastic prototype, 3d cad models, rapid prototypes [online]. Available from: http://www.alphaprototypes.com/Z-Corp-3d-Printing-Process.aspx.

[26] Keith Hillestad. Decorating methods and processes. pages 5–13 –, Rochester, NY, USA, 1996. Flexography;Pad transfer printing;.

[27] Make-up for plastics surfaces[printing and decorating]. *Kunststoffe International*, 98(1):32 – 5, 2008/01/. plastics surfaces;printing;decorating;surface refinement process;plastics trade fair;Dusseldorf;.

[28] Wikipedia. Pad printing [online]. Available from: http://en.wikipedia.org/wiki/Pad_printing.

[29] R. A. Janco. Graphics for decorating plastics: Comparison of the four most common decoration methods. pages 1136 – 1138, Los Angeles, CA, USA, 1987.

[30] Gene Collard. Pad-transfer printing - taking a new look. *Plastics Engineering*, 40(2):49 – 50, 1984. PAD-TRANSFER PRINTING;.

[31] Printex:Poway, CA, USA. http://www.printexusa.com.

[32] Monode Marking Products, Inc.: Mentor, Ohio , USA. http://www.monode.com.

[33] Ibrahim Zeid. *Mastering Cad/Cam.* McGraw-Hill, New York, 2004.

[34] Autodesk, Inc.: Inventor, San Rafael, CA, USA. http:// www.autodesk.com.

[35] Hp tij 1.0 print cartridges. Technical Report 5981-6812EN, Hewlett-Packard Development Company, L.P., West Bernardo Drive, San Diego, CA 92127, USA., Nov 2004. Available from: www.hp.com/oeminkjet/reports/TIJ1.0.pdf.

[36] Hp 51604 (51604a) refills [online]. Available from: http://inkjetrefillkit.net/inkjetcartridge.php?cartridge=hp-51604&lazySID=vrqlTGTirEkuHTZHBlofFvfXy1216532147.

[37] Matt Gilliland. *Inkjet Applications, with BASIC Stamp 2 and SX Microcontrollers.* Woodglen Press, 2005.

[38] Parallax INC. *96 dpi Serial Inkjet Printer Development Kit*, 1.1 edition, November 2005. Available from: www.parallax.com/Portals/0/Downloads/docs/prod/robo/InkjetKitDocs-v1.0.pdf [cited 2008.07.04].

[39] John A. Bosch, editor. *Coordinate Measuring Machines and systems.* Marcel Dekker, INC., New York, New York, 1995.

[40] Renishaw. *PH10 Motorised Probe Head Series User's Guide*, April 2006. Available from: `www.renishaw.com/media/pdf/en/7937578e157344a3b0f416f9cebd7a5c.pdf` [cited 2008.07.04].

[41] Ontario Specialty Coatings Corp.: inkAID, Watertown, NY, USA. `http://www.inkaid1.com`.

[42] Allan D. Spence, Harley Chan, J. Philip Mitchell, and David W. Capson. Automotive sheet metal and grid digitizing solutions. *Computer Aided Design & Applications*, 2:135–144, 2005.

[43] The Mathworks, Inc.: MATLAB®, Natick, MA, USA. `http://www.mathworks.com`.

[44] Arius3D Inc. Mississauga, ON, Canada. `http://www.pointstream.net`.

[45] Les Piegl and Wayne Tiller. *The NURBS book (2nd ed.).* Springer-Verlag New York, Inc., New York, NY, USA, 1997.

[46] Rayco Manufacturing, Inc., LLC: Rayco Fixtures, Sterling Heights, MI, USA. `http://www.raycofixture.com`.

[47] TE-CO INC. Cmm fixturing [online]. Available from: `http://www.te-co.com/CMM+Fixturing-C-2001-C-.aspx` [cited 2008.07.04].

[48] Omni-Tech Corporation: Fenton, MI ,USA. `http://www.omnicmm.com`.

[49] Milton Abramowitz and Irene A. Stegun. *Handbook of Mathematical Functions with Formulas, Graphs, and Mathematical Tables.* Dover, New York, 9th edition, 1964.

[50] B.; Sun W.; Regli W Fang, Z.; Starly. A computer-aided multi-scale modeling and direct fabrication of bone structure. *Computer Aided Design & Applications*, 2(5):627–634, 2005.

[51] Vladimir Mironov, Nuno Reis, and Brian Derby. Bioprinting: A beginning. *Tissue Engineering*, 12(4):631 – 634, 2006. Biomimetic structures;Organ engineering;Multicellular tissues;Hierarchical organizations;Bioprinting;. Available from: `http://dx.doi.org/10.1089/ten.2006.12.631`.